Atomic Energy
Control Board

P.O. Box 1046
Ottawa, Canada
K1P 5S9

Commission de contrôle
de l'énergie atomique

C.P. 1046
Ottawa, Canada
K1P 5S9

INFO-0112

DEVELOPMENT OF DIFFUSION-BASED RADON DAUGHTER DOSIMETERS

by

C.R. Phillips, A. Khan and
H. Leung, Univ. of Toronto

A research report prepared for the
Atomic Energy Control Board
Ottawa, Canada

July 1983

RESEARCH REPORT

85-5011/

DISCLAIMER

The Atomic Energy Control Board is not responsible for the accuracy of the statements made or opinions expressed in this publication, and neither the Board nor the author assumes liability with respect to any damage or loss incurred as a result of the use made of the information contained in this publication.

ACKNOWLEDGEMENTS

The cooperation of Denison Mines Ltd., particularly J. Chakravatti and Z. Zeljeznak, in the mine tests of the passive dosimeter, and the scientific liaison of Dr. H. Stocker, Atomic Energy Control Board, are gratefully acknowledged.

SUMMARY

Two passive collection principles, thermophoresis and electrostatic attraction using electrets, were examined for the collection of radon daughters in personal dosimetry in uranium mines. Radon daughters are collected well by thermophoresis under a wide range of aerosol conditions, but practical difficulties exist in maintaining the required temperature gradient. The collection efficiency of electrets, on the other hand, depends upon the properties of the radioactive aerosol; electrets, however, pose fewer practical difficulties in deployment in a dosimeter.

The thermophoretically collected radon daughter activity is linear with temperature gradient at constant Working Level (WL) and with WL at constant temperature gradient, thus confirming the theory of thermophoresis as applied to the collection of radon daughters. A constant conversion factor, dpm/°C WL, is obtained for different aerosols. The conversion factor depends, however, on the ratio of RaA:RaB:RaC.

From a comparison between thermophoretic collection and collection by a pump, the temperature gradient corresponding to 0.05 L/min was determined to be 527°C/cm. At 0.01 - 0.03 WL, typical of a uranium mine, a temperature gradient of 400°C/cm would be adequate. However, incorporation of the thermophoretic principle into a passive personal radon daughter dosimeter poses design problems, since maintenance of a temperature gradient of 400°C/cm under mine conditions appears difficult. Actual thermal velocities per unit temperature gradient found were 4.12×10^{-4} $cm^2/sec°C$ for zinc oxide aerosol and 3.14×10^{-4} $cm^2/sec°C$ for carbon fumes, compared to the theoretical value of 3.12×10^{-4} $cm^2/sec°C$.

RÉSUMÉ

Deux principes passifs de captage, la thermophorèse et le captage électrostatique utilisant des électrets, ont fait l'objet d'une étude concernant le captage des produits de filiation du radon pour les relevés dosimétriques individuels dans les mines d'uranium. Les produits de filiation du radon se captent bien par thermophorèse sous plusieurs formes d'aérosols, mais on éprouve des difficultés pratiques à conserver le gradient de température nécessaire. D'autre part, l'efficacité des électrets comme capteurs dépend des propriétés de l'aérosol radioactif; l'utilisation des électrets dans un dosimètre, toutefois, présente moins de difficultés pratiques.

L'activité des produits de filiation du radon captés par thermophorèse est linéaire par rapport au gradient de température lorsque le niveau alpha (WL) est constant et par rapport au WL lorsque le gradient de température est constant, confirmant par là la théorie de la thermophorèse appliquée au captage des produits de filiation du radon. Un facteur de conversion constant, exprimé en dpm/°C WL, est obtenu pour différents aérosols. Le facteur de conversion dépend, toutefois, du rapport RaA:RaB:RaC.

En comparant le captage par thermophorèse et celui par pompage, on a déterminé le gradient de température correspondant à 0,05 L/min comme étant 527°C/cm. À des niveaux variant entre 0,01 et 0,03 WL qui sont typiques d'une mine d'uranium, un gradient de température de 400°C/cm serait adéquat. Toutefois, l'application du principe de la thermophorèse dans un dosimètre individuel passif de détection des produits de filiation du radon pose des problèmes de conception, puisque le maintien d'un gradient de température à 400°C/cm dans un milieu minier paraît difficile. On a découvert que la vélocité thermique réelle par unité de gradient de température était de $4,12 \times 10^{-4}$ cm^2/sec°C pour l'aérosol d'oxyde de zinc et de $3,14 \times 10^{-4}$ cm^2/sec°C pour les vapeurs de carbone, comparativement à la valeur théorique de $3,12 \times 10^{-4}$ cm^2/sec°C.

In contrast, maintenance of electrostatic conditions for collection of radon daughters appears practical. Certain other constraints exist, however. The experimental results seem to indicate that the electrostatic flow rate is constant for $0.03\ \mu m <$ particle diameter $< 0.09\ \mu m$, $70{,}000/cm^3 <$ aerosol concentration $< 180{,}000/cm^3$, and unattached fraction of RaA < 0.40. The data do not allow conclusions to be drawn about the electrostatic flow rate outside of these particle diameters, aerosol concentrations and unattached fraction ranges.

Electrets were formed with two different materials, a commercial 'electret-foil' and a locally aluminized Teflon FEP film, both 25 μm thick. The former material could retain surface potentials only up to ~2000 V. The latter material could, however, retain potentials up to or greater than 3000 V for at least a week and was therefore selected for use in the final dosimeter tests.

Two dosimeter tests were carried out in Denison Mines, Elliot Lake, for a period of up to five days in each case. In the first test, although the data were marred by contamination of the track etch detectors, valuable information was obtained to allow improvements to be made in the electret surface potentials and protection of the detectors from dust. Improved dosimeters with up to -3800 V electrets were tested in Denison Mines for a five-day period. Four of the six dosimeters were compared with reference CEA dosimeters exposed simultaneously. The efficiency of the electret dosimeter was found to be about 1/3 that of the CEA dosimeter. Three of the four dosimeters agreed to within 8% of the radon daughter Working Level recorded by the CEA dosimeter and to within 25% of the thoron daughter Working Level.

En revanche, le maintien des conditions électrostatiques pour le captage des produits de filiation du radon semble pratique, mais d'autres contraintes existent. Les résultats expérimentaux semblent indiquer que le débit électrostatique est constant pour 0,03 µm < diamètre de particule < 0,09 µm, 70 000/cm^3 < concentration d'aérosols < 180 000/cm^3, et une fraction non fixée de RaA < 0,40. Les données ne permettent pas de tirer des conclusions à propos du débit électrostatique à l'extérieur de ces éventails de diamètres de particule, de concentrations d'aérosol et de fractions non fixées.

Les électrets ont été formés à partir de deux matériaux différents, un "électret-foil" commercial et une pellicule Teflon FEP enduite d'aluminium sur place, d'une épaisseur de 25 µm chacun. Le premier matériau a pu retenir des potentiels de surface allant jusqu'à ~ 2 000 V, tandis que le deuxième a pu en retenir allant jusqu'à 3 000 V et plus, pour au moins une semaine, et a donc été choisi pour servir dans les essais finals des dosimètres.

Deux essais de dosimètres ont été menés aux mines Denison d'Elliot Lake, pour une période allant jusqu'à cinq jours dans chaque cas. Lors du premier essai, bien que la contamination des détecteurs à traces ait troublé les résultats, on a quand même pu obtenir des renseignements valables qui ont permis d'améliorer les potentiels de surface des électrets et la protection des détecteurs contre la poussière. On a essayé des dosimètres perfectionnés à électrets allant jusqu'à -3 800 V, aux mines Denison, pour une période de cinq jours. Quatre des six dosimètres ont été comparés à des dosimètres CEA utilisés comme référence qui avaient été exposés en même temps. L'efficacité du dosimètre à électrets s'est avérée environ le tiers du dosimètre CEA. Trois des quatre dosimètres s'écartaient du niveau alpha (WL) des produits de filiation du radon enregistré par le dosimètre CEA par une marge ne dépassant pas 8%, tandis qu'ils s'écartaient du niveau alpha enregistré pour les produits de filiation du thoron par une marge ne dépassant pas 25%.

The major conclusions with respect to electret dosimeters can be summarized as follows:

(1) Depending on the area of the charged disc, an electrostatic flow rate for radioactive aerosols can be defined and correlated with the flow rate of a pump drawing similar aerosols through a filter. Unlike the pump flow rate, however, the electrostatic flow rate is not identical for RaA, RaB and RaC in the air. Over the 5 minute sampling time, the electrostatic flow rate of RaC was found to be negligibly small whereas for RaB it was equal to or less than that for RaA. This result could have been due to differences in the charged state of the radon daughters.

(2) The charged fraction and the unattached fraction may not be the same species but the experiments consistently indicated relatively greater electrostatically deposited activity in the presence of higher unattached fractions.

(3) An electret surface potential greater than (-)2500 V was found to be suitable for the passive dosimeter developed in this work.

(4) The electret retains its surface potential better in a covered than in an uncovered state. The proposed dosimeter configuration provides a reasonable cover for the electret in order that it may stay charged for longer periods.

(5) Electrets with surface potentials less than 1000 V have been known to be stable over long periods (∿years). However, higher surface potentials (greater than 2500 V) can be retained for no more than ∿15 days under ambient room conditions and for up to a week if exposed to a mine environment.

Voici un résumé des principales conclusions relatives aux dosimètres à électrets:

(1) Selon la superficie du disque chargé, on peut déterminer un débit électrostatique des aérosols radioactifs et établir une corrélation avec le débit d'une pompe tirant des aérosols semblables à travers un filtre. Contrairement au débit de la pompe, toutefois, le débit électrostatique n'est pas le même pour RaA, RaB et RaC dans l'air. Au cours de l'échantillonnage de cinq minutes, le débit électrostatique du RaC était négligeable, tandis que celui du RaB était égal à celui du RaA ou moindre. Ce résultat pourrait découler des différences dans l'état de charge électrique des produits de filiation du radon.

(2) La fraction chargée et la fraction non attachée peuvent ne pas être de la même espèce, mais les expériences ont toujours indiqué une activité déposée électrostatiquement relativement plus élevée en présence de hautes fractions non attachées.

(3) Un potentiel de surface des électrets supérieur à (-) 2 500 V est réputé satisfaisant pour le dosimètre passif mis au point dans le cadre de ce travail.

(4) L'électret retient mieux un potentiel de surface lorsqu'il est couvert. La configuration du dosimètre proposé offre un recouvrement raisonnable pour permettre de conserver l'électret chargé pour de plus longues périodes de temps.

(5) Les électrets avec des potentiels de surface inférieurs à 1 000 V sont reconnus pour conserver leur stabilité pendant de longues périodes (~ années). Toutefois, des potentiels de surface plus élevés (supérieurs à 2 500 V) peuvent être maintenus pour des périodes ne dépassant pas ~ 15 jours dans des conditions ambiantes normales et une semaine en milieu minier.

(6) A Teflon FEP (non-aluminized) cover provides adequate protection for the electret surface, and the electret charge (of the same sign) appears on the cover as a result of induced polarization. Changing the cover results in some loss of charge from the electret surface.

(7) Contamination from dirt or moisture settling on the electret cover does not necessarily destroy its charge.

(8) A diffusion barrier must be provided in order to make a passive dosimeter reliable. However this requirement considerably decreases the efficiency of the dosimeter.

(9) Because of the measurable effect of high or low aerosol concentrations on the electrostatic collection, appropriate calibration factors must be determined for each different situation.

(10) The dosimeter design can be used for one week in its present state. However improvements in design and in electret performance are desirable.

(6) Un recouvrement de Teflon FEP (non aluminisé) offre une protection adéquate pour la surface de l'électret, et la charge de l'électret (du même signe) apparaît sur le recouvrement comme résultat de la polarisation induite. Le changement de recouvrement entraîne une certaine perte de charge à la surface de l'électret.

(7) La contamination due à la poussière ou à l'humidité qui se dépose sur le recouvrement de l'électret ne détruit pas nécessairement sa charge.

(8) La présence d'une barrière de diffusion est essentielle pour assurer la fiabilité d'un dosimètre passif. Toutefois, cette exigence réduit considérablement l'efficacité du dosimètre.

(9) À cause de l'effet mesurable des concentrations élevées ou faibles d'aérosols sur le captage électrostatique, il faut déterminer des facteurs d'étalonnage appropriés pour chaque cas.

(10) Le dosimètre conçu peut être utilisé pendant une semaine dans son état actuel. Malgré tout, l'amélioration de la conception et du rendement des électrets serait souhaitable.

TABLE OF CONTENTS

Page No.

SUMMARY (i)

1. INTRODUCTION 1

2. ATTACHED AND UNATTACHED ACTIVITY OF MINE AEROSOLS 2

   2.1 The Physical State of Radon Daughters in a Mine Atmosphere 2

      2.1.1 Unattached Fraction of Radon Decay Products 2

      2.1.2 Attachment of Radon Daughters to Aerosols 13

   2.2 Characterization of Mine Aerosols 19

      2.2.1 Aerosol Size and Activity Size Distribution 19

      2.2.2 Constituents of Mine Aerosols 21

3. CHARGED FRACTION AND ELECTROSTATIC BEHAVIOUR OF RADON DAUGHTERS 25

   3.1 Charged Fraction of Attached and Unattached Radon Daughters 25

   3.2 Neutral Particles in an Electrostatic Field 33

4. ELECTRETS 38

   4.1 Introduction 38

   4.2 Applications of Electrets 39

   4.3 Methods and Materials for Making Electrets 41

   4.4 Electret Formation for the Present Work 45

   4.5 Theoretical Aspects of Electret Formation 50

   4.6 Charge Stability Aspects 58

Page No.

5. THERMOPHORETIC COLLECTION OF RADON DAUGHTERS 63
   - 5.1 Thermophoretic Behaviour of Aerosols 63
   - 5.2 Experimental 66
   - 5.3 Theoretical Model 71
   - 5.4 Theoretical Results 76
   - 5.5 Experimental Results 76
   - 5.6 Comparison Between the Driving Forces: Thermophoretic, Collection via a Pump, and Electrostatic 84
   - 5.7 Discussion 86
   - 5.8 Conclusions 90

6. PROPOSED PASSIVE RADON DAUGHTER DOSIMETRY BY ELECTROSTATIC DIFFUSION 91
   - 6.1 Previous Designs of Passive Dosimeters 91
   - 6.2 Theoretical Considerations 92
   - 6.3 Experimental Conditions 94

7. ELECTROSTATIC DEPOSITION: DEPENDENCE ON ENVIRONMENTAL VARIABLES 106
   - 7.1 Effect of Humidity on Electrostatic Deposition of Aerosols 106
   - 7.2 Effects of Other Parameters 109

8. PASSIVE ELECTRET DOSIMETER FOR RADON AND THORON DAUGHTERS: DESIGN AND PERFORMANCE 121
   - 8.1 Design of Dosimeter 121
   - 8.2 Mine Tests of Passive Electret Dosimeter 125
     - 8.2.1 Initial Test 125
     - 8.2.2 Second Mine Test 134

Page No.

9. DISCUSSION OF RESULTS - ELECTRETS 139

9.1 Results from Aluminum Disc Experiments 139

9.2 Results from Electret Dosimeter Tests 143

10. SUMMARY, CONCLUSIONS AND RECOMMENDATIONS - ELECTRETS 146

10.1 Summary and Conclusions 146

10.2 Recommendations 149

REFERENCES 151

NOMENCLATURE 163

APPENDICES

Appendix A: Aerosol and Activity Size Distribution Measurements. 168

Appendix B: Importance of Energy Discrimination for Radon Daughter Dosimetry. 180

Appendix C: Computer Programs 183

1. INTRODUCTION

The objective of this work is to investigate the possible application of the mechanisms of thermophoresis and electrostatic collection via electrets to the collection of radon daughters with reference to personal alpha dosimeters for use in uranium mines. The potential advantage accruing from adoption of either one of these collection mechanisms is that collection is passive and does not depend upon the use of a pump (active), and is, therefore, intrinsically much more reliable.

The mechanism of thermophoresis is based upon the migration of an aerosol particle down a temperature gradient (towards the cold temperature) by virtue of differential bombardment by gas molecules on the hot side of the particle relative to the cold side. The mechanism of electrostatic-electret collection is based primarily upon the induction of dipoles in neutral aerosols by an electric field generated by the electret, a charged insulator capable of retaining its charge for periods up to years.

In order to understand fully the potential and limitations of these mechanisms, the properties of the radon daughter aerosol in a uranium mine in terms of attached and unattached fraction and charge are first characterized. The mechanisms of thermophoresis and electrostatic collection, and the procedure for electret preparation, are then examined. Finally, suitable devices are designed from the theoretical principles, and experimental tests (including mine tests) applied.

2. ATTACHED AND UNATTACHED ACTIVITY OF MINE AEROSOLS

2.1 The Physical State of Radon Daughters in a Mine Atmosphere

In areas such as uranium mines, the radon decay products upon formation find themselves surrounded with a high concentration of aerosols (∿60,000-200,000 per cm^3). Most of the newborn daughter products readily attach to aerosols, the small fraction remaining unattached depending primarily upon the concentration of aerosols available for attachment. Although most of the attached fraction and some of the unattached fraction of radon daughters are in a neutral state, a small charged fraction (attached or unattached) of radon daughters has also been found to exist. The physical state of radon daughters is discussed below without particular reference to degree of neutralization. The charge state of radon daughters is discussed in the next chapter.

2.1.1 Unattached Fraction of Radon Decay Products

A small fraction of radon daughters (<10%) is normally found in an 'unattached' state even in mine areas with high aerosol concentrations. The unattached form of radon daughters was earlier considered to be important in inducing lung cancer in the mine atmosphere. The formula recommended by the ICRP (ICRP1959) for the maximum permissible concentration of radon took into account only the unattached fraction, f, of RaA. The formula was:

$$MPC_{Rn} = \frac{3 \times 10^{-6}}{1 + 1000\ f}$$

This formula was based on the conclusion of Chamberlain and Dyson (Ch56) that the activity deposited in lungs is mainly due to unattached RaA. They had reported an average 'f' value of 0.1 for two uranium mines and calculated that 0.3 rem/week would be received by the main bronchi of an individual inhaling 3 x 10^{-11} ci/litre of radon.

Palmer et al. (Pa64) performed lung deposition studies involving total body counting which showed that all of the radon daughter activity (attached and unattached) deposits in the respiratory tract. However, it was confirmed later that most of the unattached activity (∿65%) was deposited in nasal passages, upstream of the location where most radon daughter-related lung cancers usually develop (Ge69), and that the main hazard was due to the deposition of radon daughters attached to aerosols, less than 2% of which was retained in the nose. Results of animal studies by Cohn et al. (Co53) also identified the chief hazard as being radon daughters attached to aerosols.

There has been debate over the charge state of radon daughters. At first, all unattached radon daughters were classified as 'free ions' and the terms 'charged fraction' and 'unattached fraction' were used interchangeably. Recently, Busigin, van der Vooren, Babcock and Phillips (Bu81) presented arguments which lead to the conclusion that 'unattached' particles and 'free ions' may not be a single chemical species. They have also suggested the possibility that, depending upon prevalent conditions, RaA ions may become hydrated or react chemically with oxygen or trace gases in the atmosphere.

When an atom of radon decays to form RaA, the newly-born RaA has a recoil energy of 110 KeV and is positively charged from the stripping of orbital electrons by the departing alpha particle or by the recoil motion. The recoil atom of RaA can then stay positively charged or become neutralized depending upon the charge transfer process near the end of its recoil path. After being thermalized by collisions with air molecules, the RaA atom can recombine with negative ions and become neutralized, react with oxygen to form $p_oO_2^+$ ions, and then scavenge electrons from colliding neutral molecules (if these happen to be organic compounds or trace gases such as NO and NO_2 having low ionization potentials) or remain positively charged. Subsequently, the RaA atom can either decay immediately or interact with an aerosol particle before decay. Raabe (Ra69) has inferred from circumstantial evidence and diffusion coefficient calculations that RaA exists as a single atom or as a polonium oxide molecule, surrounded by six water molecules in either case. The exact nature of an unattached decay product of radon is, however, very uncertain and depends upon a variety of factors as outlined by Busigin, van der Vooren, Babcock and Phillips (Bu81).

Due to the lack of understanding of the nature of unattached RaA, large discrepancies can be found in the diffusion coefficient values for RaA determined by different investigators. Some reported values are for ThB (Pb-212) whose molecular weight is close to that of RaA (Po-218). Table 2.1 summarizes the reported values of diffusion coefficients of RaA and ThB in air. Similar values can be attributed to RaB and RaC because of their similar molecular weights.

On the basis of the present knowledge, the following mechanisms have been established about the nature of unattached RaA:

i) The rate of neutralization of unattached RaA particles increases sharply with increasing humidity for less than 20% R.H. and shows only a nominal increase above 20% R.H. (Ge77), as shown in Fig. 2.1a.

TABLE 2.1

Diffusion Coefficients of RaA and ThB

Species	Diffusion coefficient D (cm^2/s)	Relative humidity	Ref.	Remarks
RaA	0.045	No number given; dry air	We14	Neutral atoms
ThB	0.054	-	Ch56	
ThB	0.005-0.06	-	Ma66	D decreased with age of air
ThB	0.076 0.05	-	Po68	Higher value is for neutral atoms; lower value is for ions
RaA	0.047 0.034	15% 35%	Ra68	Neutral atoms; high radon concentration (0.15 nci/litre)
RaA	0.053 0.085	<20% >20%	Th70	Average age of RaA was less than 15-20 seconds
ThB	0.02-0.09	-	Fo69	Neutral atoms; D decreased with age of air
RaA	<0.05 <0.01	- -	Bi71	∿Four times lower value for ions
ThB	0.055	-	Ko75	
ThB	0.0545 0.0524 0.0604 0.054	5-10% 10-20% 20-80% 80-90%	Ko76	D increased with ventilation rate; no effect of thoron concentration on D; ∿90 air changes per hour

TABLE 2.1 (cont'd)

Species	Diffusion coefficient D (cm^2/s)	Relative humidity	Ref.	Remarks
RaA	0.0698) (1)	10%	Ra79	(1) 6 air changes per hour
	0.0436)	90%		
	0.0811) (2)	10%		(2) 60 air changes per hour
	0.0803)	90%		
	0.0725) (1)	10%		
	0.0713)	90%		
	0.0955) (2)	10%		
	0.C913)	90%		
ThB	0.024	<2%	Po79	Top two values are for positive ions; last value is for neutral atoms; no influence of water vapour on D
	0.068	30-90%		
	0.068	All R.H.s		

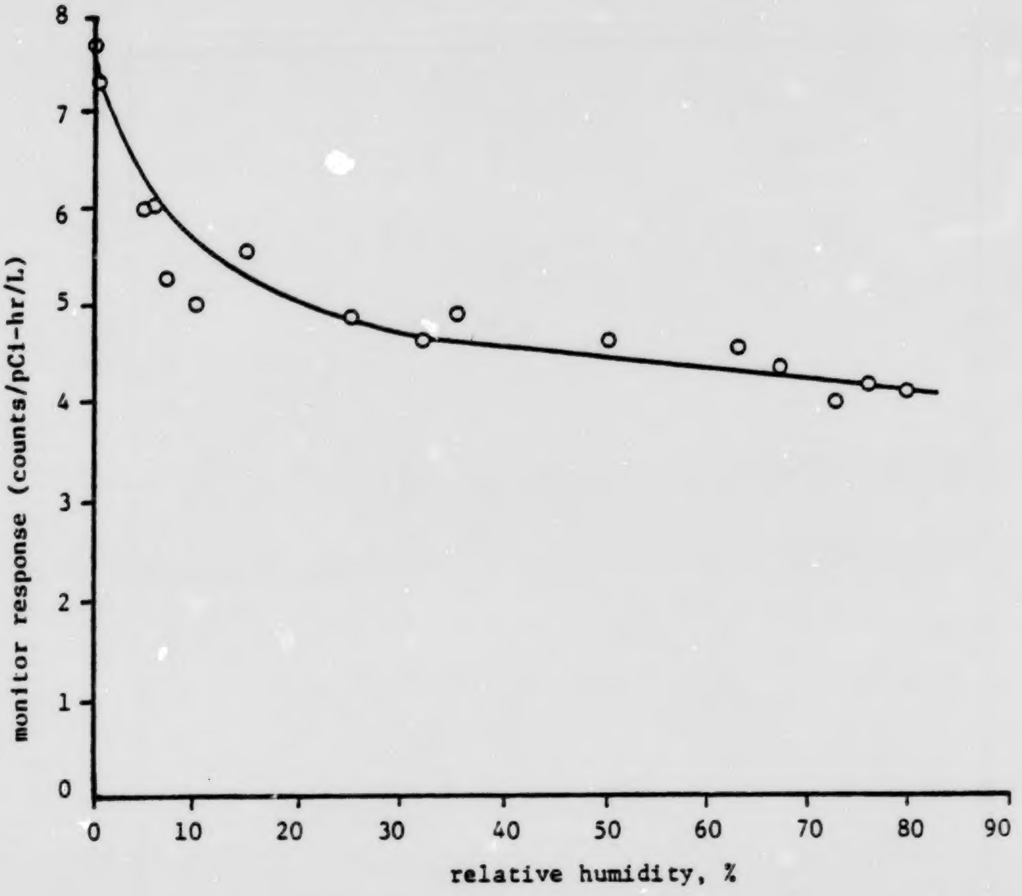

Fig. 2.1a. Variation of response with relative humidity of an integrating radon monitor based on the electrostatic collection of RaA (Ge77).

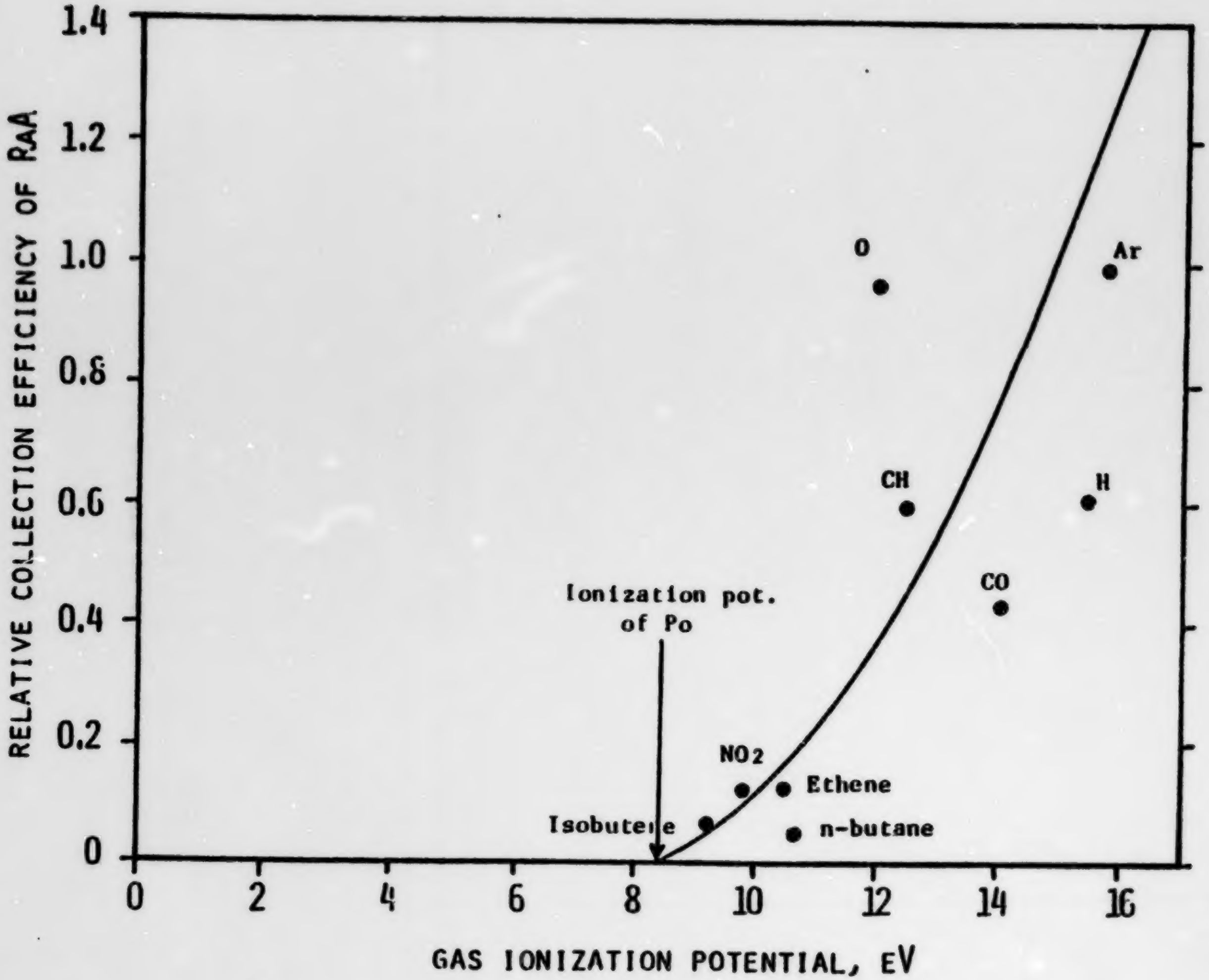

Fig. 2.1b. The dependence of the relative electrostatic collection efficiency of newly formed RaA on the ionization potential of the gaseous environment (Bu81).

ii) The diffusion coefficient of unattached RaA is in the range 0.005 to 0.1 cm^2/s and cannot adequately be represented by a single number (Bu81).

iii) The rate of neutralization of newly-born RaA depends upon the gaseous environment and increases with the decreasing ionization potential of the atmospheric constituents (Bu81) (Fig. 2.1b).

Experimental measurements on the fraction of radon daughters in the 'unattached' state have been made in both the laboratory and the mine. Results of some studies are listed in Table 2.2. However, as shown by van der Vooren, Busigin and Phillips (Va82), measurement methods for unattached fraction determination may not be accurate to more than one significant figure. Theoretical estimates of the number of unattached radon daughter atoms can be made by formulating and solving appropriate differential equations.

Unattached RaA is formed from the decay of radon and thereafter either becomes attached to aerosols at a rate, λ_s, or decays while unattached. RaB can be formed either from the decay of unattached RaA or from the decay of the fraction of RaA which becomes detached on recoil. Unattached RaB is removed either by attachment to aerosols or by radioactive decay leading to formation of unattached RaC. A fraction of the RaB can also become unattached on recoil but no experimental evidence has been found to support this possibility (Ra69; Mc72). The recoil formation term of RaC is therefore generally taken to be zero.

The following equations describe the net formation rate of the atoms of unattached RaA, RaB and RaC, whose number concentrations are

TABLE 2.2

Unattached Fractions of Radon/Thoron Daughters (ds)

Species and location	Unattached fraction	Measurement technique	Other parameters and remarks	Reference
Rn ds	0.1	Diffusion sampler	R.H. = 100%	Chamberlain and Dyson (Ch56)
Rn ds US uranium mines	0-0.73 Average = 0.25	3.7 cm dia, 60 cm long diffusion tube with filter paper at exit	R.H. = 60-90% Inadequate discrimination against attached Rn daughter	Craft et al. (Cr66)
Rn ds uranium mines	0.06-0.15 in active areas 0.09-0.25 in dormant areas	Diffusion sampler		Fusamura et al. (Fu67)
Rn ds French uranium mines	<0.05	Electrostatic sampler	R.H. >99% Aerosol concn. = $5 \times 10^4/cm^3$	Chapuis et al. (Ch70)
Rn ds 6 US uranium mines	0.002-0.12 Mean = 0.035 More than half was <0.03	Diffusion sampler	R.H. = 41-97% Temp. = 46°-67°F Aerosol concn. = $3 \times 10^3 - 10^7/cm^3$	George and Hinchliffe (Ge72)
Tn ds Thorium plant	Mean = 0.0074	Diffusion sampler collection eff. = 65%	R.H. = 70-85% Aerosol concn. = $3 \times 10^4 - 3 \times 10^5/cm^3$	Kotrappa et al. (Ko75)
Rn ds Iron mine	0.059	68.5 mesh/cm wire screen collection eff. = 86%	Particle dia. <7 μm	Stranden et al. (St82)
Rn ds Canadian uranium mines	<0.04	60 mesh/cm wire screen collection eff. = 76%	R.H. = 99-100%	Busigin, Busigin, and Phillips (Bu83)

denoted by N_{2_f}, N_{3_f} and N_{4_f}, respectively:

$$\frac{dN_{2_f}}{dt} = \lambda_1 N_1 - (\lambda_s + \lambda_2) N_{2_f} \tag{2.1}$$

$$\frac{dN_{3_f}}{dt} = \lambda_2 N_{2_f} + \alpha\lambda_2 (N_2 - N_{2_f}) - (\lambda_s + \lambda_3) N_{3_f} \tag{2.2}$$

$$\frac{dN_{4_f}}{dt} = \lambda_3 N_{3_f} - (\lambda_s + \lambda_4) N_{4_f} \tag{2.3}$$

The subscripts 1, 2, 3 and 4 refer to radon, RaA, RaB and RaC respectively. λ_i's are the radioactive decay constants, α is the recoil fraction of the RaA which beomes unattached RaB upon decay and λ_s is the rate of attachment of atoms to aerosols, given by

$$\lambda_s = BZ \tag{2.4}$$

where B = attachment coefficient (cm^3/s)

and Z = aerosol concentration (no. of particles/cm^3).

The solutions of eqns. 2.1-2.3 are given by:

$$N_{2_f} = \frac{\lambda_1 N_1}{\lambda_2 + \lambda_s} \left(1 - e^{-(\lambda_2 + \lambda_s)t}\right) \tag{2.5}$$

$$\begin{aligned} N_{3_f} = {} & \frac{\lambda_1 N_1}{\lambda_3 + \lambda_s} \left[\frac{\lambda_2 (1-\alpha)}{\lambda_2 + \lambda_s} + \alpha\right] \left(1 - e^{-(\lambda_3 + \lambda_s)t}\right) \\ & + \frac{\lambda_1 N_1 \lambda_2 (1-\alpha)}{(\lambda_2 + \lambda_s)(\lambda_3 - \lambda_2)} \left(e^{-(\lambda_3 + \lambda_s)t} - e^{-(\lambda_2 + \lambda_s)t}\right) \\ & + \frac{\lambda_1 N_1 \alpha}{\lambda_3 - \lambda_2 + \lambda_s} \left(e^{-(\lambda_3 + \lambda_s)t} - e^{-\lambda_2 t}\right) \end{aligned} \tag{2.6}$$

$$N_{4f} = \frac{\lambda_1 N \lambda_3}{(\lambda_4 + \lambda_s)(\lambda_3 + \lambda_s)} \left[\frac{\lambda_2(1-\alpha)}{\lambda_2 + \lambda_s} + \alpha\right] (1 - e^{(\lambda_4 + \lambda_s)t})$$

$$+ \frac{\lambda_1 N_1 \lambda_3}{(\lambda_4 - \lambda_3)} \left[\frac{\alpha}{\lambda_3 - \lambda_2 + \lambda_s} + \frac{\lambda_2(1-\alpha)}{(\lambda_2 + \lambda_s)(\lambda_3 - \lambda_2)}\right.$$

$$\left. - \frac{\lambda_2(1-\alpha)}{(\lambda_2 + \lambda_s)(\lambda_s + \lambda_3)} - \frac{\alpha}{(\lambda_3 + \lambda_s)}\right] (e^{-(\lambda_3 + \lambda_s)t} - e^{-(\lambda_4 + \lambda_s)t})$$

$$- \frac{\lambda_1 N_1 \lambda_2 \lambda_3 (1-\alpha)}{(\lambda_2 + \lambda_s)(\lambda_3 - \lambda_2)(\lambda_4 - \lambda_2)} (e^{-(\lambda_2 + \lambda_s)t} - e^{-(\lambda_4 + \lambda_s)t})$$

$$- \frac{\lambda_1 N_1 \lambda_3 \alpha (e^{-\lambda_2 t} - e^{-(\lambda_4 + \lambda_s)t})}{(\lambda_s + \lambda_4 - \lambda_2)(\lambda_3 - \lambda_2 + \lambda_s)} \qquad (2.7)$$

The total number of RaA, RaB and RaC atoms (N_2, N_3 and N_4, respectively) are given by:

$$N_2 = \frac{\lambda_1 N_1}{\lambda_2} (1 - e^{-\lambda_2 t}) \qquad (2.8)$$

$$N_3 = \frac{\lambda_1 N_1 \lambda_2}{\lambda_3(\lambda_2 - \lambda_3)} \left[(1 - e^{-\lambda_3 t} - \frac{\lambda_3}{\lambda_2}(1 - e^{-\lambda_2 t})\right] \qquad (2.9)$$

$$N_4 = \frac{\lambda_1 N_1}{\lambda_2 - \lambda_3} \left[-\frac{\lambda_3}{\lambda_4}(1 - e^{-\lambda_4 t}) + \frac{\lambda_2}{\lambda_4}(1 - e^{-\lambda_4 t})\right.$$

$$\left. - \frac{\lambda_2}{\lambda_4 - \lambda_3}(e^{-\lambda_3 t} - e^{-\lambda_4 t}) + \frac{\lambda_3}{\lambda_4 - \lambda_2}(e^{-\lambda_2 t} - e^{-\lambda_4 t})\right] \qquad (2.10)$$

The unattached fractions of RaA, RaB and RaC (f_A, f_B and f_C, respectively) can be calculated as:

$$f_A = \frac{N_{2f}}{N_2} \qquad (2.11)$$

$$f_B = \frac{N_{3f}}{N_3} \qquad (2.12)$$

and

$$f_C = \frac{N_{4f}}{N_4} \qquad (2.13)$$

It is noteworthy that the unattached fractions of RaA, RaB and RaC are independent of the radon concentrations because the factor $\lambda_1 N_1$ cancels out.

2.1.2 Attachment of Radon Daughters to Aerosols

Radon daughters can readily become attached to surrounding aerosols on contact because of their high mean diffusion velocities. The attachment rate of a decay product of radon to aerosols depends upon its diffusion velocity, the aerosol size and the aerosol concentration. There have been many theoretical and experimental studies in order to establish the law governing the attachment rate of radon daughter atoms and ions to aerosols. Lassen and Rau (La60), Jacobi (Ja61), Fuchs (Fu64), Baust (Ba66), Raabe (Ra 68; Ra69), Kawano et al. (Ka69), Van Pelt (Va71), McLaughlin (Mc72), Kruger and Andrews (Kr76) and Porstendorfer and Mercer (Po78, Po79) have made contributions to attachment studies on radon daughters.

Lassen and Rau (La60) experimentally studied the attachment of thoron daughter atoms to 0.08-0.12 μm diameter aerosols and found that the attached activity was proportional to $d^2/(4 + \frac{\bar{v}d}{D})$ where d is the aerosol diameter, $\bar{v}$ is the mean kinetic velocity and D is the diffusion coefficient. Raabe (Ra68) performed experiments with polydisperse polystyrene aerosols in order to study the attachment of radon daughters and concluded that the attachment rate of uncharged daughters was proportional to the surface area of the aerosol particles from 0.04 to 0.5 μm diameter. Later Raabe (Ra69) reviewed the radon daughter-aerosol interaction and postulated that this proportionality was true for all particle sizes and for all but extremely high concentrations of radon.

Porstendörfer et al. established after a series of experimental studies (Po68; Po78; Po79) that for small particles ($d < 0.1$ µm) the attachment rate is proportional to d^2 and that the process may be considered to be controlled purely by the kinetic theory of gases. Kruger and Andrews (Kr76) used thoron daughters and Kruger and Nöthling (Kr79) used radon daughters in studies which confirmed the dependence of the attachment rate on d^2. Based upon the kinetic theory of gases, the attachment coefficient, B, as defined earlier in eqn. (2.4), is given by:

$$B = \frac{\pi}{4} \bar{v} d^2 s \qquad (2.14)$$

where $\bar{v}$ = mean thermal velocity of radon daughter atoms or ions (cm/s), d = particle diameter (cm) and s = sticking probability of the atoms or ions to particle surfaces.

The underlying assumptions in eqn. (2.14), as outlined by Raabe (Ra69) are: a) the mass of an unattached radon daughter is negligibly small compared to the mass of an aerosol particle, b) the diameter of an unattached radon daughter is negligibly small compared to the diameter of a particle, c) the concentration of unattached daughters of radon with respect to the aerosol concentration is such that there is very little agglomeration of radon daughters.

The attachment rate for larger particles ($d > 1$ µm) is controlled by pure diffusion laws (Po79a) and there is no influence of electric charge. The attachment coefficient is then given by:

$$B = 2 \pi D d \qquad (2.15)$$

where D is the diffusion coefficient of radon daughter atoms or ions.

For both kinetic theory-based and diffusion-based attachment laws, the common underlying assumption is that each aerosol particle is surrounded by a number of decay product atoms and the concentration gradient thus set up around the particles then determines the rate of attachment (Me80).

Results of Porstendörfer et al. (Po79a) are shown in Fig. 2.2. The theoretical results are based on $D = 0.068$ cm^2/s, $T = 205$°K, $\bar{v} = 1.72 \times 10^4$ cm/s and the sticking probability $s = 1$.

The estimates of the sticking probability of radon and thoron daughter atoms to aerosols do not agree well. Kruger and Andrews (Kr76) found the sticking probability of ThB atoms to monodispersed polystyrene aerosols to be 0.08. Kruger and Nöthling (Kr79) confirmed the value of 0.08 for ThB but found that a value of 0.13 of the sticking probability for radon daughters seemed to fit their experimental data well. Porstendörfer and Mercer (Po78a) predicted a value of unity for the sticking probability of both radon and thoron daughters to submicron aerosols and found that a value of 0.08 made the calculated values of the attachment coefficients too low (Fig. 2.3). More experimental evidence is required in order to establish the correct value for the sticking probability.

The attachment rate, as seen in eqn. (2.4) is also directly proportional to the aerosol concentration. The dependence, as experimentally observed by Porstendörfer and Mercer (Po79), is shown in Fig. 2.4 for different aerosol diameters. The dependence becomes stronger as the particle diameter increases because the attachment coefficient is proportional to d^2.

It can be concluded from the above discussion of the attachment process that the particle size is an extremely important parameter and

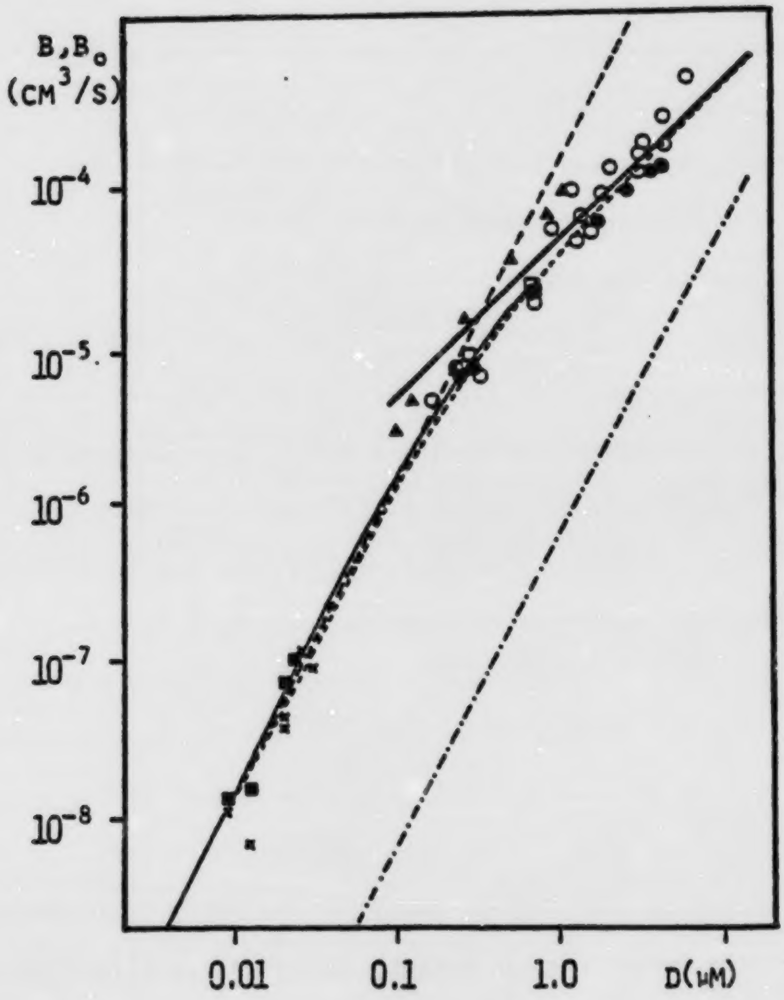

Fig. 2.2. The attachment coefficient of atoms and ions as a function of particle size (Po79a).

- ▲ Po68
- ☐ Kr76
- ■ Po78
- ✖ Po78
- ● Po79: ThB ions
- ○ Po79: ThB ions

———	Diffusion theory; atoms	$D = 0.068$ cm^2/s, $s = 1$
--------	Diffusion theory; ions	
-·-·-·-	Diffusion theory; iodine	$D = 0.076$ cm^2/s, $s = 5 \times 10^{-3}$
———	2˙Dd	
— — — —	Kinetic theory; $\frac{\pi}{4} \bar{v} d^2 s$; $s = 1$	

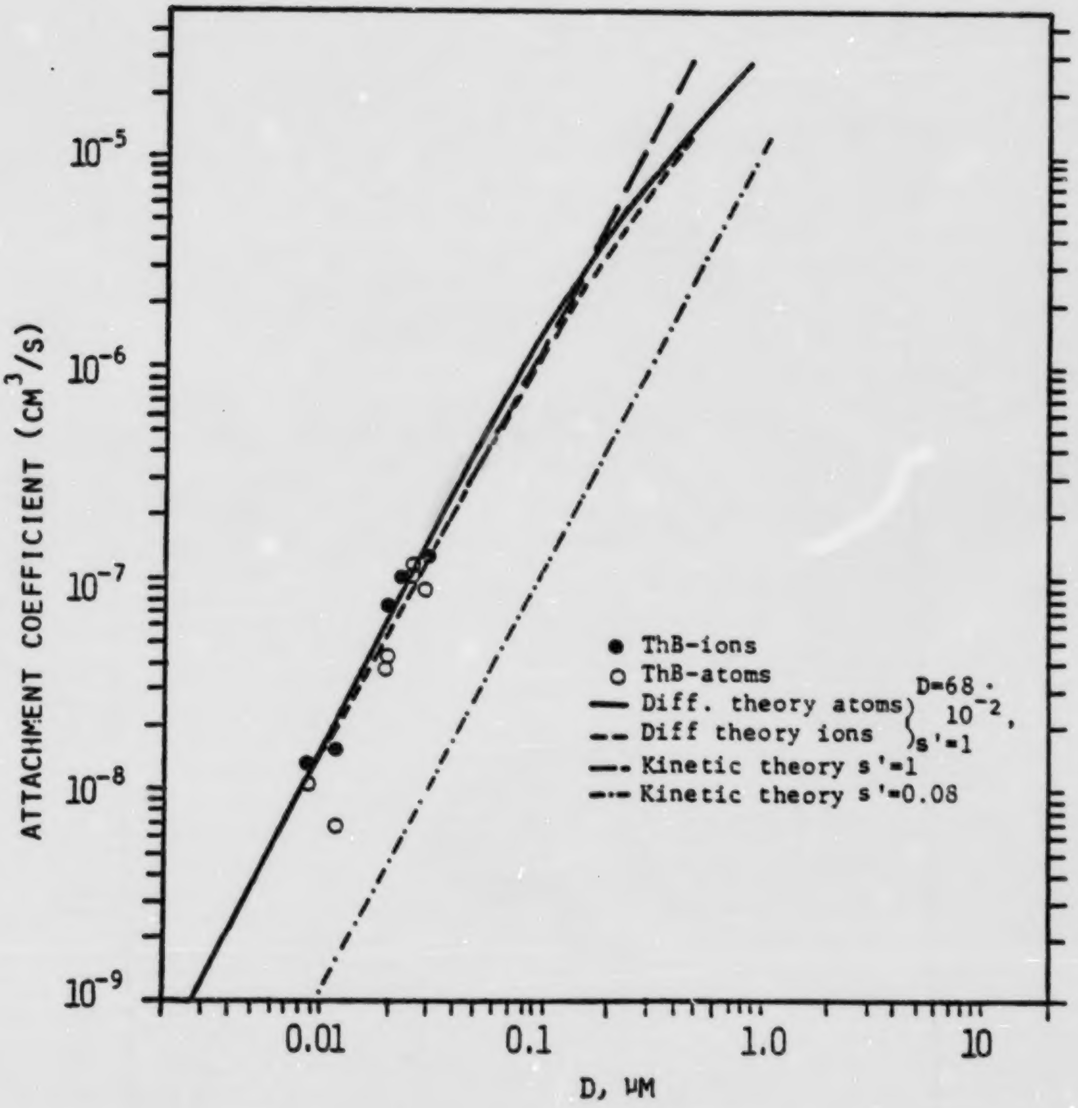

Fig. 2.3. Attachment coefficient as a function of particle size.

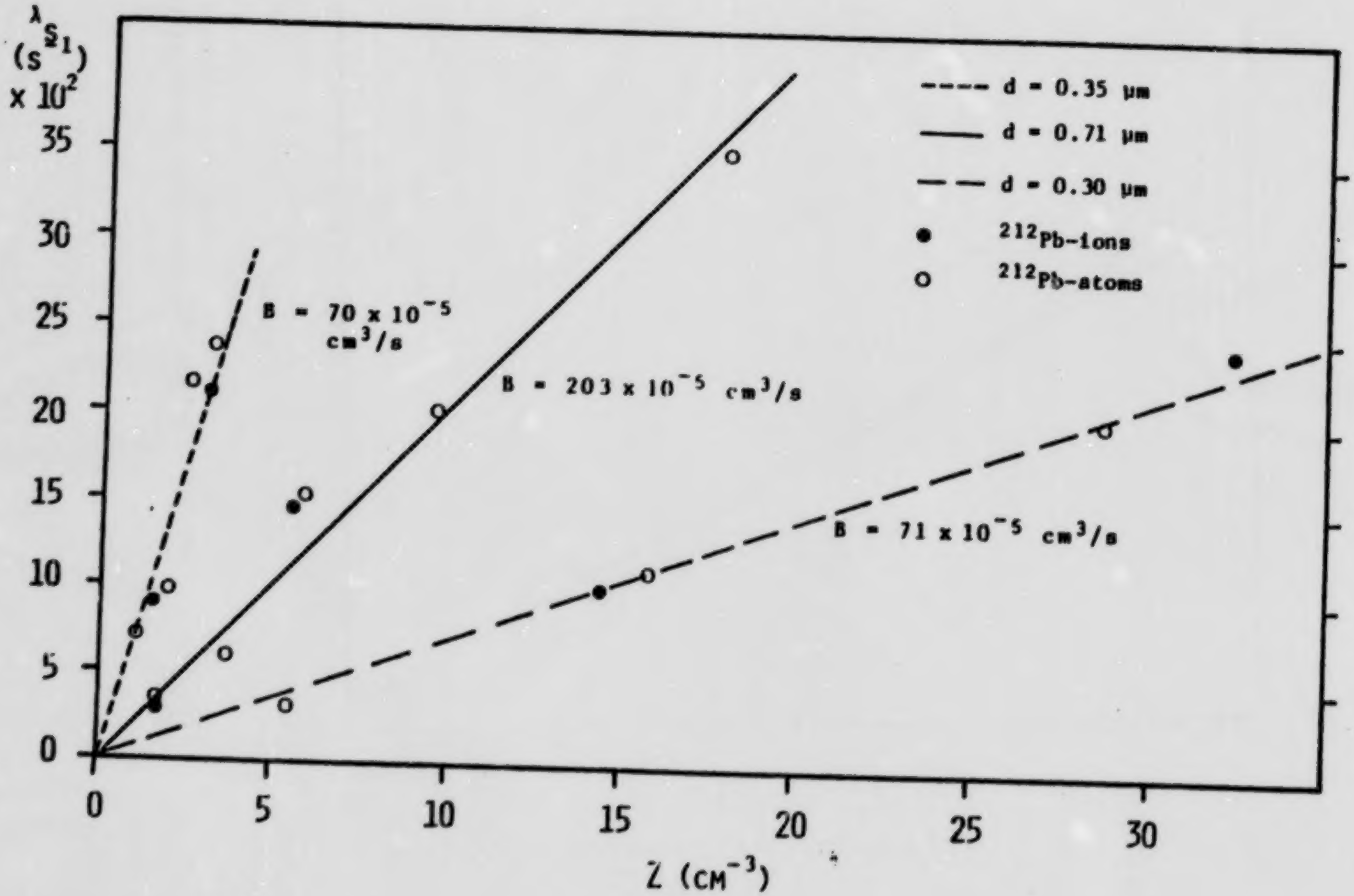

Fig. 2.4. The attachment rate for different sizes as a function of aerosol concentration (Po79).

must, therefore, be measured with great care. In actual practice, however, monodisperse aerosols, which can be represented by a single value for their diameters, do not occur, and the aerosols can only be described by a size distribution. The aerosols carrying the radon daughters can have an 'activity size distribution' of their own which may be similar to or different from the aerosol size distribution. Moreover, the chemical nature of the aerosols must also be known in order to obtain complete information on the nature of aerosols in a particular study. These important parameters are discussed in the following section.

2.2 Characterization of Mine Aerosols

2.2.1 Aerosol Size and Activity Size Distribution

An aerosol size distribution is represented in the form of a histogram by dividing the whole range of particle sizes into a number of intervals and then plotting the number of particles against the size range. The histogram can be generalized to represent the number of particles per unit diameter in each interval by dividing the number of particles in each size range by the size of the interval. A more general, normalized histogram can be obtained by dividing the number of particles per unit diameter in each interval by the total number of particles in the entire size range, so that the fraction of particles per unit diameter can be plotted against the particle size intervals. The size distribution of most commonly occurring aerosols in nature, such as atmospheric aerosols, has been found to be adequately represented by a lognormal distribution (Da74). The lognormal size distribution is defined as the distribution of aerosol sizes whose logarithms are normally distributed. The particle size distribution function C(d) in this case can be expressed as:

$$C(d) = \frac{1}{d\sqrt{2\pi}\ln\sigma_g} \exp\left(-\frac{1}{2}\left(\frac{\ln d/\bar{d}}{\ln\sigma_g}\right)^2\right) \qquad (2.16)$$

where $\bar{d}$ = count median diameter of the distribution

σ_g = geometric standard deviation of the distribution.

σ_g also serves as an index of the polydispersity of the aerosols. For monodisperse aerosols its value is unity and for polydisperse aerosols $\sigma_g > 1$.

Raabe (Ra71) has outlined details of analysis of particle sizes utilizing the log-normal distribution. Raabe also proved that any characteristic of the particle that is proportional to the qth power of the diameter (such as surface area or volume) can also be described by a lognormal distribution, with the same geometric standard deviation as the original size distribution and with a median diameter d_q given by:

$$\ln d_q = \ln \bar{d} + q(\ln\sigma_g)^2 \qquad (2.17)$$

Equation (2.16) has been widely used to describe size distributions of mine aerosols. Busigin (Bu78) developed a technique to calculate size distribution of aerosols from eqn. (2.16) based on experimental data obtained by diffusion batteries. This procedure and results of diffusion battery experiments carried out in Canadian uranium mines in the summer of 1982 are described in Appendix A. Activity size distributions can be obtained using the same technique by replacing aerosol concentrations in the experimental data by the activity obtained from a filter placed at the outlet of each diffusion battery. The activity size distribution was found to be very similar to the aerosol size distribution for Canadian mines as described in Appendix A.

2.2.2 Constituents of Mine Aerosols

For complete characterization, the chemical nature of an aerosol must also be described. Since the present work is mainly related to uranium mine aerosols, the constituents of uranium mine aerosols will now be discussed.

In elaborate studies on the physical and chemical characteristics of uranium mine aerosols, Jackson et al. (Ja82) listed the following major forms of particulates in uranium mines:

- ore dust, from ore handling operations (dumping, loading, mucking, slushing and hauling), consisting of larger particles having a composition similar to the ore.
- aerosols, from blasting operations, composed of material from blasting components, and of pulverized and vaporized ore, with smaller size distribution compared to the ore dust.
- mist, from drilling operations, composed of ore-dust, oil, water and dissolved components.
- small particles from diesel exhaust, composed of carbon-based soot.
- fume, from welding operations, composed of metals such as manganese and iron and flux components.
- additional components from ventilation air introduced in heating the incoming air.

The dynamic conditions and physical and chemical properties of the particulate constituents can further be altered by the processes of sedimentation, diffusion to walls, evaporation, condensation, growth by collisions, gain or loss of surface charge, liquid and gas phase reactions and surface adsorption. The complete characterization of such a complex system can, therefore, prove to be quite difficult.

Since most of the underground mines are generally diesel-operated, the nature of diesel particulate emissions requires some elaboration. A major characteristic of a diesel particulate emission is its extreme instability. The particle sizes in diesel exhaust emissions can vary from small single particles (∿0.01 μm) to long chains and large clusters (∿10 μm). The physical processes related to diesel particulate emission are shown in Fig. 2.5. The particles, chains or clusters can further vary widely in chemical nature and phases ranging from all liquid to all solid with mixtures including carbon, hydrocarbons, sulphate, metals and water. A schematic diagram showing the nature of diesel particles is shown in Fig. 2.6. The smallest sized spherical diesel particle is about 0.01 μm in diameter. Agglomerates and aggregates made up from individual spherical diesel particles have been measured and found to follow the lognormal size distribution (Vu76). About 90% of the mass of the particulate associated with diesel exhaust is in the form of 'soot'. Soot particles vary in size and hydrocarbon content and may contain trace metals from fuel additives, or gases and liquids adsorbed on particle surfaces. The mechanism of soot release has been investigated by Broome and Khan (Br71). The diesel soot can be important in presenting an interaction surface to radon daughters.

Jackson et al. (Ja82) found that the individual radon daughter activity size distribution showed significant changes in response to

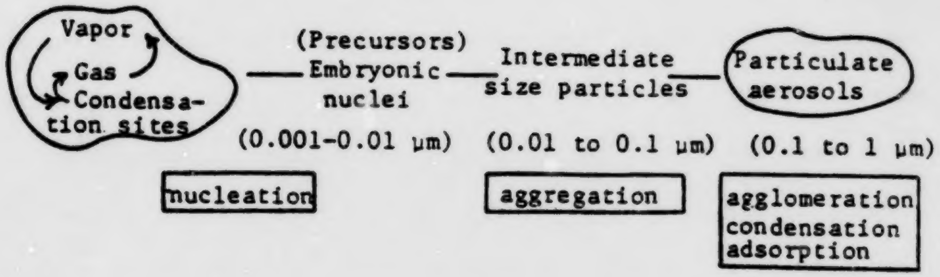
Vapor
Gas
Condensation sites
(Precursors) Embryonic nuclei
(0.001-0.01 μm)
Intermediate size particles
(0.01 to 0.1 μm)
Particulate aerosols
(0.1 to 1 μm)
nucleation
aggregation
agglomeration
condensation
adsorption

Fig. 2.5. Physical processes related to diesel particulate emissions (Vu76).

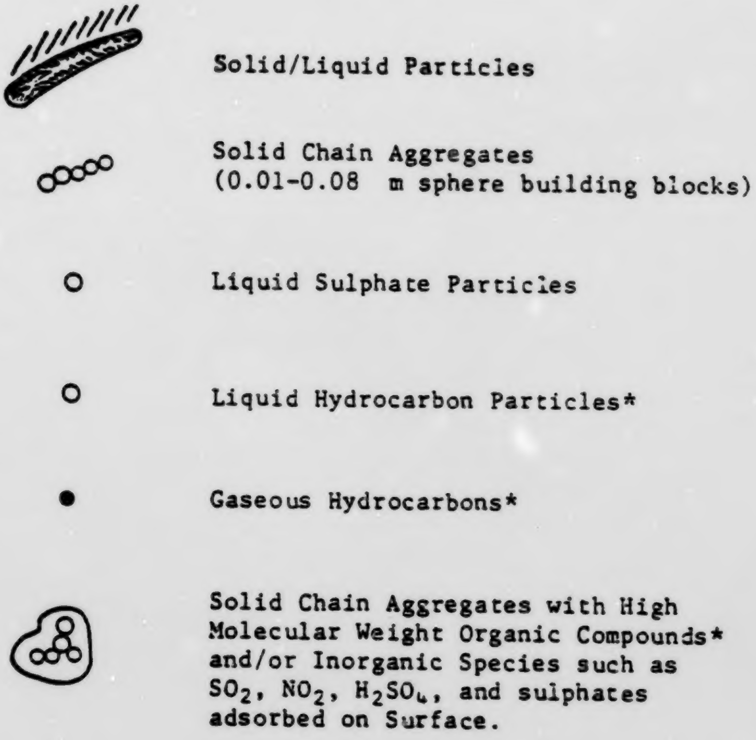
Solid/Liquid Particles
Solid Chain Aggregates (0.01-0.08 m sphere building blocks)
Liquid Sulphate Particles
Liquid Hydrocarbon Particles*
Gaseous Hydrocarbons*
Solid Chain Aggregates with High Molecular Weight Organic Compounds* and/or Inorganic Species such as SO2, NO2, H2SO4, and sulphates adsorbed on Surface.

* Unburned Hydrocarbons, Oxygenated Hydrocarbons (Ketones, Esters, Organic Acids) and Polynuclear Aromatic Hydrocarbons.

Fig. 2.6. Schematic of basic diesel particles (Vu76).

changes in the inorganic and diesel soot component of the substrate particles. Therefore, the aerosol size distributions and the activity size distributions may not be similar in all mines under all operating conditions and should be measured occasionally. Chemical characterization of aerosols is considerably more complex and may not be required in its entirety if certain assumptions, such as treating the particulate matter in diesel mines as soot, prove to be adequate. For simplified analysis, Bigu (Bi83) proposes kerosene as the chemical species most representative of the chemical nature of aerosols in diesel-operated mines.

3. CHARGED FRACTION AND ELECTROSTATIC BEHAVIOUR OF RADON DAUGHTERS

The physical state of radon daughters was discussed in Chapter 2 without reference to their charge state. However, in the presence of an electrostatic field, the behaviour of radon daughters in either the attached or the unattached form is controlled by their state of charge. Different mechanisms control the motion of charged and neutral radon daughters in an electrostatic field. The charged fraction is collected by a charged collecting surface due to coulombic forces, whereas the neutral fraction is collected due to polarization induced in the particles. These modes of collection by a charged surface are discussed in this chapter.

3.1 Charged Fraction of Attached and Unattached Radon Daughters

A small fraction of attached and unattached radon daughters is normally found to be charged. Studies have been performed to explore the differences between the attachment of charged and neutral atoms of RaA to aerosols. Using Keefe and Nolan's (Ke62) formula for the effective ion-nucleus recombination coefficient, McLaughlin (Mc72) calculated the attachment coefficients of RaA ions to condensation nuclei as a function of the degree of neutralization of the ions. His results are shown in Table 3.1 and suggest a noticeable effect of the degree of neutralization of RaA on its coefficient of attachment to aerosols. However, Porstendörfer et al. (Po79) found no significant difference between the attachment coefficients of charged and neutral atoms.

Most studies on radon daughter ions have been carried out in relation to electrical properties of the atmosphere such as the decrease

TABLE 3.1

Attachment Coefficients for RaA Particles and Condensation Nuclei (Mc72)

Particle dia. (μm) B	0.02	0.04	0.06	0.08	0.1	0.12	0.14	0.16	Degree of neutralization of RaA small ions
B_0	0.041	0.154	0.328	0.553	0.822	1.13	1.47	1.835	1.0
$B_{0.1}$	0.066	0.208	0.410	0.664	0.963	1.30	1.675	2.10	0.9
$B_{0.5}$	0.167	0.421	0.736	1.10	3.05	1.98	2.49	3.05	0.5
B_1	0.293	0.689	1.145	1.65	2.23	2.83	3.52	4.26	0.0

of the radon daughter ion content due to the electric field of a thunderstorm (Wi78). The mobility* spectrum of radon daughter ions was measured in the atmosphere by Wilkening et al. (Wi66) who found that 75% of radon daughter ions with mobilities greater than 0.06 $cm^2/V\text{-}s$ were in the range 0.25-1.5 $cm^2/V\text{-}s$. Bricard and Pradel (Br66) determined the mobility spectrum of small radioactive ions of RaA and ThB in natural unfiltered air artificially enriched with radon and thoron decay products as shown in Fig. 3.1. The mobilities of different size ranges of ions as listed by Bricard and Pradel are shown in Table 3.2.

Experiments to determine the charged fraction of radon daughters have also been carried out in uranium mines. Chapuis et al. (Ch70) obtained the mobility spectrum of charged radioactive particles by using a Zeleny tube (Ze01). These mobilities are listed in Table 3.3 for different size ranges of particles. The radioactive fraction attached to 'free ions' was found to be less than 1 percent, whereas most of the activity from the charged fraction was associated with charged aerosols of diameter greater than ~0.05 μm. After further measurements in the same series of experiments, Billard et al. (Bi71) found that 60% of the activity from radon daughters was attached to ions of diameter between 0.02-0.083 μm and that 40% of the remaining activity was attached to neutral particles larger than 0.4 μm. However the results could not be explained because it seemed quite improbable that all particles with diameter >0.4 μm should be neutral. Moreover, many neutral particles should have been present in the size range 0.02-0.1 μm because of the presence of both positively and negatively charged

---

* Mobility is defined as the proportionality constant between velocity in an electric field and the electric field strength.

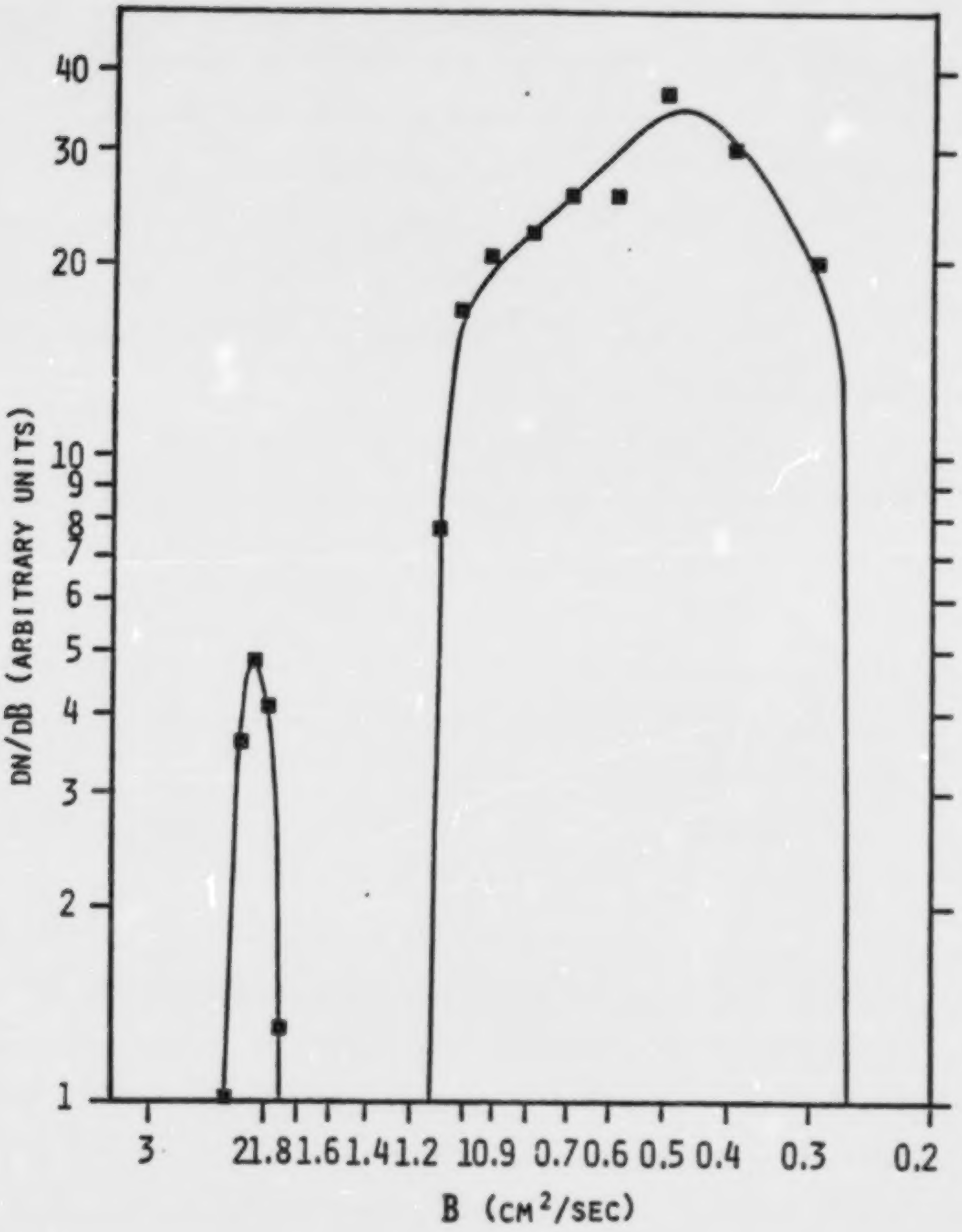

Fig. 3.1. The mobility spectrum of small radioactive ions (Br66).

TABLE 3.2

The Mobilities of Ions of Different Sizes (Br66)

	Mobility ($cm^2\ V^{-1}\ sec^{-1}$)	Dimensions (cm)
Small ions	$1.0 > K > 0.01$	$6.6 < R < 78 \times 10^{-8}$
Moderate large ions	$0.01 > K > 0.001$	$78 < R < 250 \times 10^{-8}$
Langevin ions	$0.001 > K > 0.00025$	$250 < R < 570 \times 10^{-8}$
Extra large ions	$K < 0.00025$	$R > 570 \times 10^{-8}$

TABLE 3.3

Mobilities of Ions (Ch70)

Mobility, K cm^2/V-s	Percentage of activity on ions of mobility greater than K	Particles dia. (μm)
3.75×10^{-3}	1	0.022
2.1×10^{-3}	2	0.03
1.4×10^{-3}	4	0.038
10^{-3}	6	0.044
7×10^{-4}	18	0.056
5×10^{-4}	40	0.068
4×10^{-4}	50	0.076
3.2×10^{-4}	59	0.09

particles. The ambiguities in the results of Billard et al. could have resulted from the inadequacies of the measurement technique and the variable number of charges that the particles may have carried. The use of a Zeleny tube could have led to the collection of some large neutral particles due to polarization, a mechanism explained in the next section. In such a case, the activity collected due to charged fraction could be seriously overestimated. There have also been found to be large variations in the values of the charged fraction determined in different mines. This variation could be attributed to different prevailing conditions such as ventilation rate, humidity, diesel or non-diesel machinery and other factors discussed above.

Measurements of charged fraction of radon and thoron daughters in Canadian uranium mines were carried out by Busigin, Busigin and Phillips (Bu83) using two identical Zeleny tubes as shown in Fig. 3.2. A potential of -1000 V was applied to the central wire in one Zeleny tube and the activities collected on the filters were compared to determine the charged fraction. The charged fraction of RaA was found to be <30% in both diesel and non-diesel mines. The charged fraction of ThB was found to be <54% in both mines. However, these results appear to be an overestimation, partly because at -1000 V a considerable number of neutral aerosols may be collected by the polarization mechanism (not taken into account) and partly because of the usual uncertainties associated with mine measurements.

The charged fraction can be extremely important in determining the overall behaviour of aerosols in an electrostatic field as the coulombic forces can be strong. The coulombic force which causes the

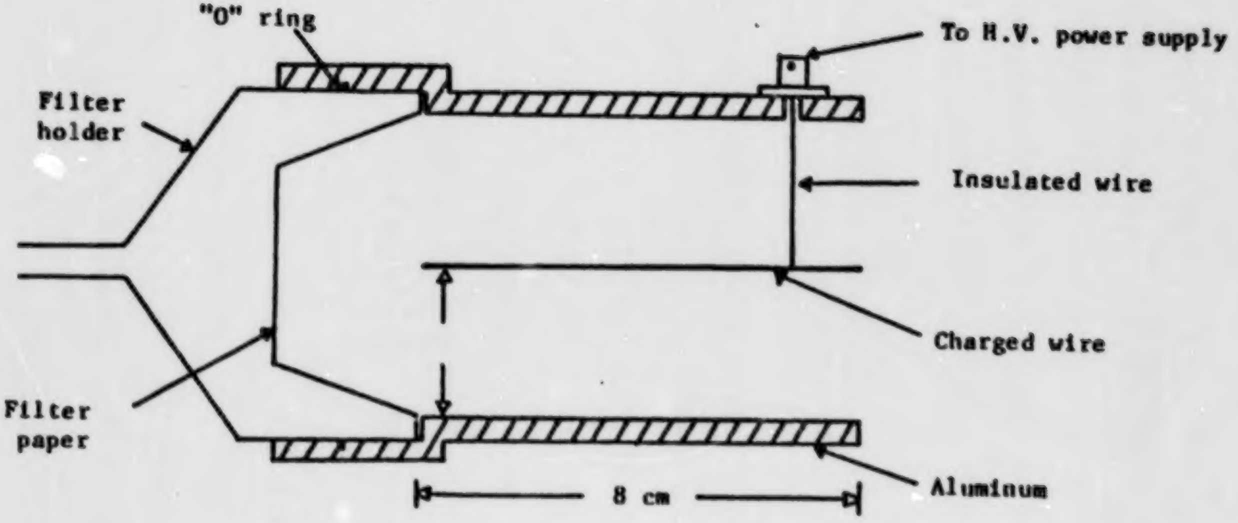
"O" ring
Filter holder
Filter paper
To H.V. power supply
Insulated wire
Charged wire
Aluminum
8 cm

Fig. 3.2. Schematic diagram of Zeleny tube used by Busigin et al. (Bu83).

attraction of an oppositely charged particle to a charged surface may be expressed as

$$F_C = neE \tag{3.1}$$

where n = number of elementary charges per particle, e is the electronic charge = 1.6×10^{-19} coulombs and E is the field strength.

Billard et al. (Bi71) have postulated that there may be up to 10 charges per particle in view of the production mode of particles in a mine (drilling, blasting, etc.). The occurrence of multiple charges would lead to complexities in the theoretical model of the system because of over- or under-estimation of the coulombic force.

3.2 Neutral Particles in an Electrostatic Field

Whenever a neutral particle enters a region in which there is an electric field, it will become polarized. 'Polarization' implies a transfer of charge within the particle so that one end of the particle acquires a negative charge and the other end a positive charge. The particle thereby becomes a dipole having an equivalent 'dipole moment' of M. The dipole moment is given by the magnitude of the charge at each end of the particle multiplied by the distance by which the charges are separated.

The induced dipole always has its positive end in the direction of the electric field intensity, E. If the field is perfectly uniform, the charges at each end of the particle experience the same force, but in the opposite directions. Thus the dipole does not experience a net force and remains suspended. In a non-uniform field, however, the forces are unbalanced because the forces at each end of the dipole are unequal.

As a result, the particle experiences a net force towards the stronger region of the field. The particle then moves in the direction of the field gradient and along the field lines towards the electrode of opposite charge.

The mechanism which results in a translational motion of neutral particles in non-uniform fields is termed 'dielectrophoresis' and may be exploited in the classification and separation of minerals, the pumping of liquids, the transportation of powders, the treatment of suspensions, the classification of microorganisms and the separation of live and dead microbial cells. The mechanism is independent of the sign of the electric field.

Particle charging applications such as industrial gas cleaning, electrostatic painting, printing, and electrostatic imaging may also be achieved by methods such as corona discharge, conductive induction and contact electrification. However, these methods are best suited to large scale applications and are, therefore, not discussed here.

For dielectrophoresis to be effective in imparting motion to suspended particles towards a charged surface, the presence of a non-uniform field is essential. Fortunately, in practice, it is easy to achieve non-uniform fields. Pohl (Po73) discusses as an example the electric field between two large, identical, flat and parallel metal electrodes separated by an insulating liquid and held at different potentials. According to conventional electrostatic theory, such a field would be uniform, but, citing Pohl, "this ideality is but a fleeting transient condition, lasting perhaps a few nanoseconds. The field rapidly warps to high inhomogeneity in microseconds ..... Field warping can continue for minutes after the application of a steady voltage."

For an insulated particle, the expression for the polarization force, F_p, can be derived as follows:

In an electrostatic field, the force on a small neutral body is,

$$F_p = (\underline{P} \cdot \nabla) E \qquad (3.2)$$

where $\underline{P}$ is the dipole vector. For a linearly, homogeneously and isotropically polarizable body,

$$\underline{P} = \alpha_p VE \qquad (3.3)$$

where V is the volume of the body and α_p is the 'polarizability' defined as the dipole moment per unit volume in unit field. Equation (3.2) then becomes

$$F_p = \alpha_p V(E \cdot \nabla) E \qquad (3.4)$$

or

$$F_p = \frac{1}{2} \alpha_p V \nabla |E|^2 \qquad (3.5)$$

For the case of a spherical particle in an electric field, it can be shown that the field inside the sphere is given by

$$E_i = \frac{3K_1}{K_2 + K_1} E \qquad (3.6)$$

where K_1 = relative dielectric constant of the medium,

and K_2 = relative dielectric constant of the particle.

The polarizability, α_p, is given by

$$\alpha_p = \frac{M}{VE} = \frac{(K_2 - K_1)\varepsilon_0}{4\pi} \frac{E_i}{E} \qquad (3.7)$$

where ε_0 = permittivity of the free space = $8.854 \times 10^{-12} \frac{C}{V\text{-}m}$

From (3.6) and (3.7),

$$\alpha_p = \frac{\varepsilon_0 (K_2 - K_1) 3K_1}{K_2 + 2K_1} \qquad (3.8)$$

On substituting the value of α_p from eqn. (3.8) and the volume of the spherical particle, $V = \frac{\pi}{6} d^3$, where d is the particle diameter, the force expression (3.5) becomes:

$$F_p = \frac{\pi}{4} d^3 K_1 \varepsilon_0 \frac{K_2 - K_1}{K_2 + 2K_1} \nabla|E|^2 \tag{3.9}$$

The special case of a conducting particle is given by the limit $K_2 \rightarrow \infty$ in the above equation:

$$F_{p'} = \frac{\pi}{4} d^3 \varepsilon_0 \nabla|E|^2 \tag{3.10}$$

The dielectrophoretic forces have been used for electrostatic air filtration by Silverman et al. (Si56), Thomas and Woodfin (Th59), Rivers (Ri62) and more recently by Nelson et al. (Ne78) and Van Turnhout et al. (Tu79). The general theory of collection of aerosol particles in electrostatic fields is outlined by Kraemer and Johnstone (Kr55) and Lapple (La70). The theoretical principles of capture of dust particles by the 'filtrete' made from permanently polarized fibres (Tu79) are given in detail by Brown (Br81).

From the above discussion it can be concluded that neutral particles can be made to move towards a charged surface. The d^3 term in eqns. (3.9) and (3.10) suggests that the net force increases rapidly with particle size. The difference in the relative dielectric constants of the particle and the medium is also important and must be >1 for a reasonably strong polarization force. The non-uniformity of the electric field, which is the primary condition for dielectrophoresis, can range from ordinary non-uniformity due to surface irregularities of the charged surface to a designed non-uniformity arising from a specially designed geometry for achieving highly divergent fields. The degree of non-uniformity of the field will directly affect the magnitude of the dielectrophoretic force on a particle suspended in the field.

The mechanism of polarization can therefore result in the collection of attached and unattached radon and thoron daughters on a charged surface, such as an electret, which by its very nature is a non-uniformly charged surface. Charge density normally varies within ±10% even on the surfaces of electrets prepared under carefully controlled conditions. This is discussed further in the next chapter. Very small radon daughter ions can be collected in an electric field owing to their coulombic forces, whereas larger particles, which are mostly neutral, can be collected by dielectrophoretic forces on an electret in areas such as uranium mines.

4. ELECTRETS

4.1 Introduction

Electrets are dielectric materials which can remain charged for long periods of time. The term 'electret' was derived from (electr)icity and magn(et) because of the close resemblance between the charge storage mechanism exhibited by some solid dielectrics and magnetism. The analogy is, however, inexact because of the following differences between electrets and magnets:

i) there is no free magnetic monopole but there is free electric charge.

ii) a magnet is usually long with small pole faces but an electret is generally short with large faces which exhibit polarization.

iii) if proper precautions are taken, a magnet can be permanent but electrets have a limited lifetime, normally ~10 years or less.

iv) magnets can be found in nature but electrets are always formed artificially.

v) magnets can be made in any desired shape but electrets are nearly always made in the form of flat circular discs.

An electret, however, gives rise to electric flux lines (and electric fields) external to itself and is therefore considered to be the electrostatic analogue of a permanent magnet. Because of its external electric field, an electret can be utilized when the primary requirement is that of an electric field alone and electric current is not important.

Electret behaviour was first observed as early as 1732 by Gray (Gr32) who described the "perpetual attractive power" of some dielectrics (waxes, resins and sulphur). After about a century, Faraday (Fa39) presented a theory about a "dielectric which retains an electric moment after the externally applied field has been reduced to zero". In 1892 Heaviside (He92) suggested the term 'electret' which was thereafter accepted and retained by researchers to designate all dielectric materials which could store charges in a semi-permanent way. The Japanese physicist Eguchi pioneered in 1919 the technique for making electrets by simultaneous application of heat and electric field on a mixture of carnauba wax and rosin (Eg19). Electrets formed by this technique are called 'thermoelectrets'. In 1935 Gemant (Ge35) introduced the now commonly used terms heterocharge (for a charge of polarity opposite to that of the forming electrode) and homocharge (for a charge of the same polarity as that of the forming electrode). Selenyi's (Se38) development of electrostatic recording with powders, using the electret effect, led to the important development of xerography in 1940. Many reviews on electrets were published in the early 1950's by researchers with an eye on the numerous proposed applications of electrets (Gu48; Ni50; Wi53; Ge53; Li56). Other important papers on electret research are those of Gross (Gr44; Gr49; Gr58; Gr71), Feaster (Fe53), Perlman (Pe68), Van Turnhout (Tu71; Tu75a; Tu75b) and Sessler and West (Se62; Se70; Se73; Se80).

4.2 Applications of Electrets

An important breakthrough in the field of electret applications is due to Sessler and West (Se62) who introduced thin polymer films for producing electrets with improved charge retention characteristics. Previously wax electrets had only limited application because of poor charge stability and sensitivity to high humidity and temperature. It is mainly due to the development of 'foil electrets' that electrets found such a variety of applications. In 1966 Sessler and West (Se66) developed the foil-electret microphone, commercial scale production of which was started by Sony in 1969. Since then, electrets have been given serious attention by researchers in many different fields. As a result, numerous applications of electrets now exist. Improved electret transducers (Se73) have found applications in sound-level meters, noise dosimeters, movie cameras, hearing aids, telephones, headphones, hydrophones and loudspeakers. Electret motors (Je70) and generators (Tu75) have been built. Some interesting applications of the electret effect have been made in biophysics in the form of attempts to improve the blood compatibility of polymers by negative charge deposition (Mu73) and investigation of electret properties of human and other bones and blood-vessel walls (Mu73). Electret bandages have been found to improve the tensile strength of skin incisions leading to quicker healing (Ko78). Electrets are also being used for radiation dosimetry because the charge decay of electrets upon irradiation by X-rays, γ-rays or thermal neutron dosages has been found to be proportional to the dose. Fabel and Henisch (Fa71) have described experiments with nylon, mylar, polystyrene and teflon for polymer thermoelectret dosimetry of X-rays and thermal neutrons. Electret ionization chambers have been reported by Bauser and Ronge (Ba78) and by Cameron and Mascarenhas (Ga80). Electret charges for pocket ion chamber dosimeters have been developed by Coover et al. (Co77) and Kotrappa et al. (Ko80). An electret dosimeter using gas multiplication has been reported by Ikeya and Miki (Ik80). A recent novel application of electrets has been the development of the 'electret air filter' (commercially available under the trade name 'filtrete') made from non-woven electret fibres (Tu79; Tu80). In the radon and radon daughter measurement area, electrets have been used for monitoring radon/thoron gas by Chittaporn et al. (Ch81) and Kotrappa et al. (Ko81; Ko82). General reviews of electret applications have been published by Johnson (Jo68) and Sessler and West (Se80).

4.3 Methods and Materials for Making Electrets

A wide variety of methods is available for making electrets. The most common methods are the following:

a) Heating the dielectric to its melting point (waxes) or softening point (polymers) and subsequent cooling under an applied electric field. This procedure has been the most popular method since pioneered by Eguchi (Eg25). Electrets made in this way are called 'thermoelectrets' (Cr67; Tu75; Pi72; Fa71).

b) Irradiating a photoconductor in the presence of an electric field with light of energy great enough to release charges in the dielectric. The resulting electrets are called 'photoelectrets' (Na37; Sc48, Fr61).

c) Irradiation with penetrating γ-rays in the presence of an electric field. The resulting electrets are called 'radioelectrets' (Gr63).

d) Heating the dielectric just above its melting point and applying a uniform magnetic field by a stabilized direct current through an electromagnet (Bh64). The electrets made by this method are called 'magnetoelectrets'.

e) Injection of low energy (20-40 KeV) electron beams into thin polymers in vacuum (Se70; Se75).

f) Application of high breakdown fields across a sandwich consisting of a polymer film on a dielectric support between two metallic electrodes (Se72). This method is carried out at room temperature and yields high charge densities ($\sim 10^{-7}$ C/cm^2).

g) Use of liquid contacts between the polymer film surface to be charged and a metallic electrode (Ch72; Ch76). This method yields electrets with very uniform charge densities.

h) Charging by corona (Ty55).

It has been established that maximum stability of charge results from homocharged electrets which are made from unilaterally metallized polymer films (Tu75). For practical applications homocharged electrets are preferred because they are made from non-polar materials which have a low ohmic conducitivity and low water absorption, thereby resulting in stable electrets. The metallization on one side of the film is important in that it reduces the macroscopic dipole to a monopole by compensating charges on one of the two sides. The external field of the electret therefore becomes stronger by virtue of metallization on one side.

A wide variety of materials has been used to make electrets, including: plexiglass, lucite, nylon (Wi53), mylar, polystyrene (Fa71), silicone resin (Pe79), polycarbonate (Pe72), various synthetic polymers (Tu75), as well as the more conventional material, wax (mixture of carnauba wax, rosin and beeswax) (Co77). However, none of the materials mentioned retain charge at high humidity and high temperature except the polymers Teflon FEP (fluoroethylene propylene) and Teflon PFA (polyfluoroalkyl).

By virtue of its excellent charge retaining capability, Teflon FEP is at present the most widely used material for making electrets. It is commercially available under the name 'electret foil'* in 25 µm and 12 µm thicknesses with chromium deposited on one side. Teflon FEP was chosen by the National Bureau of Standards (US) as the standard reference material for measuring the dielectric constant and dissipation factor because its dielectric constant does not change significantly with relative humidity even over long periods of time, and because it contains no plasticizers or other additives which would cause a gradual change in its properties. Its chemical structure can be represented as

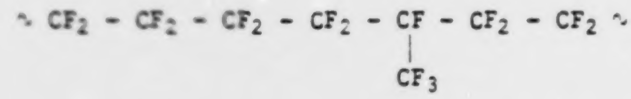

$$\sim CF_2 - CF_2 - CF_2 - CF_2 - \underset{\displaystyle CF_3}{\underset{|}{CF}} - CF_2 - CF_2 \sim$$

The dielectric constant of Teflon FEP is 2.1, its water absorption is <0.01%, melting point 255-280°C and its weather and chemical resistance are excellent. Figure 4.1 shows the charge stability of different polymer electret materials as determined by the thermally stimulated discharge method (TSD) (Tu75). The stability of Teflon FEP and Teflon PFA is excellent relative to that of other materials. Teflon PFA is superior to Teflon FEP in both mechanical strength and charge stability but, as a relatively new commercial product, it is more expensive than Teflon FEP.

---

* Sheldahl Company, Minnesota.

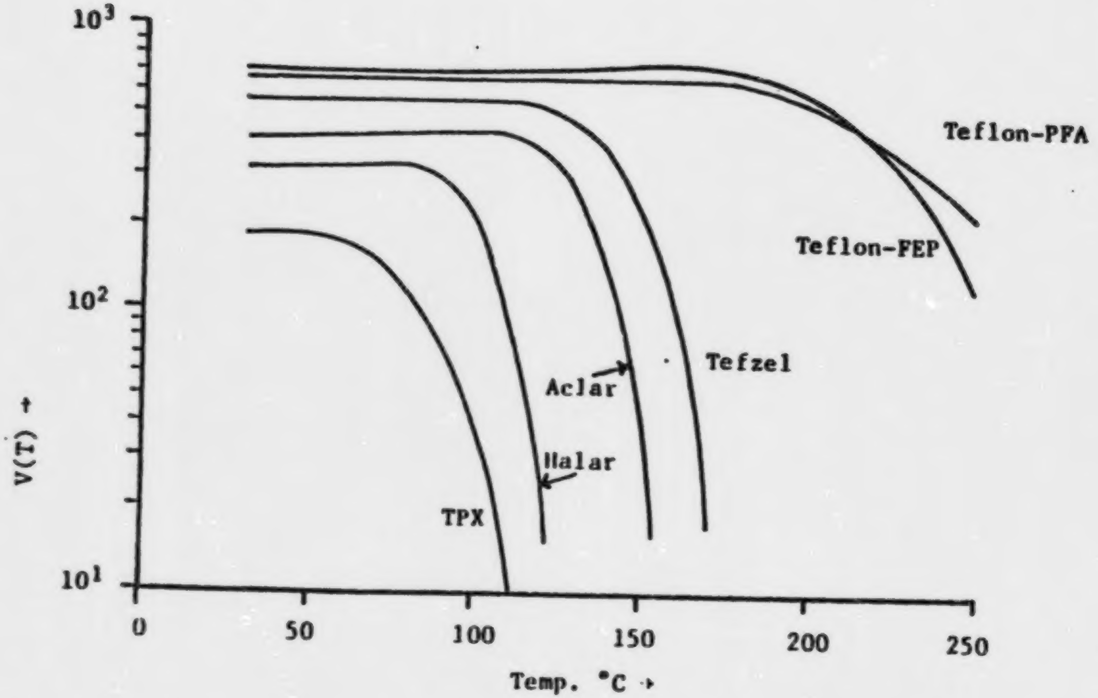

Fig. 4.1. Thermal charge stability of various electret foils of 25 μm charged with 1.7 kV in 1 min at the following temperatures: TPX (50 μm) 80°, Halar and Aclar 130°, Tefzel, Teflon-FEP and Teflon-PFA 200°C. The heating rate during thermally stimulated discharge (TSD) was 1°C/min (Tu75).

However, the latter seems to be adequate for most applications since it is a proven material for making stable electrets. Under ambient conditions Teflon FEP loses no more than 5% of its charge in three years. Even at a temperature of 70°C and 100% relative humidity, it retains at least 50% of its charge after two years (Tu75). The process of thermal aging improves its stability further as shown in Figs. 4.2 and 4.3.

4.4 Electret Formation for the Present Work

In the preliminary experiments with electrets the method based on simultaneous application of heat and high voltage was attempted. Brass electrodes were installed inside a Blue-M oven and machinable glass ceramic rings were constructed to hold the electret. The positive electrode was held by means of a micrometer attachment through the oven top. The negative electrode was placed on a glass ceramic support on the top rack inside the oven. Insulated high voltage terminals were installed on top of the oven and connections were made between a high voltage power supply and the electrodes through these terminals.

A circular piece of aluminized Teflon FEP (25 μm) was cut and sandwiched between the ceramic rings and placed on top of the negative electrode such that the non-aluminized surface of the film stretched across the negative electrode. The positive electrode was then lowered until it barely touched the film. The oven was heated to a temperature of ~150°C, well above the glass-rubber transition temperature of the polymer (77°C) and safely below its melting point (205°C). The high voltage (1-2 KV) was then switched on and the oven was switched off so that the mobilized dipoles could freeze while oriented in the direction

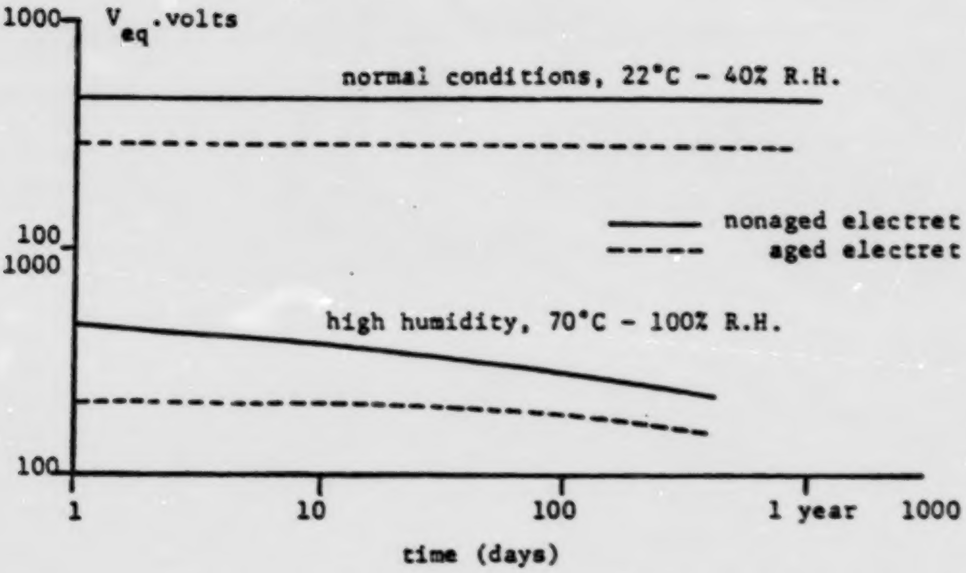

Fig. 4.2. Charge stability of Teflon FEP at normal and adverse environmental conditions (Tu75).

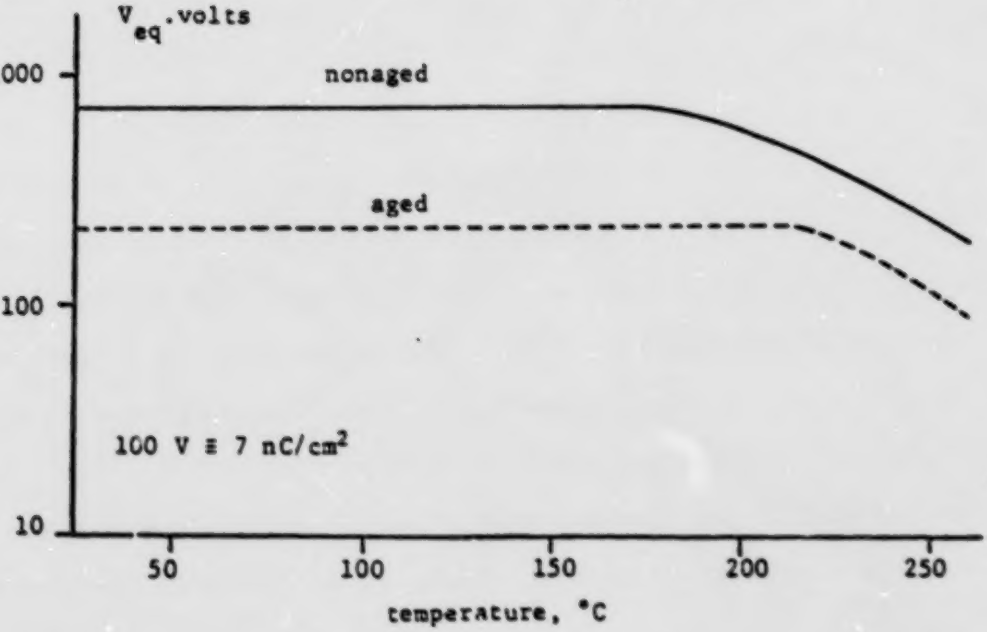

Fig. 4.3. Thermal charge stability of Teflon FEP w.r.t. aging (Tu75).

of the field. The oven was allowed to cool to room temperature. The electrets formed in such a manner were found to acquire and retain up to 1000 V. However this was not sufficient to serve the purpose since in the mean time the aluminum disc experiments described in Chapter 6 had indicated a requirement of ≥2000 V electrets for passive radon daughter dosimetry.

The only alternative for making higher surface potential electrets was by 'application of breakdown fields' (Se72). The apparatus for this method was similar to that for the thermal method except that an oven was not required. It was decided to use the same apparatus without using the heater in the oven (Fig. 4.4). The fragile ceramic rings were replaced by teflon rings which also served as guard rings for the electrodes. One square piece of 1.5 mm thick dielectric support of soda lime glass was inserted between the electrodes and a circular piece of aluminized Teflon FEP (25 μm thick) was stretched across the dielectric support. The aluminized side of the film faced the positive electrode. The arrangement is shown in Fig. 4.5. The positive electrode is lowered to make good contact with the electret. After applying high voltage (≥7 KV) for an appropriate formation time (10 sec - 1 minute), the voltage was switched off. The positive electrode was quickly raised and the charge recovery process initiated (Fig. 4.6) by joining the metallized side of the electret to the negative electrode through a wire with appropriate connections at each end. The dielectric support was then removed and the electret peeled off. The recovery process protects the high charge densities on the electret from discharge due to leakage currents through the

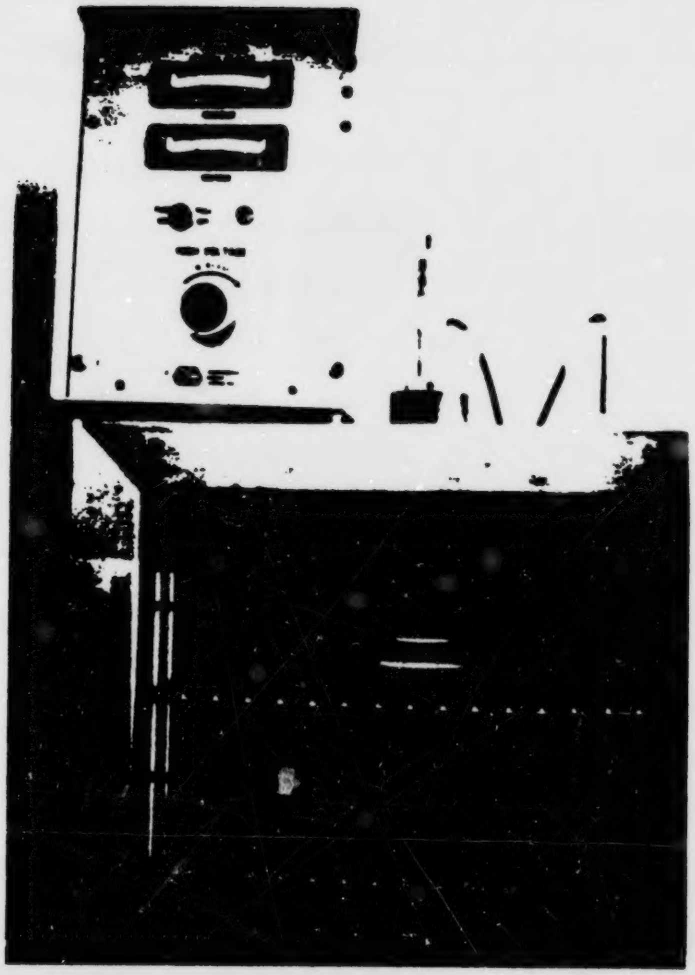

Fig. 4.4. The experimental apparatus for making electrets.

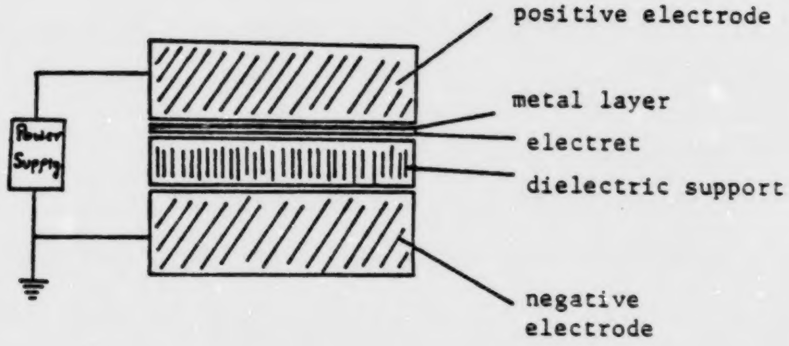
positive electrode
metal layer
electret
dielectric support
negative electrode
Power Supply

Fig. 4.5. Schematic cross-section of charging set-up.

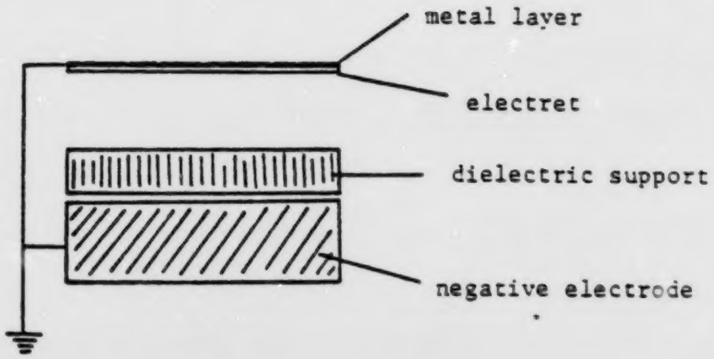
metal layer
electret
dielectric support
negative electrode

Fig. 4.6. Schematic representation of foil recovery after charging.

dielectric support. The charge density acquired by the foil is limited only by the dielectric strength of the polymer as discussed later in this chapter.

4.5 Theoretical Aspects of Electret Formation

The complicated nature of acquisition and retention of charge in electret materials is not completely understood. However, based upon present knowledge, the charges imparted to an electret can be (i) deposited surface charges, (ii) space charges injected into the electret, (iii) charges displaced within domains (Maxwell-Wagner effect) and (iv) microscopically displaced (or aligned) dipolar charges.

For an electret metallized on one side, compensation charges reside on the metallized portion. The schematic cross-section of a negatively-charged electret, metallized on one side, showing the nature of possible charges, is shown in Fig. 4.7.

Dielectric absorption involving dipolar orientation in polar substances or ionic migration in other materials is believed to be responsible for 'heterocharge' whereas interfacial charging between electrode and dielectric is linked to 'homocharge' (Gr49). Elevated temperatures can render mobile the molecules or molecule chains in a dielectric. On application of an electric field, the dipoles align themselves in the direction of the field and are frozen in this state upon cooling the material. This procedure results in a permanent polarization based on the heterocharge of the dielectric. (In thermoelectret formation, heterocharge is obtained at relatively small forming fields (10-50 kV/cm) depending upon the sample thickness, and is proportional to the forming voltage.)

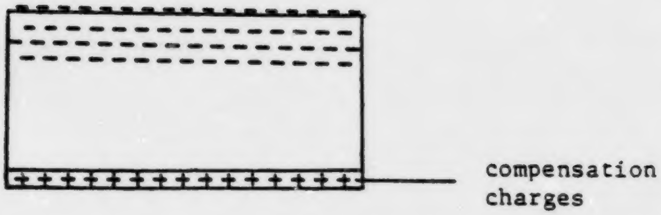
compensation
charges

(a) Surface and space charges.

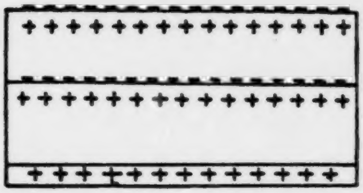

(b) Maxwell-Wagner effect.

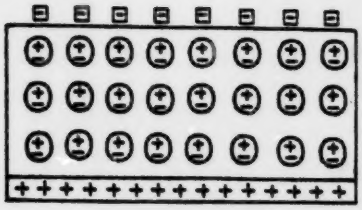

(c) Dipolar charges ⊕

Bound counter charges ⊟

Fig. 4.7. Schematic cross-section of an electret metallized on one side.

Surface charges can be deposited and space charges can be injected in a dielectric material by electrodes at a high electric field. The surface-charge deposition leads to a homocharge which is related to the breakdown in the small air gaps between the electrode and the dielectric surface and higher fields of ~100-800 kV/cm are required. The microscopic irregularities on the electrode and the dielectric surfaces can also provide a small air gap for making homocharge injection possible. This is illustrated in Fig. 4.8. Such space charge injection can occur in highly insulating materials with strong trapping. In this case the charging leads to the formation of a space-charge layer (Schottky layer) in the vicinity of the injecting electrode.

Moreover, conduction between interfaces such as domain boundaries (Maxwell-Wagner effect) or over the entire thickness of the electret can cause internal polarization due to charge separation within the dielectric.

All of the above-mentioned charge-imparting mechanisms exhibit time dependence. This time dependence is discussed in detail by Sessler (Se79).

The only limits imposed on electret charges are those due to internal and external breakdown. The former depends upon the dielectric strength of the material and the latter depends upon the air gap between the non-metallized surface of an electret and the closest metallic electrode.

Regarding the internal breakdown, the maximum charge density that can be retained by a 25 μm Teflon FEP film can be calculated from the relation

$$\varepsilon E_i = \frac{\sigma}{\varepsilon_0} \qquad (4.1)$$

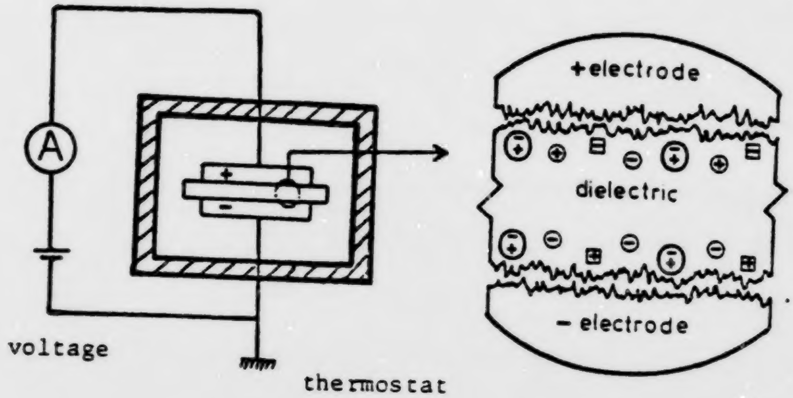
A
+
-
voltage
thermostat
+electrode
dielectric
- electrode

Fig. 4.8. Illustration of the injection of homocharges ⊕ The internal heterocharging by dipole orientation ⊙ and ion migration ⊟ is also shown (Tu71).

where E_i is the internal field of the electret, ϵ (=2) is the dielectric constant of the film, ϵ_0 is the permittivity of free space = 8.854×10^{-14} C/Vcm and σ is the surface charge density. Substituting the dielectric strength limit of $\sim 2 \times 10^6$ V/cm for teflon FEP as E_i in eqn. (4.1) gives $\sigma \cong 3.7 \times 10^{-7}$ C/cm^2.

The corresponding surface potential limit, V_m, for a 25 μm teflon FEP film is

$$V_m = \frac{\sigma \times \ell}{\epsilon\, \epsilon_0} \quad , \qquad \text{where } \ell = 25\ \mu\text{m}$$

Using the value of $\sigma \cong 3.7 \times 10^{-7}$ C/cm^2, $V_m \cong 5000$ volts. (For 25 μm teflon FEP the surface charge density can be easily converted into surface potential by the relation 100 V = 7 nC/cm^2.)

The maximum retainable charge density by a PET (polyethylene terephthalate) electret has been estimated by Sessler and West (Se72) from its dielectric strength limit (Fig. 4.9). This figure also shows the charge density obtained as a function of the formation time and applied voltage.

The external breakdown limit is governed by the Paschen curve for breakdown in air between parallel plate electrodes. Figure 4.10 shows the voltage across an air gap with or without a dielectric support used for controlling breakdown between the charged electret surface and the electrode. Figure 4.11 shows the theoretical estimate of charge densities that can be held by different thicknesses of Teflon FEP at different air gaps between the film and a metallic electrode. From this figure the minimum distance at which a metallic surface can be held above an electret surface, without risk of breakdown, can be estimated. Breakdown has important implications in passive dosimeter design because

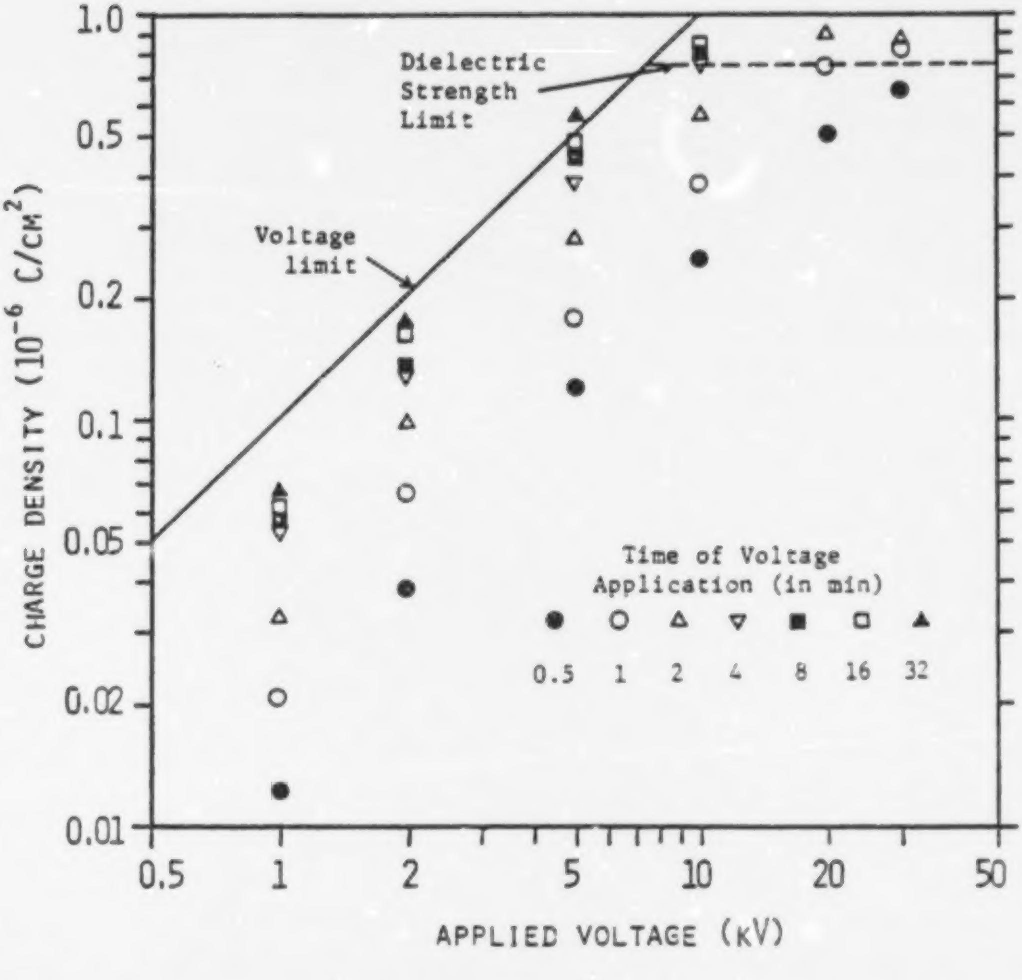

Fig. 4.9. Initial charge density on negatively breakdown charged 25 μm PET as a function of charging voltage with charging time as parameter. During charging, one sheet of 0.15 cm soda-lime glass is used as resistive spacer between PET film and negative electrode (Se72).

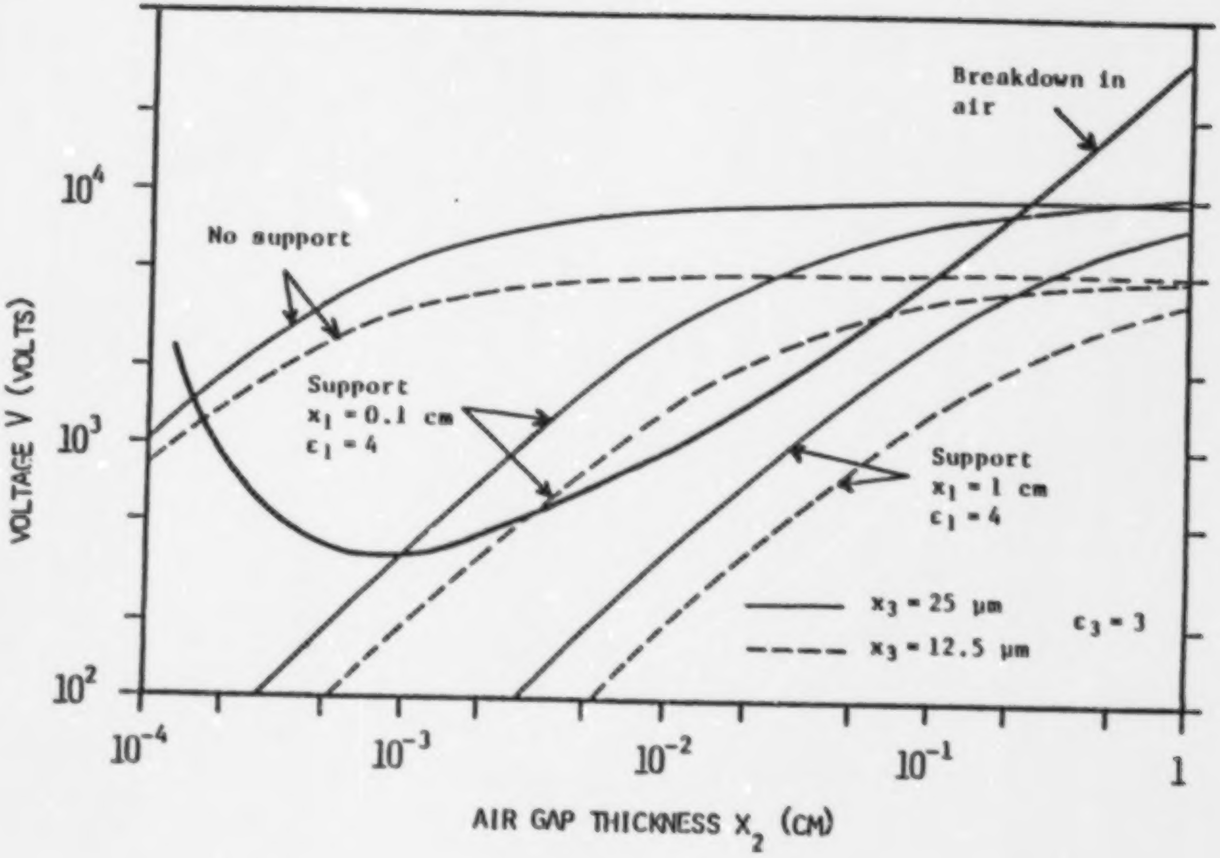

Fig. 4.10. Voltage across air gap when electret with $\sigma = 10^{-6}$ C/cm^2 is taken off from dielectric support. Paschen curve for breakdown in air between parallel flat plates is also shown (Se72).

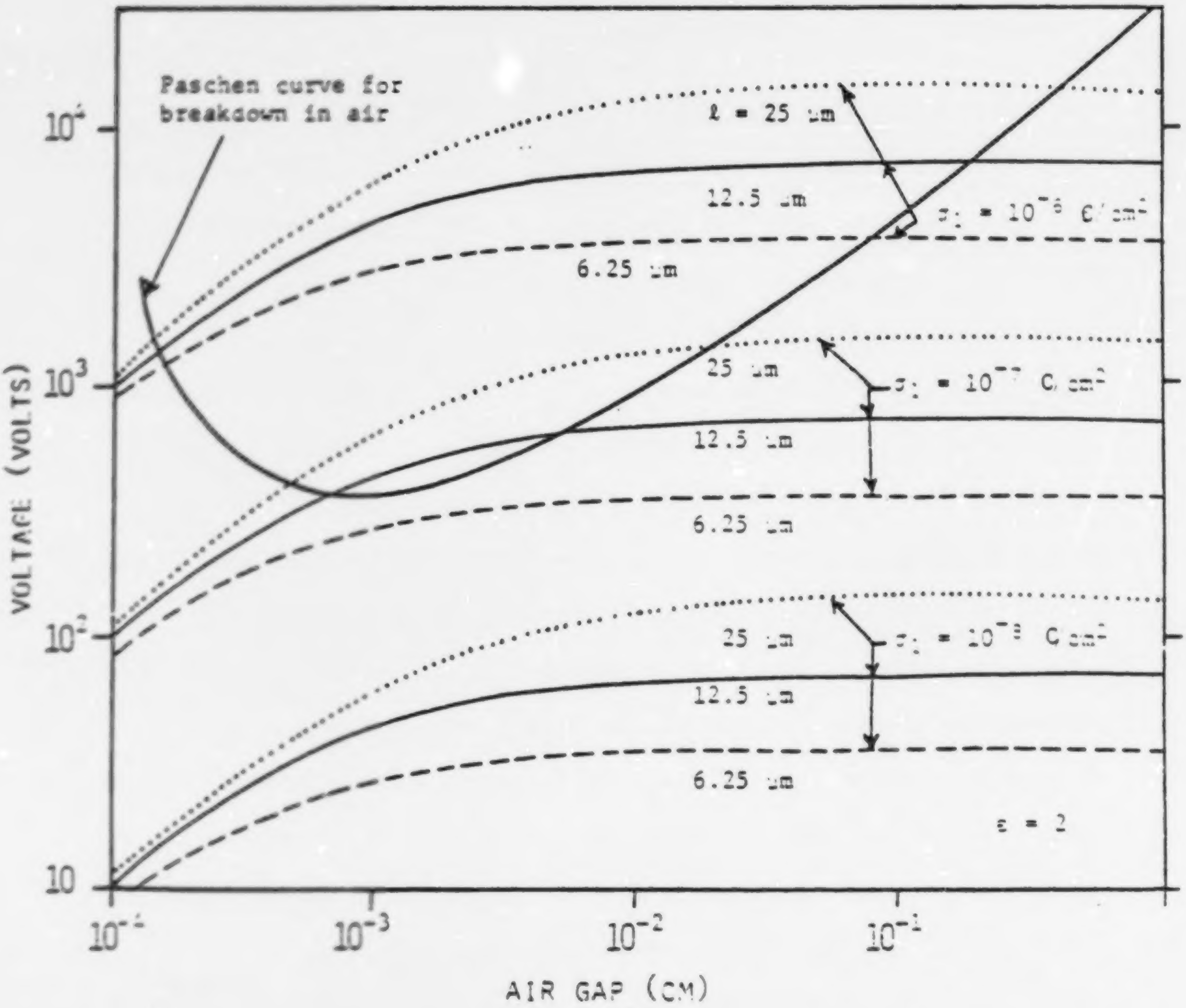

Fig. 4.11. Theoretical estimate of charge densities that Teflon FEP can hold at different air gaps between the film and the electrode (Se80).

the metallic detection head is held 6 mm above the electret surface. From Fig. 4.11, the electret can safely have a surface potential of up to 4000 V without risk of external breakdown.

4.5 Charge Stability Aspects

In the quest to find and develop better electret materials, it is important to be able to check the long-term charge stability of electret materials over short periods of time. This check was accomplished using the technique of 'thermally stimulated discharge' (TSD). This technique is capable of revealing the mechanisms responsible for charge decay of an electret and it can also help in optimizing the charging conditions. Sectioning of an electret before TSD can reveal the charge distribution within the electret. The TSD technique is based upon the principle that the charges in an electret become mobile and therefore easier to discharge when heated. An electret connected to two electrodes generates a weak current when heated at a linear rate due to heat stimulated discharge. The current recorded as a function of temperature shows a number of peaks, the shapes and locations of which are characteristic of the mechanisms by which electrets store their charges. Important information on the permanent dipoles (density, relaxation time, activation energy) and trapping parameters (energies, concentration and capture cross-section of traps) can be obtained by carefully analyzing the peaks. A comprehensive treatment of TSD of polymer electrets has been undertaken by Van Turnhout (Tu75).

The TSD technique can be used either for obtaining a current-temperature diagram with an electret metallized on both sides (current TSD) or a charge-temperature diagram with unilaterally metallized electrets (charge TSD). The latter method has been found to be suitable for foil electrets. Figure 4.1 shows measurements made by the charge TSD method. A fully automated apparatus for charge TSD measurements on foil electrets has been described by Turnhout (Tu79) (Fig. 4.12). A commercial instrument for current TSD studies is available under the name "Electret thermal analyzer"*, manufactured by Toyo Seiki Sasaku-Sho Ltd. The equipment includes a picoammeter, a 4 KV dc power supply, a U-line temperature program controller coupled to a power regulator, and a dual channel strip chart recorder.

Observations of actual charge decay of different types of electrets stored under different conditions have been made over long periods of time as shown in Figs. 4.13, 4.14 and 4.15. Similar observations were also attempted in the present work. The results are shown in Fig 4.16. In this figure the 'open' notation means that no cover was provided for the electret surface and the electret was left exposed in the open atmosphere (the bottom curve) or in a drawer (top two curves). The notation 'covered' means that a piece of non-aluminized Teflon FEP film (25 μm thick) was placed on the electret so as to cover its surface completely.

---

* Distributed in U.S.A. by Atlas Electric Devices Co., Chicago, Ill. 60613.

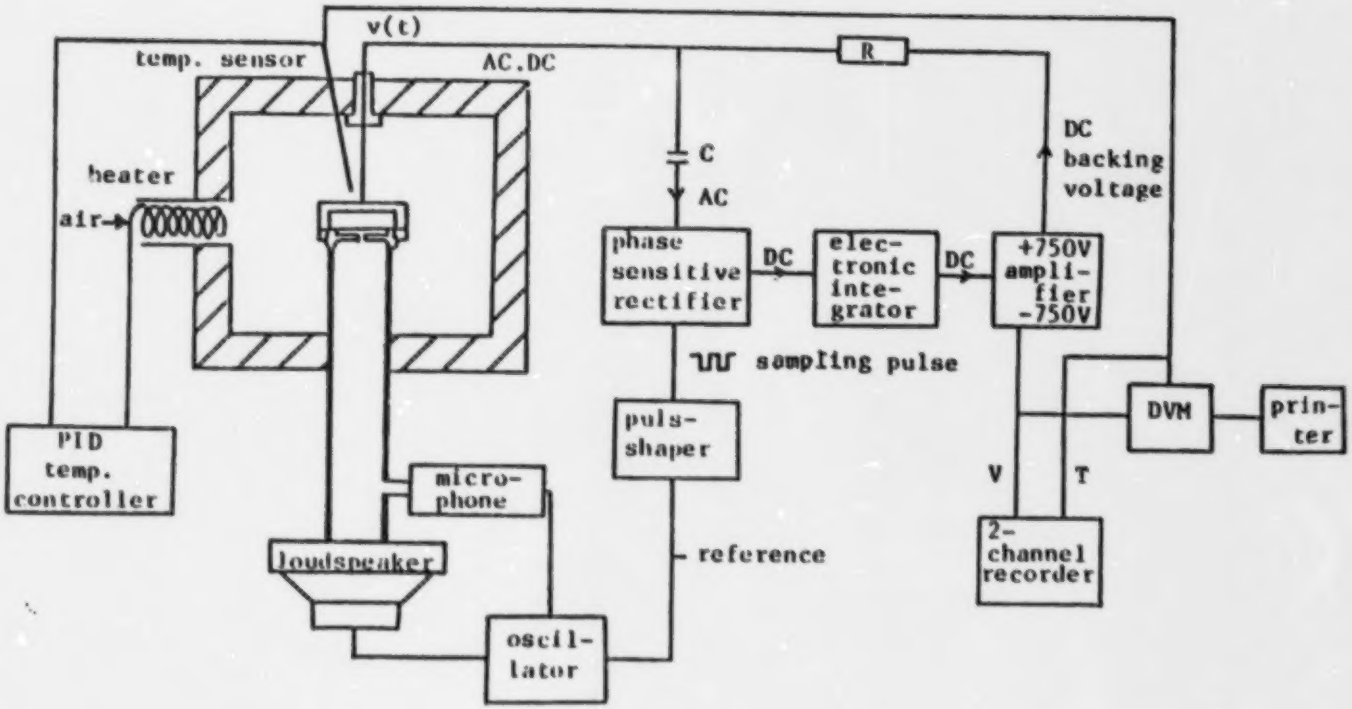
v(t)
temp. sensor
AC.DC
heater
air
PID
temp.
controller
loudspeaker
micro-
phone
oscil-
lator
C
AC
R
phase
sensitive
rectifier
DC
elec-
tronic
inte-
grator
DC
+750V
ampli-
fier
-750V
DC
backing
voltage
sampling pulse
puls-
shaper
reference
V
T
DVM
prin-
ter
2-
channel
recorder

Fig. 4.12. An automated charge TSD set-up (Tu79).

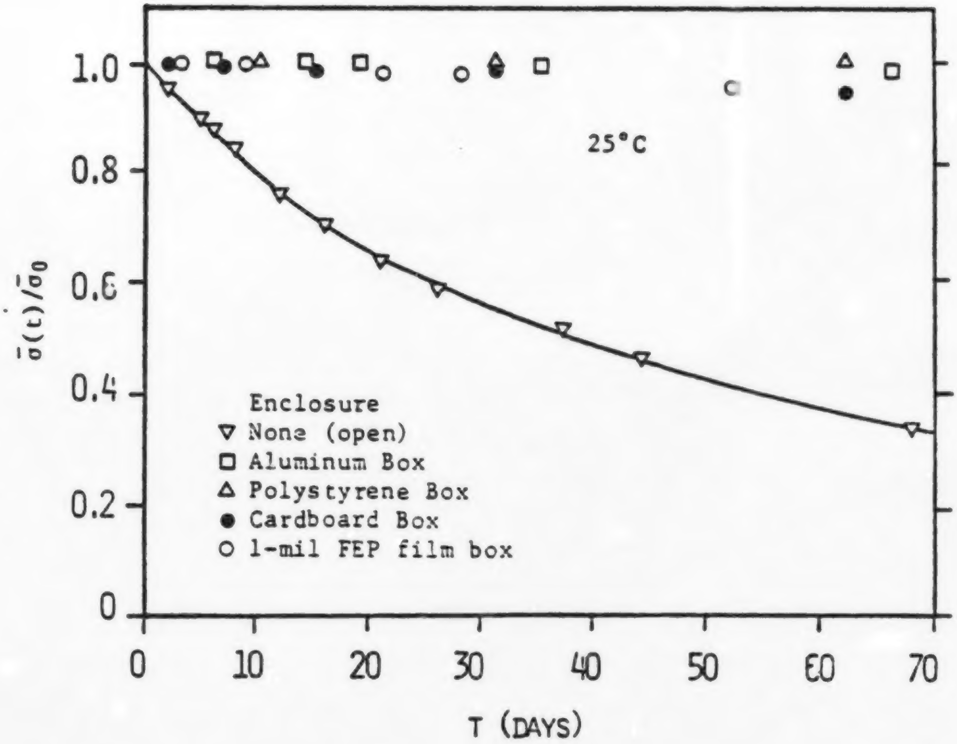

Fig. 4.13. Charge decay at 25°C for corona charged 25 μm, Teflon FEP electrets differently stored (An73).

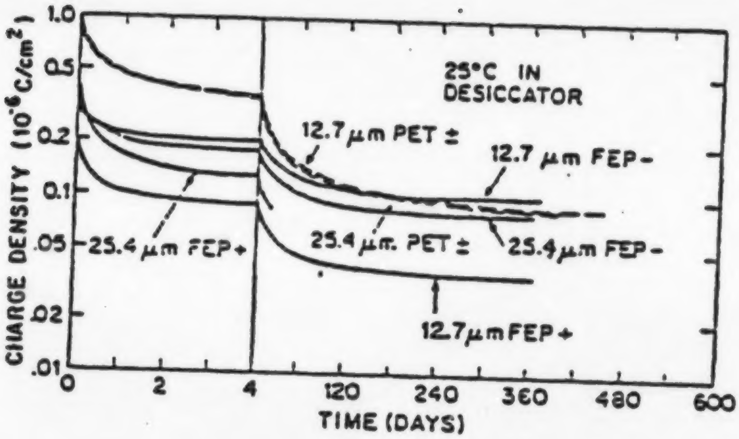

Fig. 4.14. Measured charge density on various polymer foils as function of time after charging. Charging conditions: 30 kV, 90 sec. Foils stored in noncontacting trays in desiccator at 25°C. Curves are smoothed averages of two or more electrets (Se72).

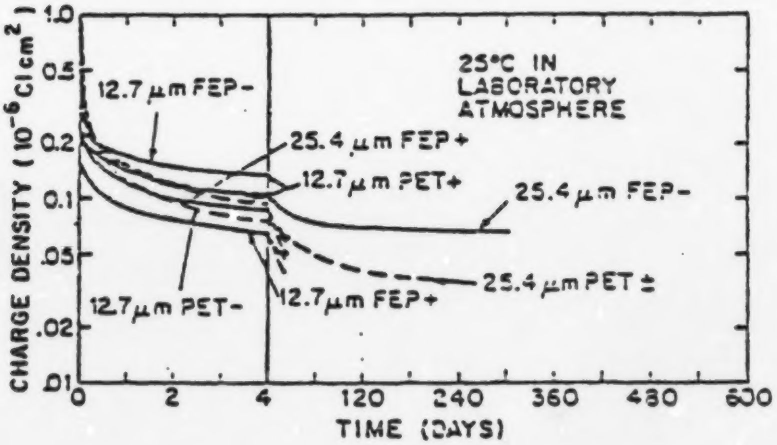

Fig. 4.15. Measured charge density on various polymer foils as function of time after charging. Charging conditions: 30 kV, 90 sec. Foils stored in noncontacting trays in laboratory atmosphere at 25°C. Curves are smoothed averages of two or more electrets (Se72).

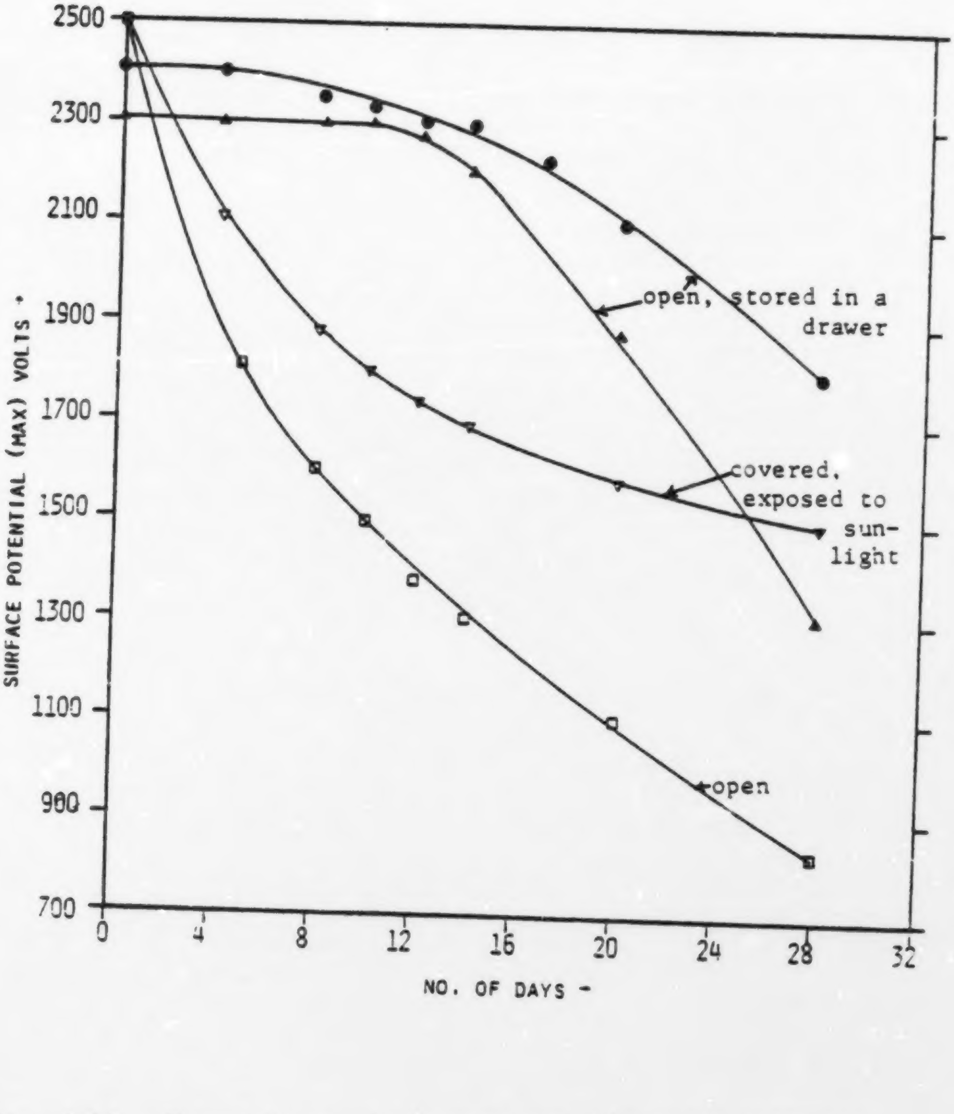

Fig. 4.16. Charge decay of electrets at 25°C under different storage conditions.

5. THERMOPHORETIC COLLECTION OF RADON DAUGHTERS

5.1 Thermophoretic Behaviour of Aerosols

Under the influence of a temperature gradient, aerosol particles drift down the gradient and deposit on cold surfaces. The mechanism of thermophoresis has been studied by relatively few investigators.

In the free molecule range ($d_p \ll \ell$), the thermophoretic velocity can be calculated from the kinetic theory of gases (Wa66):

$$C_t = -\frac{3\nu\nabla T}{4\left(1 + \frac{\pi\alpha}{8}\right)T} \tag{5.1}$$

where ν = kinematic viscosity of the gas

α = accomodation coefficient, usually about 0.9

d_p = particle size

ℓ = mean free path of the gas, about 0.065 μm in air at normal temperature and pressure

C_t = thermophoretic velocity

T = temperature

In the continuum region ($d_p \gg \ell$), the thermophoretic velocity can be obtained by solving the equation of fluid motion with a slip velocity condition (Ep24):

$$C_t = -\frac{2k\sigma}{2k + k_p}\left(\frac{k}{p}\right)\nabla T \tag{5.2}$$

where k = thermal conductivity of the gas

k_p = thermal conductivity of the particle

σ = dimensionless coefficient defined in the relationship between the slip velocity at the particle surface and the temperature gradient in the gas, ∇T:

$$V_{slip} = \sigma \frac{k}{p} \nabla T; \ \sigma \text{ usually taken as } 1/5$$

p = pressure.

In the transition region between the continuum and free molecule ranges ($0.03 < \frac{\ell}{d_p} < 1.25$), the thermophoretic force is given by (Br67):

$$F = -a \frac{d_p^2}{2} \left(\frac{\ell}{d_p} \right) C \nabla t \tag{5.3}$$

where F = thermophoretic force

a = $12\pi\mu Q$

μ = coefficient of viscosity of the gas

Q = thermal creep first order coefficient, $\frac{3}{4} \left(\frac{d_p}{\nabla T} \right)^{1/2}$

$$C = \frac{1}{\left[1 - 6S_m \left(\frac{\ell}{d_p}\right)\right]} \left[\frac{\frac{k}{k_p} - 2S_t \left(\frac{\ell}{d_p}\right)}{1 - 2\frac{k}{k_p} - 4S_t \left(\frac{\ell}{d_p}\right)} \right]$$

S_m = constant related to the reflection coefficient of molecules striking the particle surface

S_t = constant related to the thermal accommodation coefficient.

It should be noted that the thermophoretic velocity, C_t, is independent of particle size in both the continuum and free molecule ranges. However, in the transition region, C_t depends on particle size as seen in Fig. 5.1 (Pr79).

The principle of thermophoresis can be applied to collection of radioactive aerosols such as radon daughter aerosols in a uranium mine. In a diesel operated mine, median diameters of radon daughter aerosols are about 0.1 μm (Bu78). The thermophoretic velocity per unit temperature

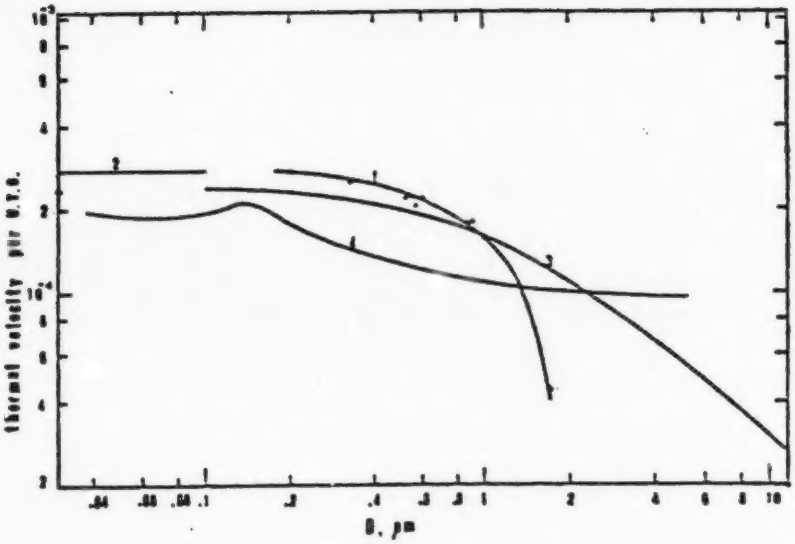

Fig. 5.1. Thermal velocities per unit temperature gradient as a function of particle size (1) Measurements by Prodi (Pr79), (2) Waldman's theory, (3) Brock's theory for thermal conductivity of sodium chloride (0.015 cal/cm sec K), (4) empirical curve presented by Mercer (Me73).

gradient can be estimated from Eq. (5.1) and Eq. (5.2):

$d_p << \ell, \quad C_t/\nabla T = 3.125 \times 10^{-4} \frac{cm^2}{s°C}$

$(\nu = 1.67 \times 10^{-5}\ m^2/s, \quad T = 20°C)$

$d_p >> \ell, \quad C_t/\nabla T = 4.28 \times 10^{-6} \frac{cm^2}{s°C}$

$k_p = 5.02$ W/mK (graphite), $k = 2.34 \times 10^{-2}$ W/mK (air),

$p = 101$ kPa

At $d_p = 0.1$ μm, $\quad C_t/\nabla T = 3.125 \times 10^{-4} \frac{cm^2}{s°C}$ $(k_p = 6.28 \frac{W}{mK}$ (NaCl)) (from Fig. 5.1).

5.2 Experimental

The apparatus is shown schematically in Fig. 5.2. The top and bottom plates are made up of aluminum discs, 8.3 cm in diameter, 0.6 cm thick. The top plate is kept at a high temperature by means of a heating disc and regulated by a temperature controller (YSI Thermistemp model 63RC with YSI 632 probe) capable of maintaining temperature within 5°C of a desired point in the temperature range from -75°C to +260°C. The top plate is protected by a metal cover plate. The bottom plate is cooled by tap water circulation. Temperatures are monitored at the top and bottom plates by means of thermocouples attached to a thermometer (Simpson model 388). The two plates are separated by three spacers equally distributed. The spacing can be adjusted from 1 mm up to a few cm.

The bottom plate is constructed with a depression for an aluminum disc (3.75 cm diameter) which may be removed and counted for gross alpha using a Trimet counter (Model TM372A) fitted with a ZnS scintillator and a photomultiplier tube.

In use, the experimental apparatus is placed in the radon chamber (Bu78) into which zinc oxide aerosols of median diameter $0.03\ \mu m < d_p < 0.07\ \mu m$ are introduced after passage through a Kr-85 neutralizer to remove any pre-existing charge. Instead of zinc oxide, carbon fume can be used as an aerosol. (Zinc oxide was generated by an aerosol generator based on the principle of mixing zinc metal vapour rich air, produced by induction heating of zinc with cool air. Carbon fume was generated by heating the unit to 400°C, at which temperature the insulation material on the unit decomposed to produce a carbon aerosol). After equilibrium is established (about 2 hr), the unit is operated at the chosen temperature gradient (in the range 0-400°C/cm). The temperature gradient can be adjusted by changing either the temperature of the top plate or the spacing between the two plates. The sampling time is 15 min. After 3 min waiting time, the disc is counted for 5 min (a fresh aluminum disc is used for each experiment). Simultaneously, measurements are made of RaA, RaB and RaC using the optimized modified Tsivoglou method (Bu78). A Duraire pump (model PV-200 is used at a constant flowrate of 3 L/min. Sampling is carried out with a Millipore filter (0.8 μm pore size) for five minutes, followed by counting at 2-5, 7-15, 25-30 min. (Prior to the experiment, the background counts due to diffusive deposition are obtained in the absence of a temperature gradient.)

Aerosol concentration is measured by a condensation nuclei counter (Environment One). The aerosol concentration in the chamber varied from 60K - 2M cm^{-3} (Tables 5.1 and 5.2). Diffusion battery measurements were made for the aerosol size distribution. Humidity and temperature inside the chamber are recorded using a hygrometer (YSI model 90). The ambient temperature was about 24°C, and the ambient relative

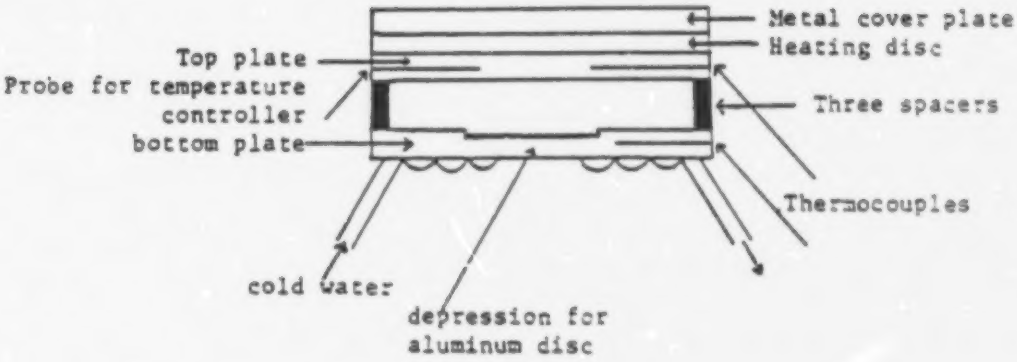
Metal cover plate
Heating disc
Top plate
Probe for temperature controller
bottom plate
Three spacers
Thermocouples
cold water
depression for aluminum disc

Fig. 5.2. Experimental apparatus.

TABLE 5.1

Experimental Results for Thermophoretic Collection of Radon Daughters

(Zinc oxide aerosol, ambient temperature = 24°C, humidity 20 mmHg (R.H. 87%))

Experi-mental run	$\frac{dpm}{\nabla T}$ $\frac{dpm\ cm}{°C}$	∇T Temp. gradient (°C/cm)	Background* counting rate dpm	Average** dpm	Atmospheric concentration (pCi/l.)			VL	Aerosol concen-tration (cm^{-3})	d_p (μm)	Unattached fraction***			$C_t/\nabla T \times 10^6$ $\frac{cm^2}{°C\ sec}$
					RaA	RaB	RaC				RaA	RaB	RaC	
1	1.06	295	204	314	578	131	90	1.6	280K	0.030	0.126	0.035	6.2×10^{-4}	3.02
2	3.69	360	204	1327	1551	335	235	4.2	180K	0.030	0.184	0.057	1.45×10^{-3}	3.98
3	4.76	164	210	781	1281	509	291	5.0	220K	0.034	0.121	0.018	3.2×10^{-5}	4.52
4	4.88	110	210	536	1281	509	291	5.0	100K	0.034	0.232	0.043	8.23×10^{-5}	4.63
5	4.67	227	64	1101	1178	516	310	5.1	60K	0.039	0.277	0.055	1.135×10^{-4}	4.29
6	7.16	236	138	1689	1154	785	586	7.4	160K	0.065	0.049	4.44×10^{-3}	4.63×10^{-6}	4.06
7	8.30	135	138	1120	1595	991	632	9.0	60K	0.065	0.171	0.013	1.52×10^{-5}	4.31

* Background counts due to diffusive deposition (averaged over 5 min counting interval)

** Background counts due to diffusive deposition are subtracted from the total counts and averaged over 5 min counting interval.

*** Unattached fraction is predicted according to the equations in Chapter 2 (eqn. (2.5)-(2.13)).

TABLE 5.2

Experimental Results for Thermophoretic Collection of Radon Daughters

(Carbon fume aerosol, ambient temperature = 24°C, humidity 20 mmHg (R.H. 87%))

Exp. Run	$\frac{\text{dpm}}{\nabla T}$ $\frac{\text{dpm cm}}{°\text{C}}$	∇T Temp. gradient (°C/cm)	Background* counting rate dpm	Average** dpm	Atmospheric concentration (pCi/L) RaA	RaB	RaC	WL	Aerosol concentration (cm^{-3})	d_p (μm)	Unattached fraction*** RaA	RaB	RaC	$C_t/\nabla T \times 10^4$ $\frac{\text{cm}^2}{°\text{C sec}}$
8	0.91	402	71	367	616	131	25	1.39	2M	0.041	0.011	2.60×10^{-3}	3.06×10^{-5}	3.08
9	0.80	402	71	322	427	149	92	1.54	2M	0.059	5.0×10^{-3}	5.96×10^{-4}	1.02×10^{-6}	2.42
10	0.91	402	72	369	701	148	37	1.60	2M	0.059	5.17×10^{-3}	1.16×10^{-3}	8.82×10^{-6}	2.86
11	1.25	402	71	502	448	259	143	2.31	2M	0.059	5.0×10^{-3}	4.79×10^{-4}	6.05×10^{-7}	2.60
12	1.71	402	71	688	578	337	175	2.95	2M	0.041	0.010	9.96×10^{-4}	1.26×10^{-6}	2.79
13	3.74	402	95	1516	2235	539	141	5.56	2M	0.059	5.17×10^{-3}	1.16×10^{-3}	8.82×10^{-6}	3.42
14	6.35	402	239	2551	2154	872	366	8.00	1.8M	0.041	0.011	1.62×10^{-3}	3.53×10^{-6}	3.95
15	8.40	402	174	3404	2091	1321	744	11.60	1.8M	0.056	6.15×10^{-3}	5.47×10^{-4}	6.22×10^{-7}	3.48
16	9.26	402	174	3721	2244	1331	708	11.70	2.1M	0.056	5.28×10^{-3}	5.06×10^{-4}	6.39×10^{-7}	3.52
17	8.91	402	239	3581	2214	1397	852	12.51	2M	0.041	0.010	9.21×10^{-4}	1.05×10^{-6}	3.35
18	9.45	402	174	3800	2002	1450	921	12.81	2M	0.056	5.54×10^{-3}	4.38×10^{-4}	4.24×10^{-7}	3.46

* Background counts due to diffusive deposition (averaged over 5 minute counting interval).

** Background counts due to diffusive deposition are subtracted from the total counts and averaged over 5 min counting interval.

*** Unattached fraction is predicted according to the equations in Chapter 2 (eqn. (2.5)-(2.13)).

humidity about 87% (inside the chamber). The unattached fraction was predicted according to the equations given in Chapter 2 (eqn. (2.5)-(2.13)) and found to be less than 0.3 in all experiments (Tables 5.1 and 5.2).

Comparisons can be made between the average dpm (over 5 min counting period) obtained using thermophoretic collection and working levels obtained by modified Tsivoglou method.

5.3 Theoretical Model

The collection system consists of two plane parallel circular discs of radius a separated by a distance H as shown in Fig. 5.3. Radioactive aerosols enter from all sides and are collected on the bottom plate by thermophoresis. The top plate is held at a constant temperature of T_1 whereas the bottom plate is maintained at T_0.

The equation of continuity for component i in cylindrical coordinates at steady state is given by

$$C_t \frac{\partial n_i}{\partial z} = D_i \left[\frac{1}{r} \frac{\partial}{\partial r} \left(r \frac{\partial n_i}{\partial r} \right) + \frac{\partial^2 n_i}{\partial z^2} \right] - \lambda_i n_i \qquad (5.4)$$

where n_i = concentration of the radioactive aerosols (where $i = 1$ for RaA, $i = 2$ for RaB and $i = 3$ for RaC)

r = radial coordinate

z = axial coordinate

D_i = diffusion coefficient of the radioactive aerosols

λ_i = radioactive decay of the aerosol, $\sec^{-1}$.

Dimensionless variables are defined as:

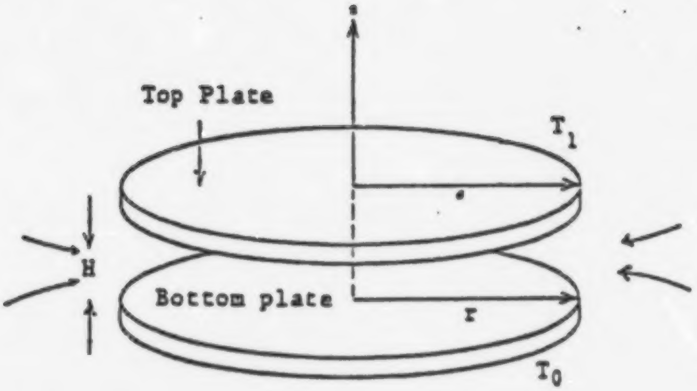
z
Top Plate
T$_1$
a
H
Bottom plate
r
T$_0$

Fig. 5.3. Model for theoretical calculation of thermophoretic collection of radioactive aerosols.

$$n_i^* = \frac{n_i}{n_{i\infty}}$$

$$r^* = \frac{r}{a}$$

$$z^* = \frac{z}{H}$$

(where $n_{i\infty}$ = atmospheric concentration of radioactive aerosols), which, when introduced into eqn. (5.4), results in

$$\frac{\partial n_i^*}{\partial z^*} = \frac{1}{Pe}\left[\frac{1}{r^*}\frac{\partial}{\partial r^*}\left(r^* \frac{\partial n_i^*}{\partial r^*}\right) + \frac{a^2}{H^2}\frac{\partial^2 n_i^*}{\partial z^{*2}}\right] - \frac{1}{\Pi} n_i^* \qquad (5.5)$$

where $Pe = \frac{a^2 C_t}{D_i H} = \frac{\text{thermophoretic collection}}{\text{diffusion}}$

$$\Pi = \frac{C_t}{\lambda_i H} = \frac{\text{thermophoretic collection}}{\text{radioactive decay}}$$

The expected magnitude of the dimensionless groups, Pe and Π can be estimated by inserting $C_t = 0.13$ cm s^{-1} (400°C), $a = 4.1$ cm, $D_i = 6.75 \times 10^{-6}$ cm^2/sec ($d_p = 0.1$ μm), $H = 0.6$ cm and $\lambda_A = 3.79 \times 10^{-3}$ sec^{-1} (for RaA). It is apparent that both Pe and Π are very large (Pe $\sim 5.4 \times 10^5$, $\Pi \sim 60$). Thermophoretic collection is therefore dominant. Equation (5.5) can then be simplified to

$$\frac{\partial n_i^*}{\partial z^*} = 0 \qquad (5.6)$$

or

$$n_i^* = 1 \qquad (5.7)$$

The flux to the disc (detector plate) is mainly due to thermophoresis for $D_i \frac{\partial n_i}{\partial x} \ll 1$ so that

$$J_i = - C_t \, n_i$$

$$= -C_t\, n_{i\infty} \tag{5.8}$$

where J_i = flux of radioactive aerosols to the disc, atoms/cm^{2}sec.

The number of atoms of radioactive aerosol transferred to the disc per unit time, atoms/sec, M_i, is given by

$$M_i = C_t\, n_{i\infty} S = -J_i S \tag{5.9}$$

where S = area of the aluminum collecting disc, cm^2.

The buildup of radioactive aerosols on the disc is then:

$$\frac{dN_i}{dt} = \lambda_{i-1} N_{i-1} + M_i - \lambda_i N_i \tag{5.10}$$

where N_i = number of atoms of radioactive aerosols on the disc surface.

Integration of eqn. (5.10) with t = T yields

$$\overline{N}_1 = \frac{M_1}{\lambda_1}(1 - e^{-\lambda_1 T})$$

$$\overline{N}_2 = M_1\left[\frac{(1 - e^{-\lambda_2 T})}{\lambda_2} - \frac{(e^{-\lambda_2 T} - e^{-\lambda_1 T})}{(\lambda_1 - \lambda_2)}\right] + M_2\left[\frac{(1 - e^{-\lambda_2 T})}{\lambda_2}\right]$$

$$\begin{aligned}\overline{N}_3 = M_1 &\left[\frac{(1 - e^{-\lambda_3 T})}{\lambda_3} - \frac{(e^{-\lambda_2 T} - e^{-\lambda_3 T})}{(\lambda_3 - \lambda_2)} - \frac{\lambda_2(e^{-\lambda_2 T} - e^{-\lambda_3 T})}{(\lambda_3 - \lambda_2)(\lambda_1 - \lambda_2)}\right.\\ &\left. + \frac{\lambda_2(e^{-\lambda_3 T} - e^{-\lambda_1 T})}{(\lambda_1 - \lambda_3)(\lambda_1 - \lambda_2)}\right] + M_2\left[\frac{(1 - e^{-\lambda_3 T})}{\lambda_3} - \frac{(e^{-\lambda_2 T} - e^{-\lambda_3 T})}{(\lambda_3 - \lambda_2)}\right]\\ &+ M_3\left[\frac{(1 - e^{-\lambda_3 T})}{\lambda_3}\right]\end{aligned} \tag{5.11}$$

where T = sampling time, sec

$\overline{N}_i$ = number of atoms of radionuclide at the end of sampling period.

Decay after collection is described by the following equations:

$$N_1 = \bar{N}_1 \, e^{-\lambda_2\theta}$$

$$N_2 = \bar{N}_1 \frac{\lambda_1(e^{-\lambda_2\theta} - e^{-\lambda_1\theta})}{(\lambda_1 - \lambda_2)} + \bar{N}_2 e^{-\lambda_2\theta}$$

$$N_3 = \bar{N}_1 \left[\frac{\lambda_1\lambda_2(e^{-\lambda_2\theta} - e^{-\lambda_3\theta})}{(\lambda_3 - \lambda_2)(\lambda_1 - \lambda_2)} - \frac{\lambda_1\lambda_2(e^{-\lambda_3\theta} - e^{-\lambda_1\theta})}{(\lambda_1 - \lambda_3)(\lambda_1 - \lambda_2)} \right] + \bar{N}_2 \left[\frac{\lambda_2(e^{-\lambda_2\theta} - e^{-\lambda_3\theta})}{(\lambda_3 - \lambda_2)} \right] + \bar{N}_3 \, e^{-\lambda_3\theta} \qquad (5.12)$$

where θ is the time after collection, sec.

The number of alpha particles recorded by the detector per unit time (assuming counting efficiency is the same for RaA and RaC) is given by:

$$C = \eta(\lambda_1 N_1 + \lambda_3 N_3) \qquad (5.13)$$

where η = counting efficiency

C = counts per unit time, counts/sec.

Integration of eqn. (5.13) with respect to θ over the counting interval α to β yields:

$$D = \eta \left\{ \bar{N}_1 \left[-\left(1 + \frac{R_2}{\lambda_1}\right) (e^{-\lambda_1\beta} - e^{-\lambda_1\alpha}) - \frac{R_1}{\lambda_2} (e^{-\lambda_2\beta} - e^{-\lambda_2\alpha}) + \frac{(R_1 + R_2)}{\lambda_3} (e^{-\lambda_3\beta} - e^{-\lambda_3\alpha}) \right] + \bar{N}_2 \left[- \frac{R_3}{\lambda_2} (e^{-\lambda_2\beta} - e^{-\lambda_2\alpha}) + \frac{R_3}{\lambda_3} (e^{-\lambda_3\beta} - e^{-\lambda_3\alpha}) \right] + \bar{N}_3 \left[- (e^{-\lambda_3\beta} - e^{-\lambda_3\alpha}) \right] \right\} \qquad (5.14)$$

where D = counts recorded between the counting interval (α, β)

α = beginning of counting interval, sec

β = end of counting interval, sec

$$R_1 = \frac{\lambda_1\lambda_2\lambda_3}{(\lambda_1 - \lambda_2)(\lambda_3 - \lambda_2)}$$

$$R_2 = \frac{\lambda_1\lambda_2\lambda_3}{(\lambda_1 - \lambda_2)(\lambda_1 - \lambda_3)}$$

$$R_3 = \frac{\lambda_2\lambda_3}{(\lambda_3 - \lambda_2)}$$

The thermophoretic velocity can be obtained by solving eqn. (5.9), (5.11) and (5.14), using experimental data for D and $n_{i\infty}$.

5.4 Theoretical Results

Experimental and theoretical results are tabulated and presented in Tables 5.1 and 5.2.

The thermophoretic velocity is obtained by solving eqn. (5.9), (5.11) and (5.14) using experimental data for counts recorded over the counting interval, D (counting efficiency is 0.423 for all cases) for various concentrations of RaA, RaB and RaC. Average thermal velocities per unit temperature gradients for zinc oxide and carbon fume are compared in Table 5.3 with literature results for sodium chloride.

From the values of $C_t/\nabla T$ in Table 5.3, the conversion factor dpm/($\frac{°C}{cm}$WL) is predicted theoretically for different ratios of RaA:RaB:RaC (pCi/L). The conversion factors at the test experimental conditions (T = 15 min, α = 3 min, β = 8 min, S = 11.04 cm^2) are listed in Table 5.4. Conversion factors at T = 5 min, α = 3 min, β = 8 min, and S = 2.54 cm^2 (experimental conditions for comparison with electrostatic collection) are given in Table 5.5.

5.5 Experimental Results

In order to test the applicability of the principle of thermo-

TABLE 5.3

Thermal Velocities per Unit Temperature Gradient

Aerosol	$C_t/\nabla T$ $\frac{cm^2}{°C\ sec} \times 10^4$	Thermal conductivity $\frac{W}{mK}$
Zinc oxide	4.12	-
Carbon fume	3.14	5.02 (graphite)
Sodium chloride (Fig. 5.1)	3.125	6.28

TABLE 5.4

Conversion Factors (dpm/$\frac{^\circ C}{cm}$ WL) for Thermophoretic Collection

($T = 15$ min, $\alpha = 3$ min, $\beta = 8$ min, $S = 11.04$ cm^2)

RaA:RaB:RaC (pCi/L)	Zinc oxide ($C_t/\nabla T = 4.12 \times 10^{-4}$ cm^2/°C sec)	Carbon fume ($C_t/\nabla T = 3.14 \times 10^{-4}$ cm^2/°C sec)
1 : 1 : 1	0.969	0.738
1 :0.8:0.4	0.834	0.636
1 :0.6:0.4	0.890	0.678
1 :0.4:0.2	0.854	0.651
1 :0.3:0.2	0.903	0.689
1 : 0 : 0	0.978	0.745
Average	0.905	0.690

TABLE 5.5

Conversion Factors (dpm/($\frac{°C}{cm}$ WL) for Thermophoretic Collection

($T = 5$ min, $\alpha = 3$ min, $\beta = 8$ min, $S = 2.54\ cm^2$)

RaA : RaB : RaC (pCi/L)	Zinc oxide ($C_t/\nabla T = 4.12 \times 10^{-4}\ cm^2/°C\ sec$)	Carbon fume ($C_t/\nabla T = 3.14 \times 10^{-4}\ cm^2/°C\ sec$)
1 : 1 : 1	0.083	0.063
1 : 0.8 : 0.4	0.071	0.054
1 : 0.6 : 0.4	0.079	0.060
1 : 0.4 : 0.2	0.079	0.060
1 : 0.3 : 0.2	0.087	0.066
1 : 0 : 0	0.132	0.101
Average	0.089	0.067

phoresis to the collection of radon daughters (on an aluminum disc), experiments were conducted at constant WL (5.0 WL). Zinc oxide aerosols were used. Average alpha disintegrations per minute (over a 5 minute counting period) were obtained at different temperature gradients across the two plates. (Background counts due to diffusive deposition were subtracted from the results (Tables 5.1 and 5.2)). The results of such experiments are presented in Fig. 5.4. The straight lines shown are theoretical predictions using a conversion factor of 0.905 $\frac{\text{dpm}}{(^\circ\text{C/cm WL})}$ (Table 5.4) for zinc oxide. The thermophoretic collection of radon daughter activity is seen to be linear with applied temperature gradient up to 400°C/cm (Fig. 5.4).

Since the maximum temperature gradient that can be achieved is about 400°C/cm, further experiments were performed at this temperature gradient. In order to apply the principle of thermophoretic collection to radon daughters, linearity of collected radon daughter activity with working levels is required so that a constant conversion factor can be applied to all conditions. Figure 5.5 shows the results of such experiments. The straight lines shown are theoretical predictions using the conversion factor of 0.69 $\frac{\text{dpm}}{(^\circ\text{C/cm WL})}$ for carbon fume in Table 5.4. Linearity is observed up to 12.8 WL.

The results of all experimental data can be plotted in one single figure (Fig. 5.6). The straight lines shown are theoretical predictions using conversion factors of 0.905 $\frac{\text{dpm}}{(^\circ\text{C/cm WL})}$ and 0.69 $\frac{\text{dpm}}{(^\circ\text{C/cm WL})}$ for zinc oxide and carbon fume respectively.

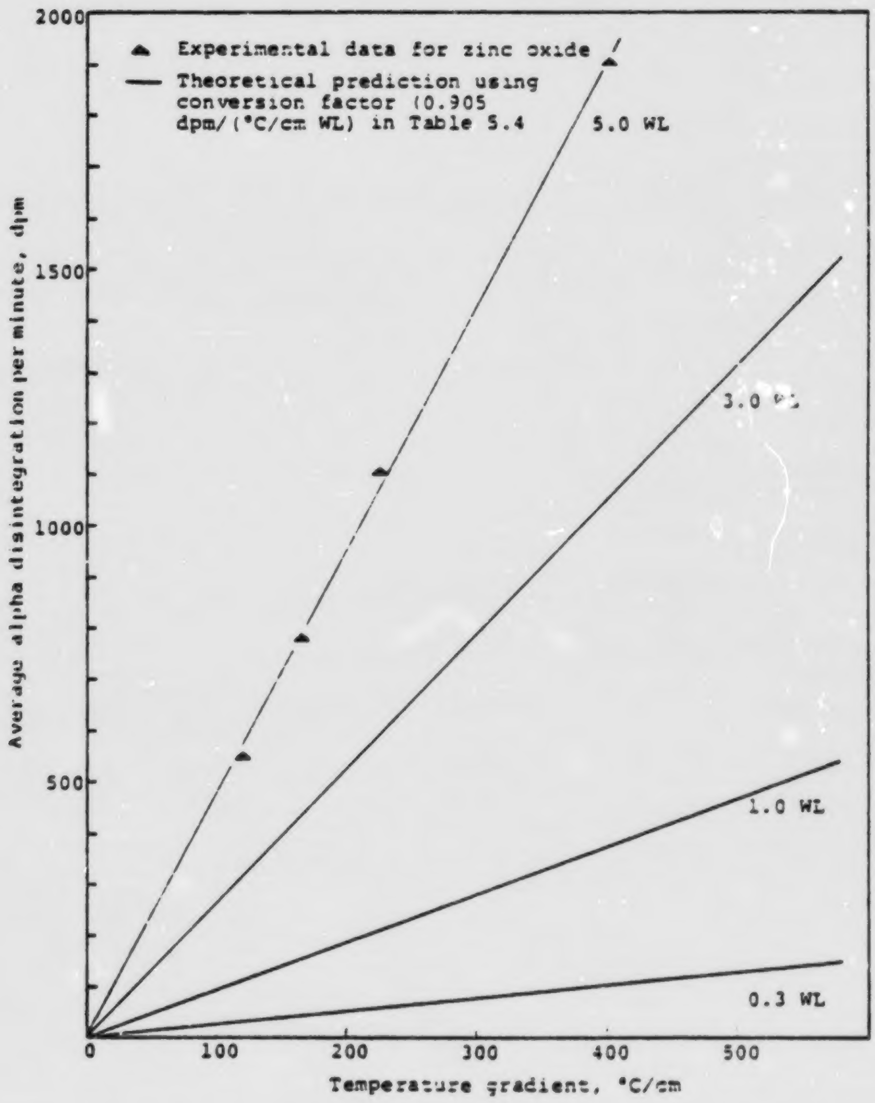

Fig. 5.4. Average alpha disintegrations per minute (over 5 min counting period) against temperature gradient across the two plates ($T = 15$ min, $\alpha = 3$ min, $\beta = 8$ min, $S = 11.04$ cm^2, relative humidity 87% at 24°C) at constant WL.

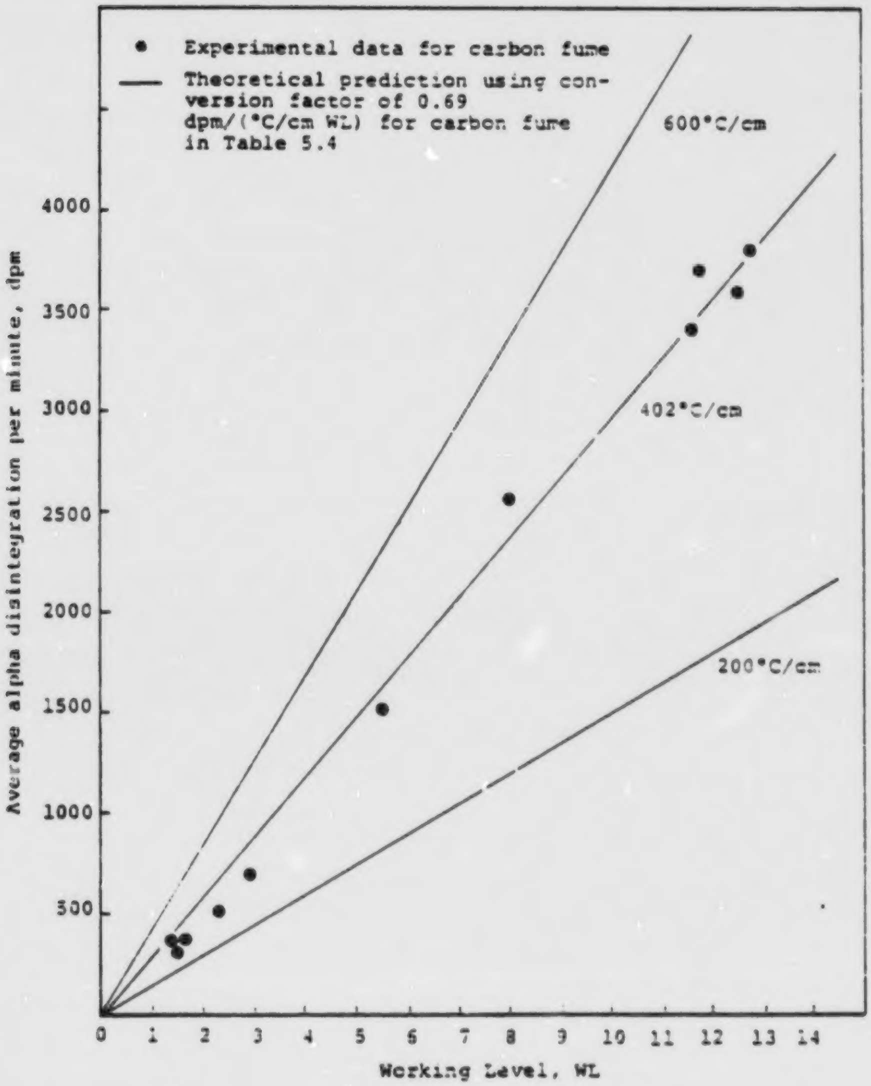

Fig. 5.5. Average alpha disintegrations per minute (over 5 min counting period) against WL at constant temperature gradient across the plates (T = 15 min, α = 3 min, β = 8 min, S = 11.04 cm^2, relative humidity = 87% at 24°C).

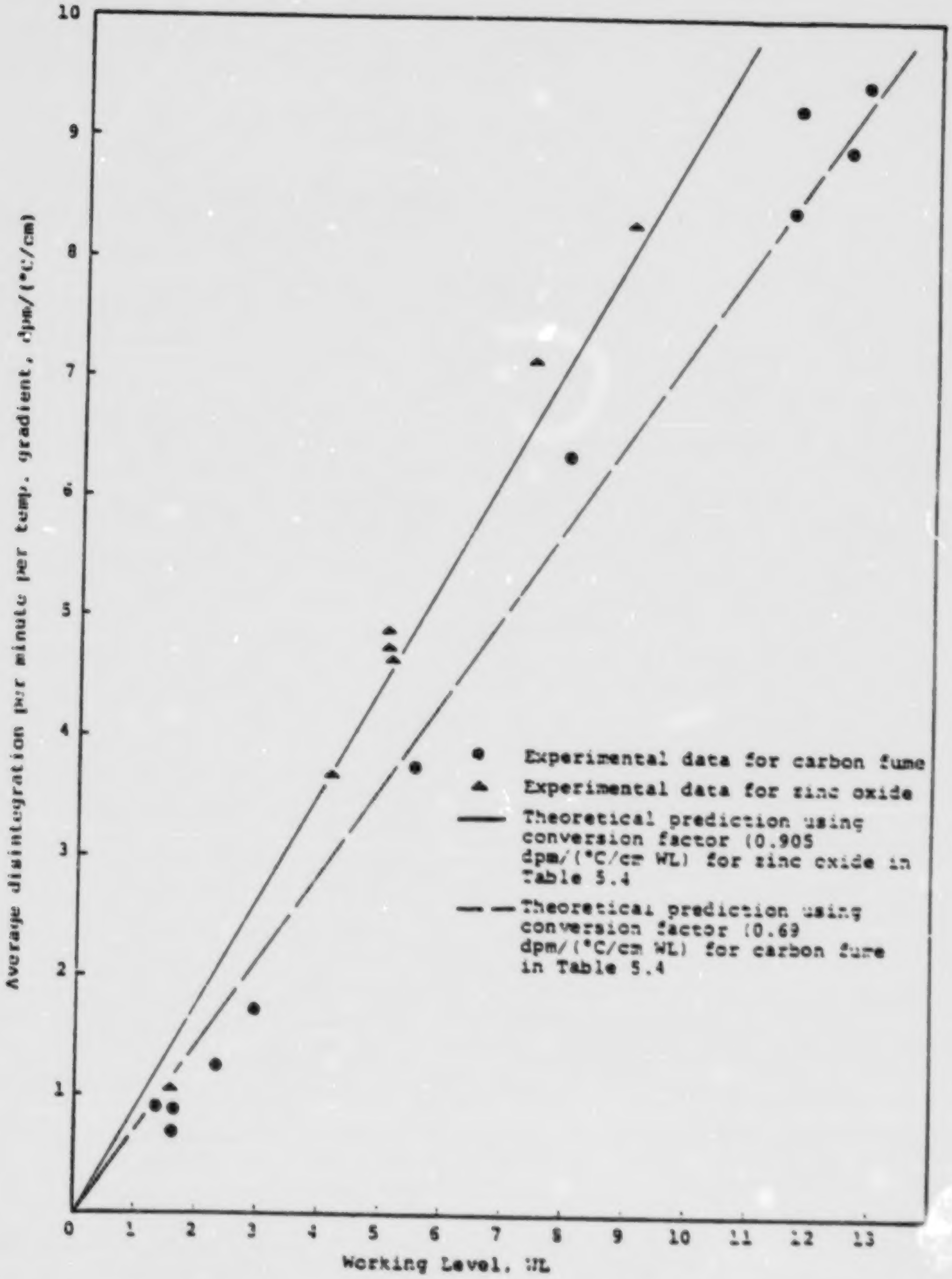

Fig. 5.6. Conversion factors for thermophoretic collection (T = 15 min, α = 3 min, β = 8 min, S = 11.04 cm^2, relative humidity = 87% at 24°C).

5.6 Comparison Between the Driving Forces: Thermophoretic, Collection via a Pump, and Electrostatic

In order to compare collection of radon daughters by thermophoresis with collection by means of a pump, comparison may be made with the experimental data for collection by a pump (refer to Section 6.3) (an open face filter-pump assembly is used; Duraire pump model PV-2000). After a sampling time of five minutes, the filter is removed and counting started 3 minutes after sampling. The filter is counted for five minutes. Typical concentration ratios of RaA, RaB and RaC (pCi/L) are 100:60:40. (Experimental data are taken from Fig. 6.2 using data points for a radon daughter concentration of 4.5 WL. By assuming a linearity of dpm per unit flowrate with working level, a conversion factor of 833 $\frac{\text{dpm}}{\text{L/min WL}}$ is obtained.)

Thermophoretic collection is predicted theoretically using the conversion factor of 0.079 $\frac{\text{dpm}}{(°\text{C/cm WL})}$ for zinc oxide at a RaA, RaB and RaC concentration ratio of 100:60:40 in Table 5.5 (reduced to the same experimental condition as for the collection of a pump, i.e., $T = 5$ min, $a = 3$ min, $\delta = 8$ min, $S = 2.54$ cm^2). Such a comparison is made in Fig. 5.7. At 0.05 L/min (normal operating flow rate of the CEA dosimeter used in the mine), the corresponding temperature gradients are about 527°C/cm.

Further comparisons are made between thermophoretic and electrostatic collection. For electrostatic collection, experimental conditions are given in Section 6.3. (Experimental data for electrostatic collection are taken from Fig. 6.1 using data points for a radon daughter concentration of 4.5 WL. By assuming a linearity of average disintegration per minute per unit applied voltage with working level, a conversion factor of 0.31 $\frac{\text{dpm}}{\text{V WL}}$ is obtained.) Theoretical prediction is

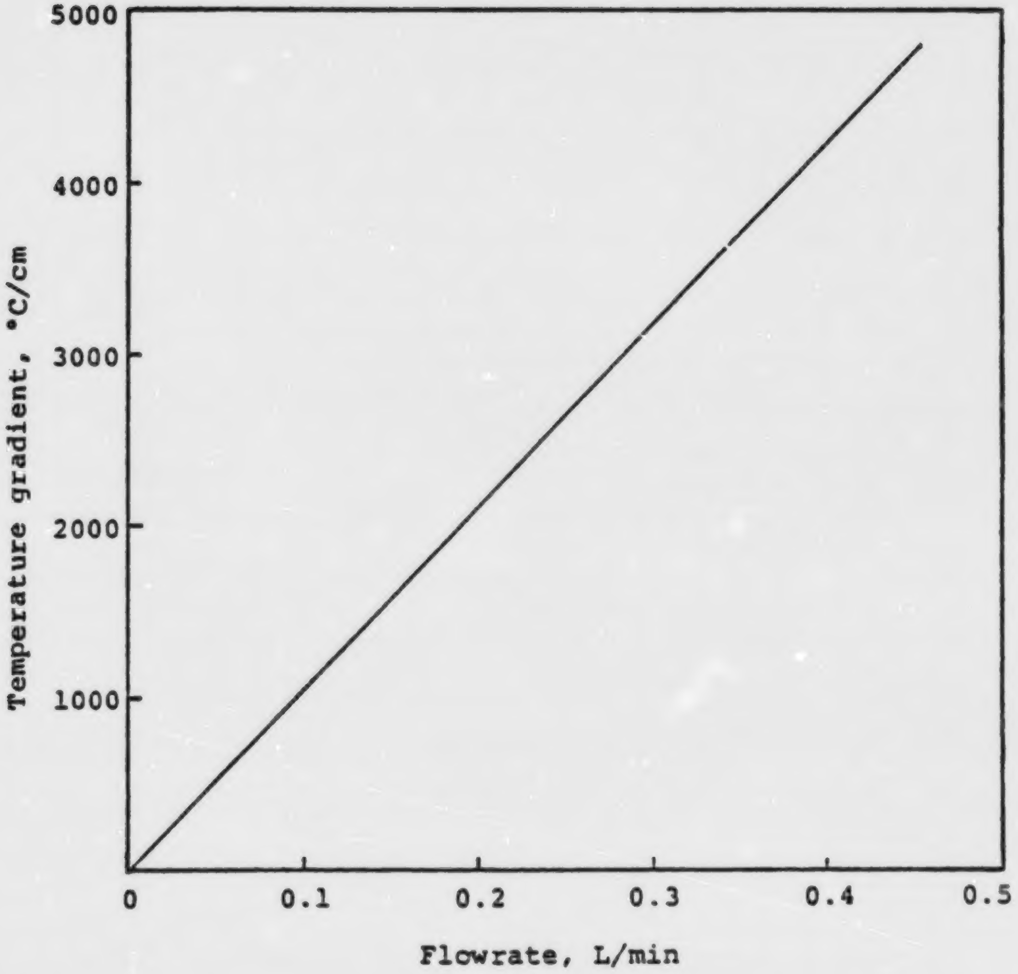

Fig. 5.7. Comparison between thermophoretic collection and collection by means of a pump for identical average dpm and Working Level (T = 5 min, α = 3 min, β = 8 min, S = 2.54 cm^2). [Data for collection by means of a pump are taken from Fig. 6.2 using data points for a radon daughter concentration of 4.5 WL. Thermophoretic collection is predicted theoretically using the conversion factor of 0.079 (dpm/°C/cm WL) from Table 5.5.]

made for thermophoretic collection using a conversion factor of 0.079 $\frac{\text{dpm}}{°\text{C/cm WL}}$ for zinc oxide (Table 5.5). These comparisons are given in Fig. 5.8. At -1000 V, a satisfactory working applied voltage for electrostatic collection, the corresponding temperature gradients are about 3920°C/cm. (It should be noted that, for these comparisons, the thermophoretic and electrostatic collection, and collection via a pump are operated in the open condition, i.e. no protection is provided against the effects of wind velocity in the mine environment).

5.7 Discussion

The temperature gradient can be varied by changing either the temperature of the top plate, or the spacing between the two plates. However, resistance to air flow increases significantly with decrease in the spacing between the two plates. At 0.3 cm, the resistance to flow greatly influences the thermophoretic collection. It is therefore desirable that the spacing between the two plates should not be less than 0.5 cm. Because of this constraint, the maximum achievable temperature gradient is only about 400°C/cm.

From Table 5.3, it can be seen that thermal velocities per unit temperature gradient for zinc oxide and carbon fume are close to the values predicted theoretically by Waldman (eqn. (5.1)) (3.125 x 10^{-} cm^2/°C sec). From the theory, the thermal velocities per unit temperature gradient, $C_t/\nabla T$, do not depend on the physical properties of the aerosol. Although zinc oxide has a higher thermal velocity per unit temperature gradient than carbon fume (Table 5.3), both carbon fume and sodium chloride have the same $C_t/\nabla T$. It is interesting to note that for

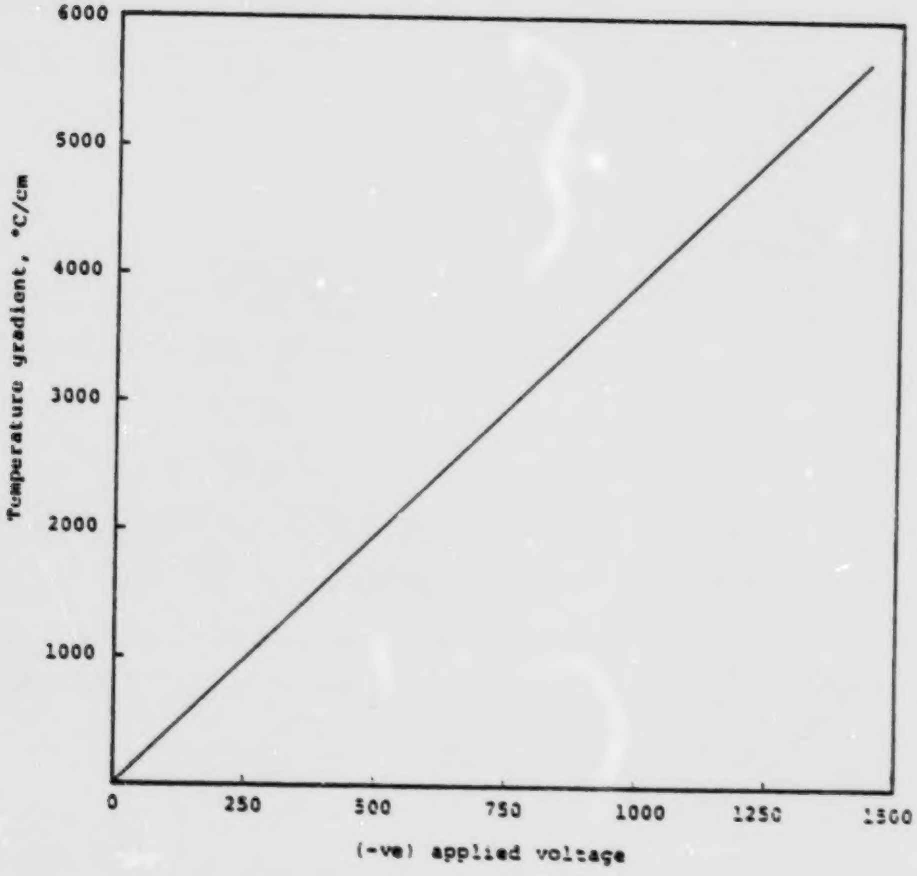

Fig. 5.8. Comparison between thermophoretic collection and electrostatic collection for identical average dpm and Working Level (T = 5 min, α = 3 min, β = 8 min, S = 2.54 cm^2). [Data for electrostatic collection are taken from Fig. 6.1 using data points for a radon daughter concentration of 4.5 WL. Thermophoretic collection is predicted theoretically using the conversion factor of 0.079 dpm/°C/cm WL (Table 5.5).]

carbon fume and sodium chloride, the thermal conductivities are very close (5.02 W/mK for graphite and 6.28 W/mK for sodium chloride).

If the temperature of the top plate can be controlled more precisely, the present technique provides a convenient means of obtaining values for $C_t/\nabla t$. (In the work of Prodi (Pr79), an electron microscope is used to detect the number of the deposited particles on the mica sheet.)

From Table 5.4 and 5.5, conversion factors for the thermophoretic collection depend slightly on the equilibrium ratios of RaA, RaB and RaC. A 1:1:1 concentration ratio of RaA, RaB and RaC (pCi/L) corresponds to equilibrium, whereas 1:0:0 corresponds to very "young" air. Concentration ratios of RaA, RaB and RaC are typically 1:0.6:0.4 in uranium mines. In thermophoretic collection, the concentration ratios of RaA, RaB and RaC vary considerably. Average conversion factors are therefore used in the theoretical predictions (Fig. 5.4, 5.5 and 5.6).

The thermophoretically collected radon daughter activity is linear with temperature gradient at constant WL (5.0 WL) (Fig. 5.4), and with WL at constant temperature gradient (402°C/cm) (Fig. 5.5), thus confirming the theory of thermophoresis as applied to the collection of radon daughters. A constant conversion factor is obtained for different aerosols (Fig. 5.6). Scattering of experimental data about the theoretical lines is primarily due to the following:

1. As mentioned above, conversion factors depend slightly upon concentration ratios of RaA, RaB and RaC. During the experiments, concentration ratios of RaA, RaB and RaC varied considerably. The theoretical lines are obtained by using average conversion factors from Table 5.4.

2. The sampling period varies within 30 sec.

3. The temperature gradient fluctuates about 10°C/cm.

However, if the concentration ratios of RaA, RaB and RaC (pCi/L) do not vary significantly in the mine, a constant conversion factor may be used for thermophoretic collection.

From the comparison between thermophoretic collection and collection by a pump (Fig. 5.7), it can be seen that at the normal operating flowrate of the CEA dosimeter in the mine (0.05 L/min), the corresponding thermophoretic temperature gradient is 520°C/cm. At 0.01-0.03 WL (typical of a uranium mine), the corresponding temperature gradient is expected to be lower than 527°C/cm. A temperature gradient of 400°C/cm is adequate for a personal radon daughter dosimeter in the mine. However in order to provide a sufficient barrier against the effects of wind velocity, the whole dosimeter should be enclosed by a protective screen. Thus the efficiency of the dosimeter is greatly reduced. In order to compensate for the loss of efficiency, a five to ten times increase in the temperature gradient is required, thus bringing the required temperature gradient to about 2000-4000°C/cm.

However, thermophoretic collection cannot be used for grab sampling. At a flowrate of 3 L/min (commonly used for grab sampling), a very high temperature gradient >10,000°C/cm, has to be applied to provide the same performance (same dpm) as that of the pump. Such a high temperature gradient is almost impossible to achieve.

In Fig. 5.8, thermophoretic collection is compared with electrostatic collection. For electrostatic collection, -1000 V can easily be achieved by an electret. The corresponding temperature gradients are around 4000°C/cm, which cannot easily be achieved.

The principle of thermophoresis works satisfactorily for the collection of radon daughters. However, incorporation of such a principle into a passive personal radon daughter dosimeter poses several design problems. A high temperature gradient around 2000-4000°C/cm has to set up across the two plates. A constant temperature gradient across the two plates may not be practical in the mine atmosphere due to difficulty in controlling the temperatures of both the 'hot' and 'cold' plates. Further work has to be undertaken on the design of a practical dosimeter.

5.8 Conclusions

Thermal velocities per unit temperature gradient are obtained experimentally for zinc oxide and carbon fume ($C_t/\nabla T = 4.12 \times 10^{-4} \frac{cm^2}{sec°C}$ for zinc oxide; $C_t/\nabla T = 3.14 \times 10^{-4} \frac{cm^2}{sec°C}$ for carbon fumes). Values for $C_t/\nabla T$ are close to those predicted theoretically ($C_t/\nabla T = 3.125 \times 10^{-4}$ $cm^2/sec°C$).

A constant conversion factor for thermophoretic collection ($\frac{dpm}{°C\ WL}$) can be used in all conditions provided that the concentration ratios of RaA, RaB and RaC (pCi/L) do not vary significantly.

An applied temperature gradient of about 400°C/cm is adequate for a personal radon daughter dosimeter in order for it to perform comparably with the CEA dosimeter (0.05 L/min). However in order to compensate for the loss of efficiency due to wind protection, a temperature gradient around 2000-4000°C/cm is required. The achievement and maintenance of this required temperature gradient in a working dosimeter constitutes a design challenge.

6. PROPOSED PASSIVE RADON DAUGHTER DOSIMETRY BY ELECTROSTATIC DIFFUSION

The need for a passive radon daughter dosimeter arises from the fact that pumps in active dosimeters have proved to be unreliable and to require considerable and costly maintenance. Passive dosimeters designed to date for monitoring radon daughter exposures have proved to be inherently inaccurate as described earlier. The major deficiencies of previous designs and possible remedies are discussed below.

6.1 Previous Designs of Passive Dosimeters

Existing passive dosimeter designs are sensitive to wind because of their open configuration, and have low sensitivity because of their reliance upon ordinary diffusion for collection of the radon daughters. Rose and Perkins (Ro82) have pointed out the importance of the often ignored effect of wind velocity (sometimes referred to as 'face velocity') in passive dosimeter design. Diffusion alone cannot match the sensitivity offered by pumps in active dosimeters.

'Face velocity' effects are important in areas such as mine tunnels in which high ventilation rates are adopted. The exposure recorded by an open face passive dosimeter in such conditions is dominated by and is roughly proportional to the radon daughter flux (product of concentration and face velocity) and is thus not independent of ventilation rate. The problem can be remedied by use of a diffusion barrier to isolate the external air flow from the detector, thereby ensuring stagnant conditions in the proximity of the detector (aerosol collector). Such a diffusion barrier is easily provided in passive dosimeters for organic vapours by use of a selective permeation membrane which passes the organic vapour but does not transmit bulk airflow. However, for collection of aerosols, such a membrane does not exist. An alternative solution is to surround the dosimeter with an external shield. Such a shield, however, may reduce the sensitivity of a diffusion-based dosimeter to an unacceptable level. In order to make the shield workable, the movement of aerosols must be facilitated by an external force, for example, a thermophoretic, electrostatic, gravitational, inertial, diffusiophoretic, sonic or photophoretic force. For small particles (∿0.1 μm) such as found in mine atmospheres, thermophoretic (movement of aerosols down a temperature gradient) or electrostatic (movement of aerosols across a potential gradient) forces appear to be most suitable. A device such as a semi-permanently charged 'electret' can be incorporated into a passive dosimeter to facilitate diffusion of aerosols electrostatically.

6.2 Theoretical Considerations

For theoretical assessment of the feasibility of the collection of aerosols by means of an external force such as an electric field, the basic laws governing the motion of aerosols must be applied.

The motion of particles towards a collecting surface is always opposed by the frictional drag exerted by the gas on the particles. The friction coefficient, f, is given by the equation (Fr77)

$$f = \frac{3\pi\mu d}{c_p} \qquad (6.1)$$

where $$c_p = 1 + \frac{2\ell}{d}\,(1.257 + 0.4\,e^{-0.55\,d/\ell}) \qquad (6.2)$$

In the above relations, μ = viscosity of the gas, d = particle diameter and ℓ = mean free path of the gas.

Equation (6.1) is valid for the entire range of values of d from the continuum ($d \gg \ell$) to the free molecule range ($d \ll \ell$).

If a balance exists between the external force field and the drag on the particle, the migration velocity of the particle is given by:

$$v = \frac{F}{f} \tag{6.3}$$

where v is the migration (or drift) velocity in the external force field, F is the force and f is the friction coefficient given by eqn. (6.1).

The electrostatic force F_e on an aerosol, a fraction of f_1 of which is charged, is given by

$$F_e = f_1 F_c + (1 - f_1) F_p \tag{6.4}$$

where F_c is the coulombic force on charged aerosols given by eqn. (3.1) and F_p is the polarization force on neutral particles given by eqn. (3.9) and eqn. (3.10) for dielectric and conducting particles respectively. The electrostatic drift velocity is then given by F_e/f. On multiplying the electrostatic drift velocity v_e $(\frac{cm}{s})$ by the cross-sectional deposition area, A (cm^2) of the charged surface, an electrostatic flow rate $Q_e = v_e A$ (cm^3 s^{-1}) is obtained which can be interpreted as the electrostatic analogue of the pump flow rate in active dosimeters.

One possible concern about the use of electrets for radon daughter aerosol collection is the possibility of positively charged alphas being trapped on a negatively charged electret surface. This concern can be checked by simple calculation.

The minimum alpha energy of radon/thoron daughters of interest is that of RaA, i.e. 6 MeV = 9.6×10^{-13} J per alpha. The energy corresponding to 3000 V on the surface of an electret is 4.8×10^{-16} J per negative charge. The energy of each RaA alpha particle is thus 2000 times greater than that of a negative charge corresponding to a surface potential of 3000 V, which is about the maximum potential that can be retained on the surface of an electret. The radon daughter alphas should therefore be able to escape the electric field due to the electret and reach the detector unhindered.

6.3 Experimental Considerations

For preliminary experimental investigations of the behaviour of radon daughter aerosols in an electric field, an open face aluminum disc electrode (1.8 cm) dia with a Teflon guard ring was used. A high voltage cable connector at the back of the electrode holder was connected to a high voltage power supply. The experiments were carried out inside a radon chamber in which zinc oxide aerosols were introduced from an aerosol generator located on top of the chamber (Bu78). The aerosols entered the chamber after passing through a KR-85 source in order to neutralize any charges on them. The aerosol concentrations could be varied from 0-300,000 cm^{-3}. The count median diameter of the aerosols generated was from 0.02-0.08 μm which is similar to the size of aerosols in Canadian uranium mines (Bu78).

For preliminary experiments a negative voltage of 250-1750 V was applied to the aluminum electrode. For ease of counting the electrostatically collected activity, 0.75 mm thick, 1.8 cm dia aluminum discs were employed. For each experimental point a fresh aluminum disc was placed on the aluminum electrode, the desired voltage was applied and, after a sampling time of 5 minutes, the high voltage was switched off. The disc was then carefully transferred to a Trimet ZnS alpha counter (Trimet Instruments Ltd., Model 372A) sample holder and counting commenced at three minutes after the voltage was switched off. The results of three different sets of such experiments are presented in Fig. 6.1. The straight lines shown are least square fits to the data for each experiment. In an additional experiment, an open face filter mounted on a CEA dosimeter (Ch78) pump-filter assembly (0.067 L/min flow rate) was three times sampled and counted in exactly the same manner as the aluminum discs. The average of the three results is also shown in Fig. 6.1. The purpose of this experiment was to compare the driving force of the dosimeter pump with the electrostatic driving force for the collection of radon daughters.

For verifying the results obtained by using the Trimet counter, a silicon surface barrier detector (ORTEC) and a multichannel analyzer (Canberra) was used as an alpha spectrometer. The surface barrier detector was placed on top of the aluminum disc after five minutes exposure in the radon chamber with the desired applied voltage, and counting was started after three minutes. Results of this experiment confirmed that the electrostatically collected radon daughter activity is linear with applied voltage up to -1750 V, which was the maximum voltage applied.

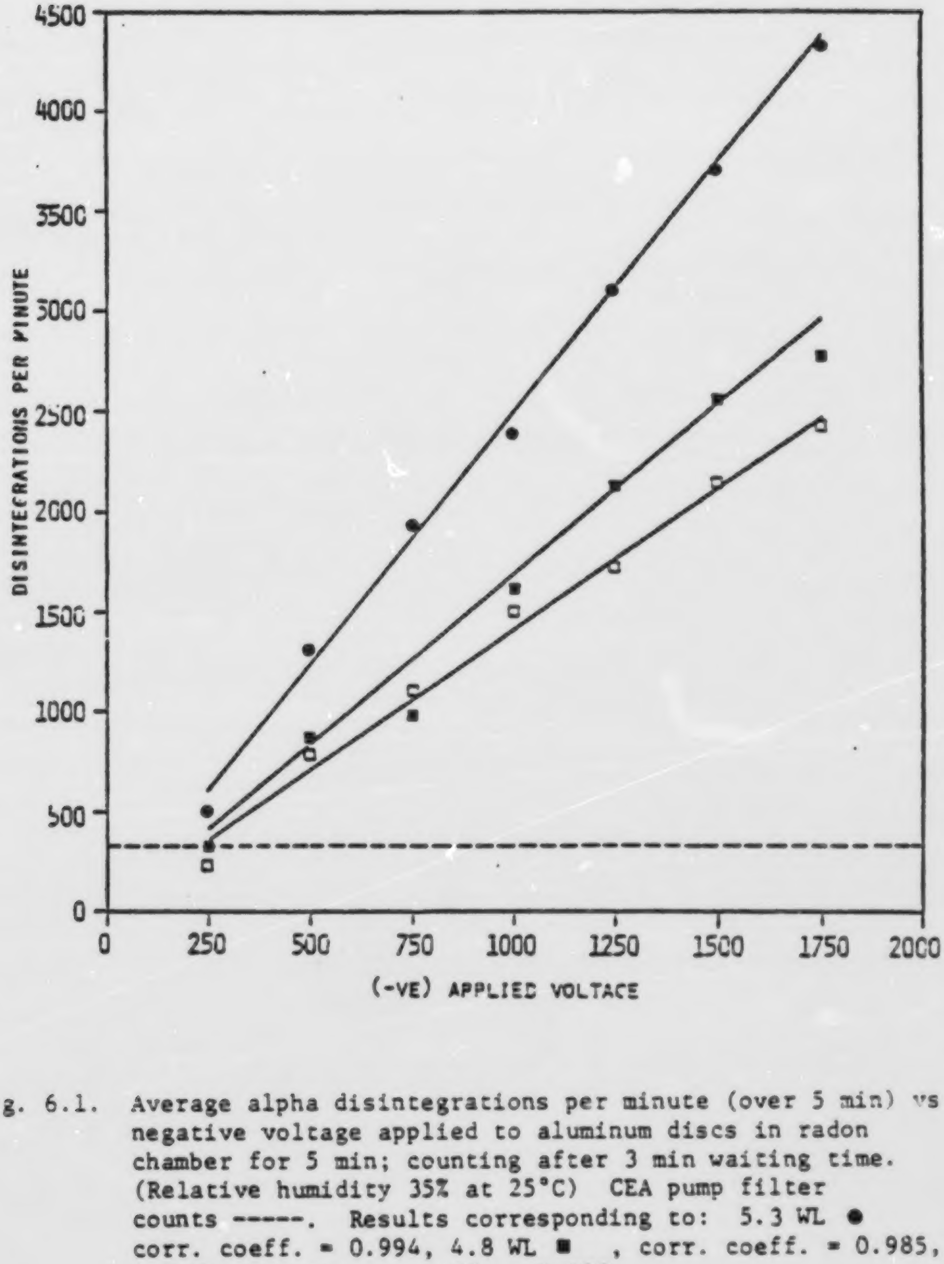

Fig. 6.1. Average alpha disintegrations per minute (over 5 min) vs negative voltage applied to aluminum discs in radon chamber for 5 min; counting after 3 min waiting time. (Relative humidity 35% at 25°C) CEA pump filter counts -----. Results corresponding to: 5.3 WL ● corr. coeff. = 0.994, 4.8 WL ■ , corr. coeff. = 0.985, 4.5 WL □ , corr. coeff. = 0.988.

In order to compare the collection of radon daughters by electrostatic force with collection by a pump, experiments were performed with filter sampling at different flow rates. A Duraire pump (model PV-200) was used in conjunction with a pre-calibrated flowmeter. Two different levels of radon daughter concentrations (WLs) were used with flow rates ranging from 0.5 L/min to 2 L/min. Results of these experiments are shown in Fig. 6.2. Direct comparison between applied voltage and flow rates for equal counts (dpm) for one of these working levels is made in Fig. 6.3.

It was important to confirm that electrets and aluminum discs behave in a similar manner with respect to electrostatic deposition of aerosols. Therefore, electrets of different surface potentials were prepared by the method described in Chapter 7, and exposed in the radon chamber for a 1000 sec period. Simultaneous sampling and counting was carried out by using a silicon surface barrier detector held 6 mm above the electret. Three sets of measurements were obtained using electrets of different surface potentials mounted on aluminum discs (1.8 cm dia) and results were compared with a set of measurements based on aluminum discs with similar applied potentials. Results are presented in Fig. 6.4.

Experiments were then carried out to observe the behaviour of aerosol deposition with a cylindrical barrier held above the open face aluminum disc. The arrangement is shown in Fig. 6.4a. These experiments were performed in order to determine the decrease in electrostatic deposition in the presence of the shield. Deposition in the presence of the shield was found to decrease by a large factor. The ratio of counts with the cylindrical shield located 6 mm above the disc to open face counts for

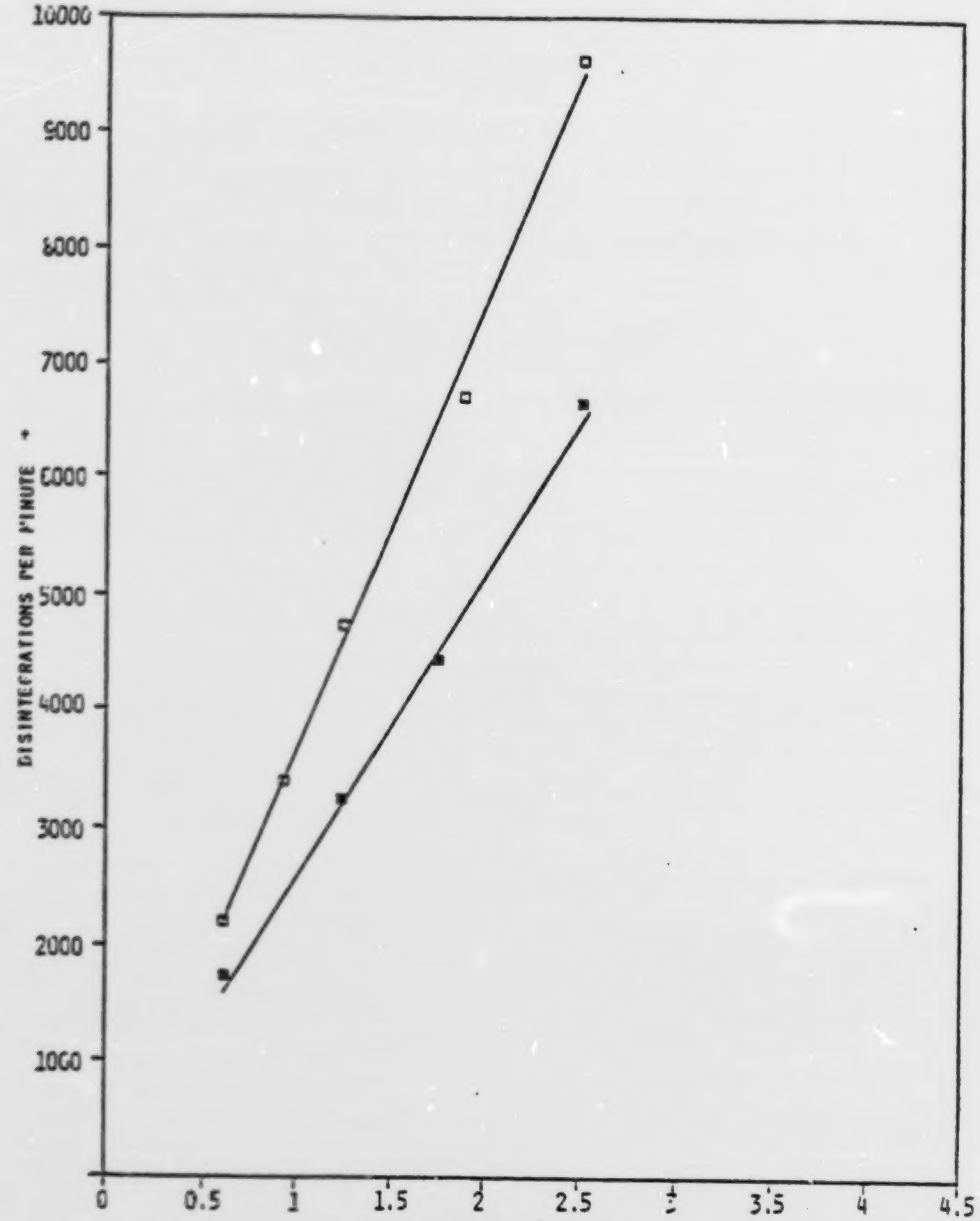

Fig. 6.2. Average alpha disintegrations per minute (over 5 min) vs flowrate for an open-face filter pump assembly. (Relative humidity 35% at 25°C). Results corresponding to:

4.5 WL □ corr. coeff. = 0.098
3.8 WL ■ Corr. coeff. = 0.991

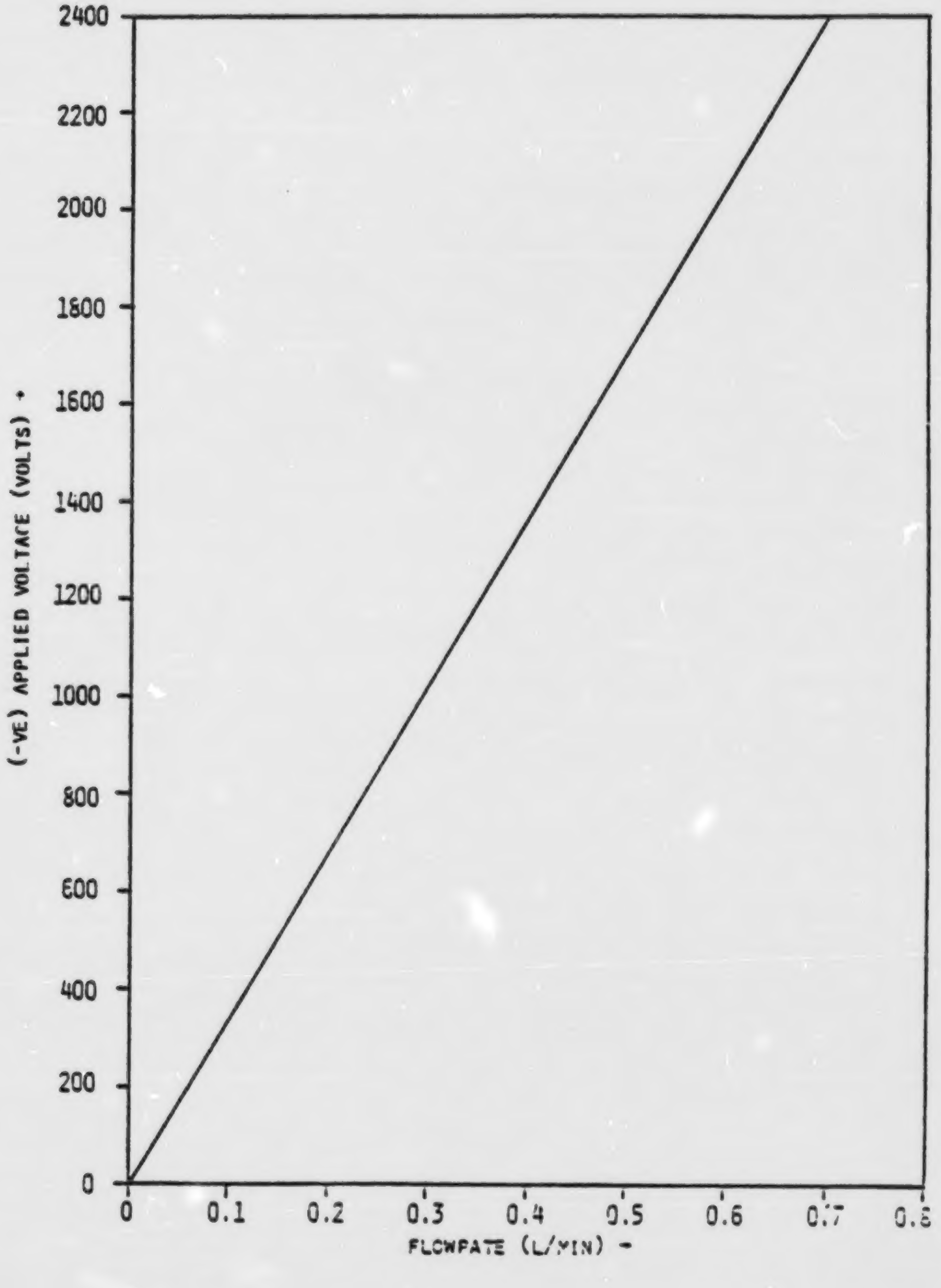

Fig. 6.3. Voltage applied to aluminum discs vs. flowrate of a pump for filter sampling, for identical dpm (averaged over 5 min of counting with 3 min delay after 5 min sampling) for a radon daughter concentration of 4.5 WL as deduced from Fig. 6.1 and Fig. 6.2.

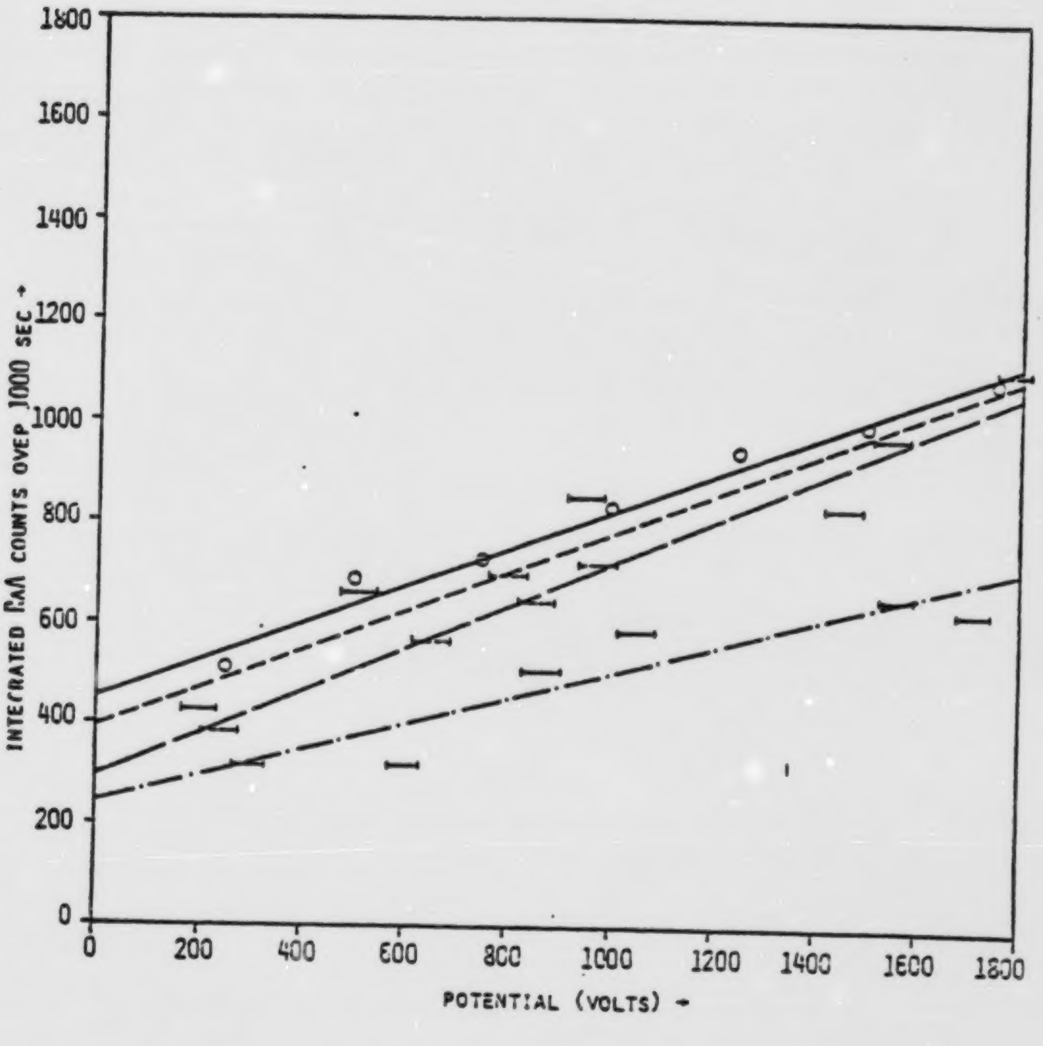

Fig. 6.4. Integrated 1000 sec RaA counts from α-spec. vs negative surface potential in case of electrets and applied potential in case of aluminum discs. Simultaneous sampling and counting (R.H. 35%, temp. 25°C). The non-uniformity of electret surface potential is represented by horizontal bar.

Electret data: Expt. 1 ⊢ - - ⊣ , 4.3 WL — — corr. coeff. = 0.875
Expt. 2 ⊢——⊣ , 3.5 WL —·— corr. coeff. = 0.856
Expt. 3 ⊢·····⊣ , 4.8 WL - - - - corr. coeff. = 0.957
Aluminum disc data ○ 5 WL —— corr. coeff. = 0.983

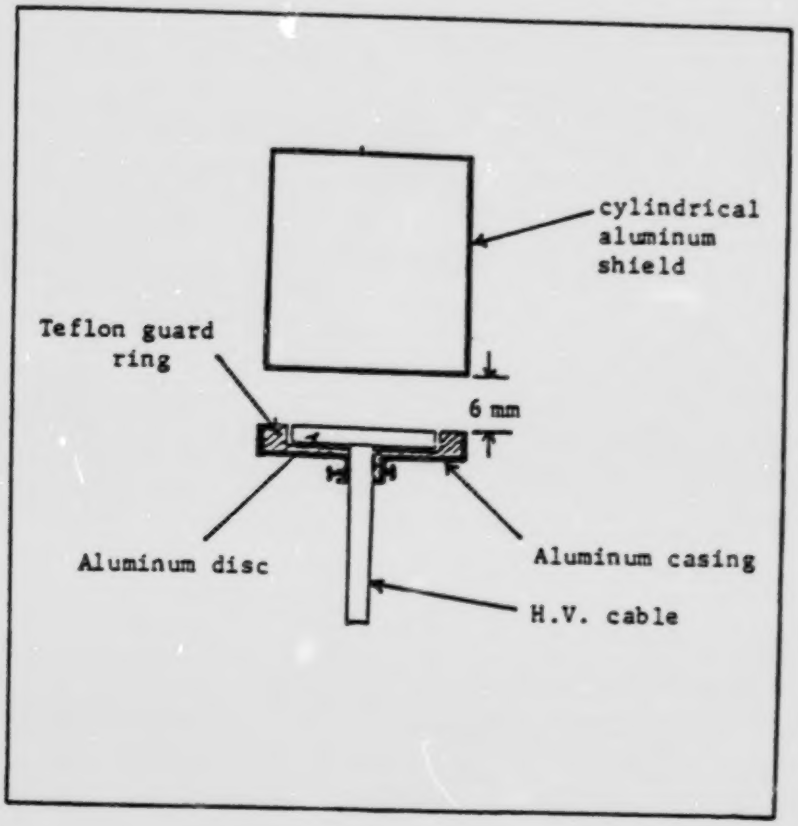
cylindrical aluminum shield
Teflon guard ring
6 mm
Aluminum disc
Aluminum casing
H.V. cable

Fig. 6.4a. The shielded configuration for the aluminum disc electrode. The cylindrical shield and the disc electrode are held by means of clamps at the specified distance apart.

negative applied voltages ranging from 500 to 2500 V is presented in Fig. 6.5. In the same experiment, shielded, electrically charged aluminum discs were counted in a similar manner with negative applied voltages ranging from 500-2500 V, and the metallic cylindrical barrier located 6 mm from a disc. In order to compare electrostatic deposition under these conditions with deposition in an active dosimeter, a CEA dosimeter filter (flowrate = 0.067 L/min) was counted for 5 minutes after 5 minute sampling and 3 minute waiting in three measurements. The counts obtained from the CEA filter and the discs, as shown in Fig. 6.6, coincide at aroun -2000 V. The difference in the three CEA points in Fig. 6.6 is due to the randomness of radioactive decay and slightly different conditions with respect to radon daughters and aerosol concentrations. This result is further confirmed in four different experiments involving simultaneous measurements with the CEA pump-filter and the -2000 V aluminum disc complete with barrier (Fig. 6.7). Since it was observed (Fig. 6.6) that the collected activity appears to become constant above 2000 V, another experiment was carried out to check this hebaviour. With conditions similar to those in the experiment of Fig. 6.6, the data obtained established that in a restricted field configuration, the deposited activity becomes insensitive to a further increase in applied voltage. These results are plotted in Fig. 6.8. All of the above experiments were carried out at ∿4 WL.

The experimental results to date can be summarized as follows:

i) The deposition of radon daughter aerosols on a charged disc is linear with applied potential and similar in behaviour to that on a filter driven by a pump.

ii) Electrets can collect radon daughter aerosols with efficiencies which are similar to the efficiencies of aluminum discs held at a potential equal to easily achieved surface potentials of electrets.

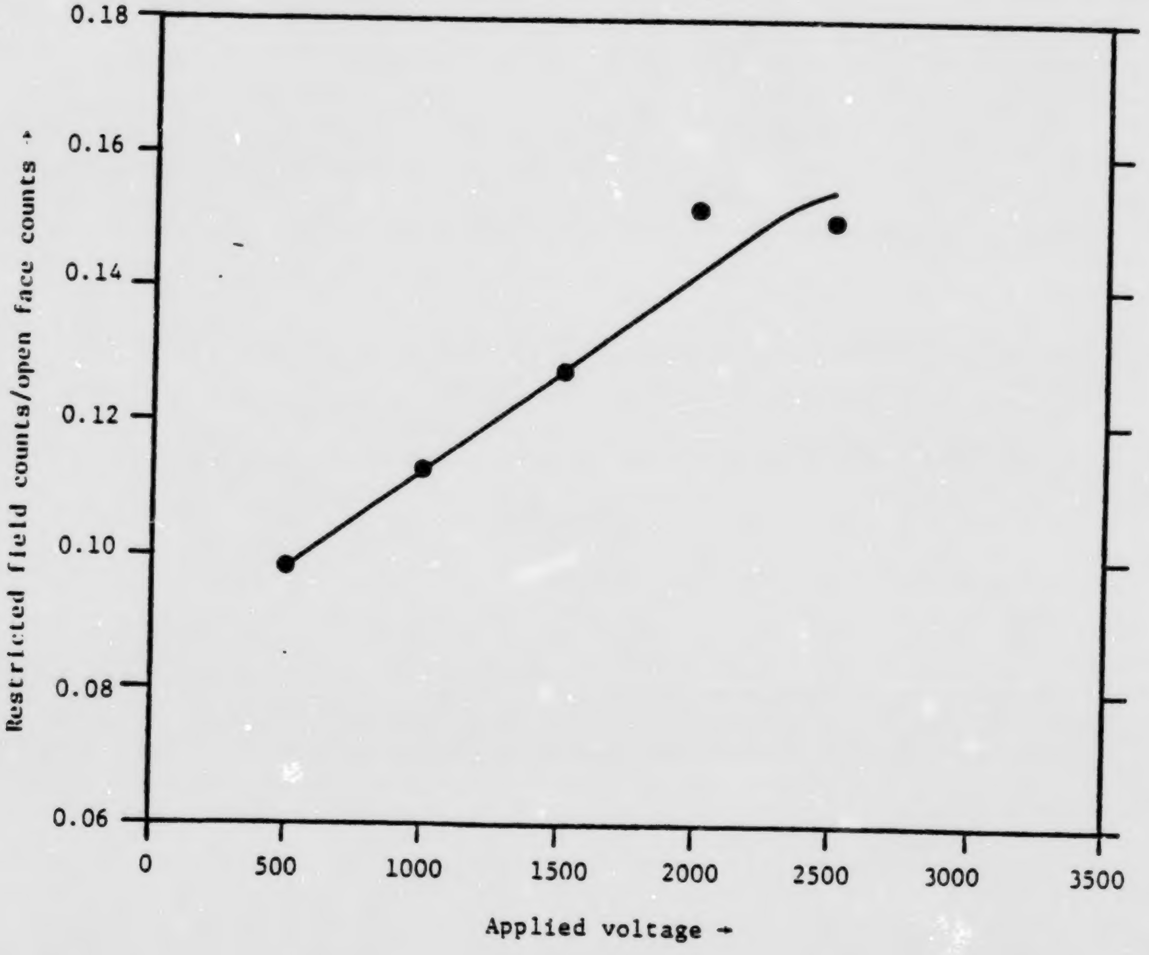

Fig. 6.5. Ratio of restricted field counts to open face counts versus applied voltage.

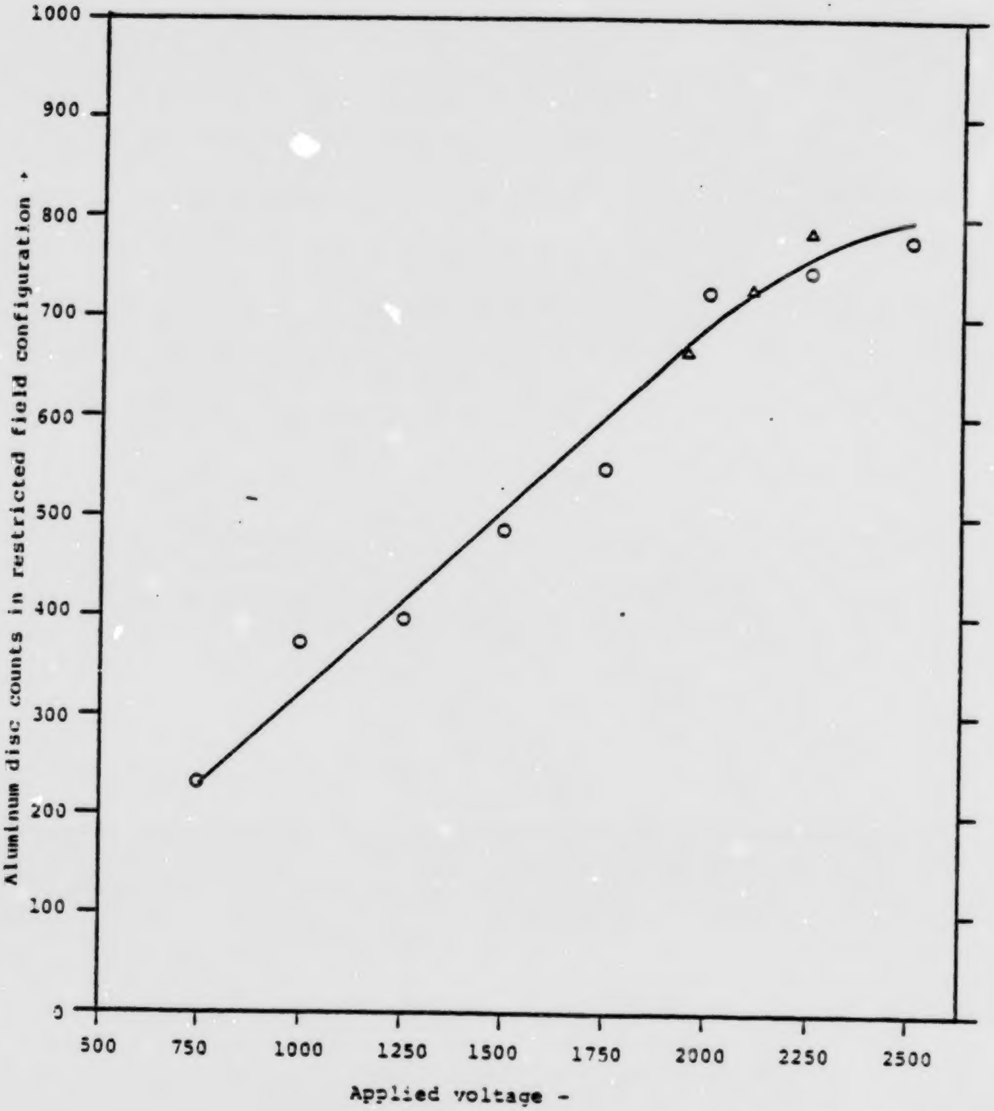

Fig. 6.6. Counts obtained from aluminum disc (with cylindrical barrier held above it) vs applied voltage ○
Counts obtained from CEA dosimeter filter. △

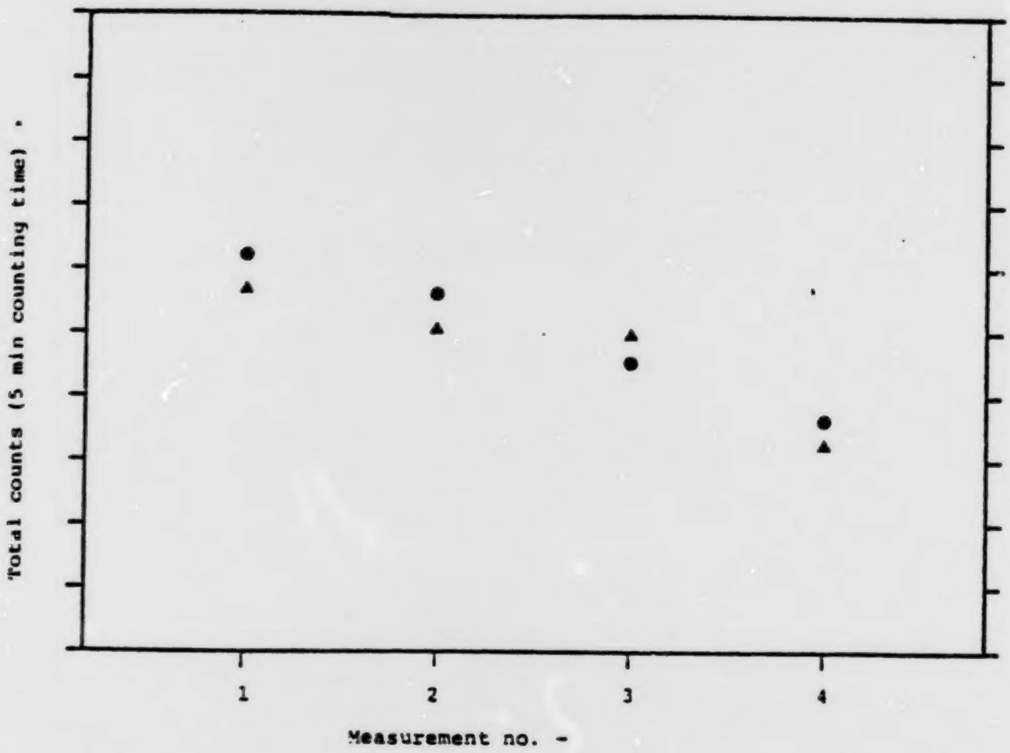

Fig. 6.7. Comparison of CEA dosimeter-filter counts (▲) with -2000 V aluminum disc counts (●) exposed and counted under similar conditions.

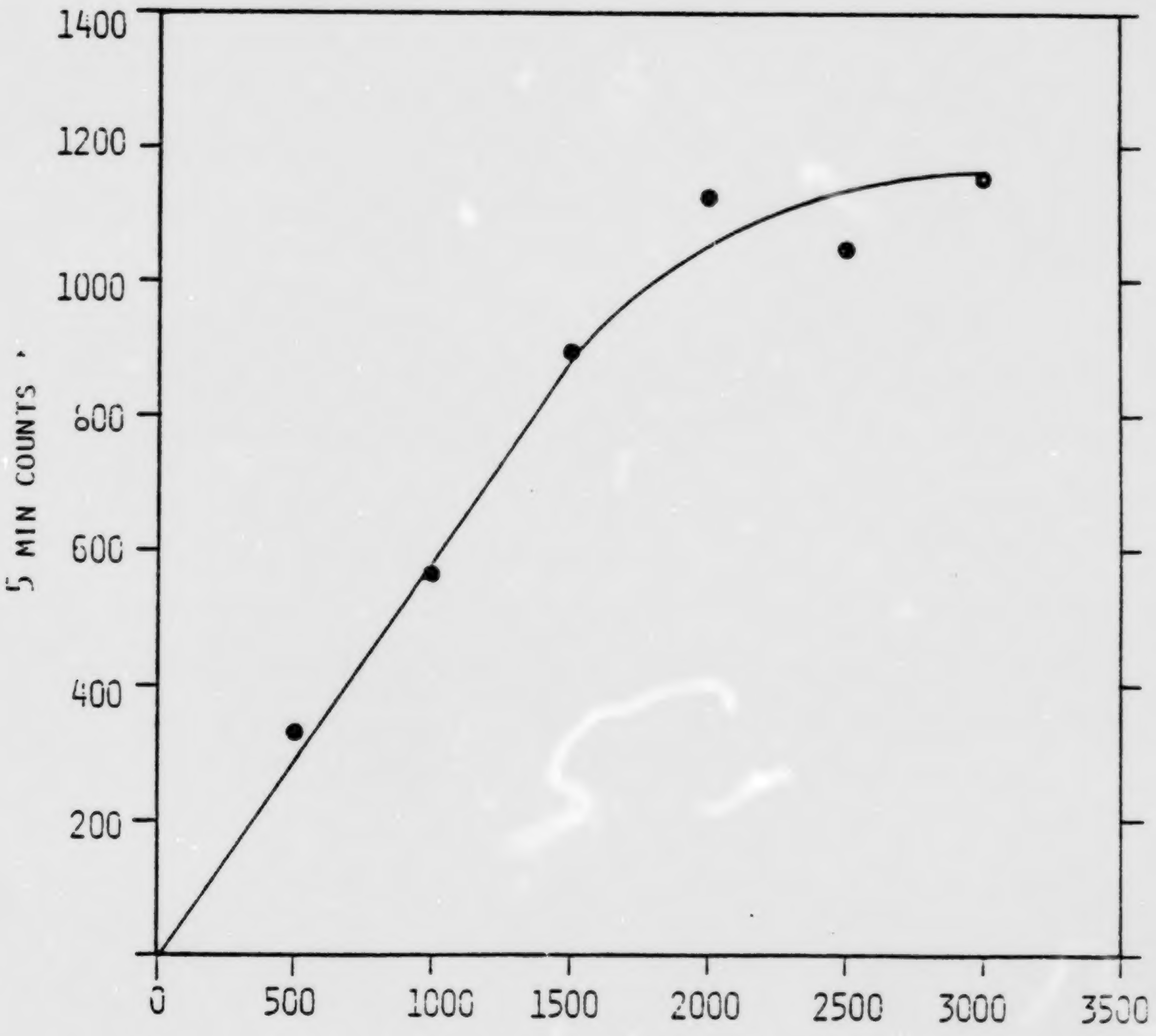

Fig. 6.8. Activity collected on aluminum disc (5 min sampling, 3 min waiting, 5 min counting) in dosimeter configuration versus applied voltage.

iii) Electrostatic deposition on an open face disc is severely reduced by placing a cylindrical barrier a small distance from the collection disc. The dependence of collected activity on applied voltage in this case is linear to about -2000 V.

iv) The potential required for a collecting surface in the chosen passive dosimeter configuration to produce a collection efficiency of aerosols similar to that in the CEA active dosimeter is -2000 V.

v) The activity collected by a charged disc in a dosimeter configuration is insensitive to increases in applied voltage above (-)2000 V.

Given these results for the electrostatic collection of aerosols on a charged disc, more elaborate experiments were undertaken. Electret formation was studied and electrets prepared as described in Chapter 7. The dependenceof electrostatic deposition on radon daughter concentrations was determined. Effects of humidity and unattached fractions, particle size and aerosol concentrations were also studied (Chapter 7). An electret passive dosimeter was designed and tested in both laboratory and mine environments. The dosimeter design and the results of the laboratory and mine trials are reported in Chapter 8.

7. ELECTROSTATIC DEPOSITION: DEPENDENCE ON ENVIRONMENTAL VARIABLES

The preliminary experiments outlined in Chapter 6 were carried out without taking into account the effects of important parameters such as radon daughter concentrations, humidity, unattached fraction, particle size and aerosol concentrations. The effects of these parameters are now investigated in order to obtain a complete understanding of the mechanism of electrostatic deposition of aerosols. Most of the experiments were carried out with open face aluminum discs held at -1000 V, since in the open face configuration, this voltage is adequate for collection.

7.1 Effect of Humidity on Electrostatic Deposition of Aerosols

The effect of humidity on collection of radon daughters on a -1000 V aluminum disc (5 minute sampling time, 3 minute waiting and 5 minute counting time) was investigated. Humidity was increased or decreased in the chamber by controlling the rate of bubbling of air through a series of water reservoirs placed inside the radon chamber. Humidity and temperature were monitored by a YSI Model 90 Hygrometer with its probe located inside the chamber. Results are presented in Fig. 7.1. Similar experiments at different applied voltages confirmed that the linearity of electrostatic deposition with respect to the applied voltage is preserved at any level of humidity under the experimental conditions used. However, experiments carried out at lower unattached fractions of radon daughters (<10%) and higher humidity (>67% R.H.) suggested that electrostatic deposition becomes less strongly dependent upon the applied voltages as shown in Fig. 7.2. In the presence of a cylindrical barrier it was found that the electrostatic deposition becomes constant with

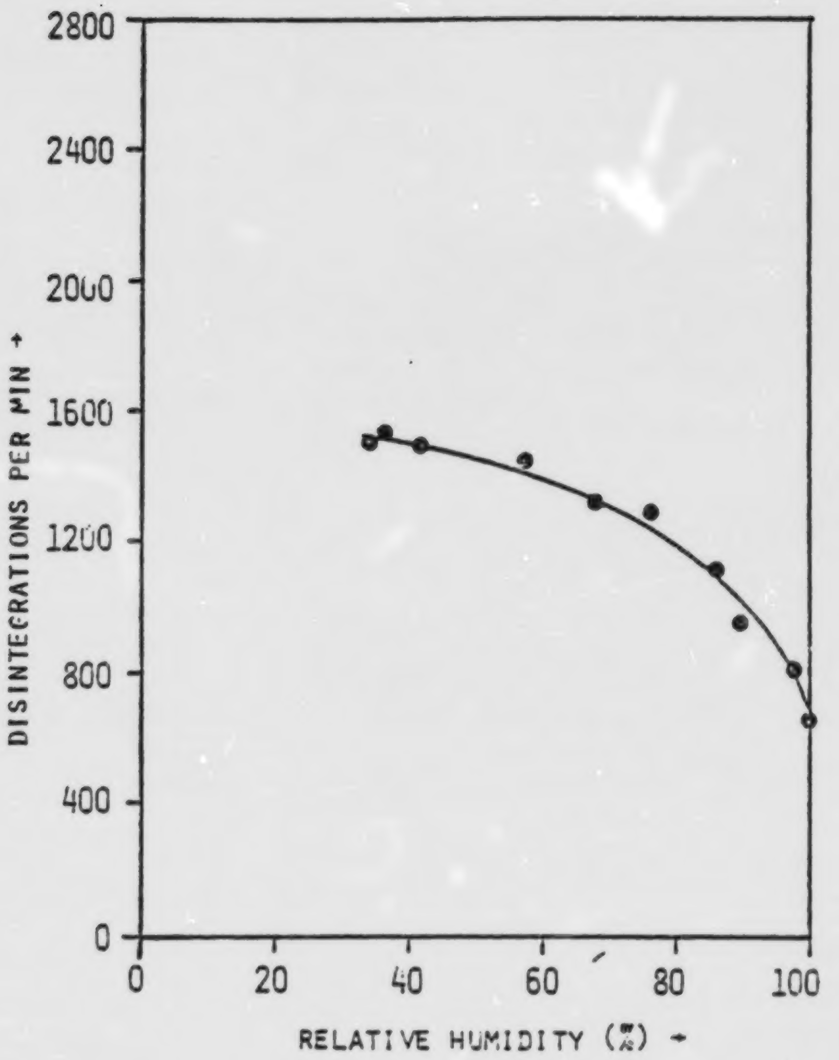

Fig. 7.1. Average alpha disintegrations per minute (over 5 min) for -1000 V aluminum discs (5 min sampling, 3 min waiting, 5 min counting) vs relative humidity (%) inside the radon chamber (temperature 22-25°C; each data point corresponds to a different WL (in the range 3-4 WL) and was obtained on a different day.

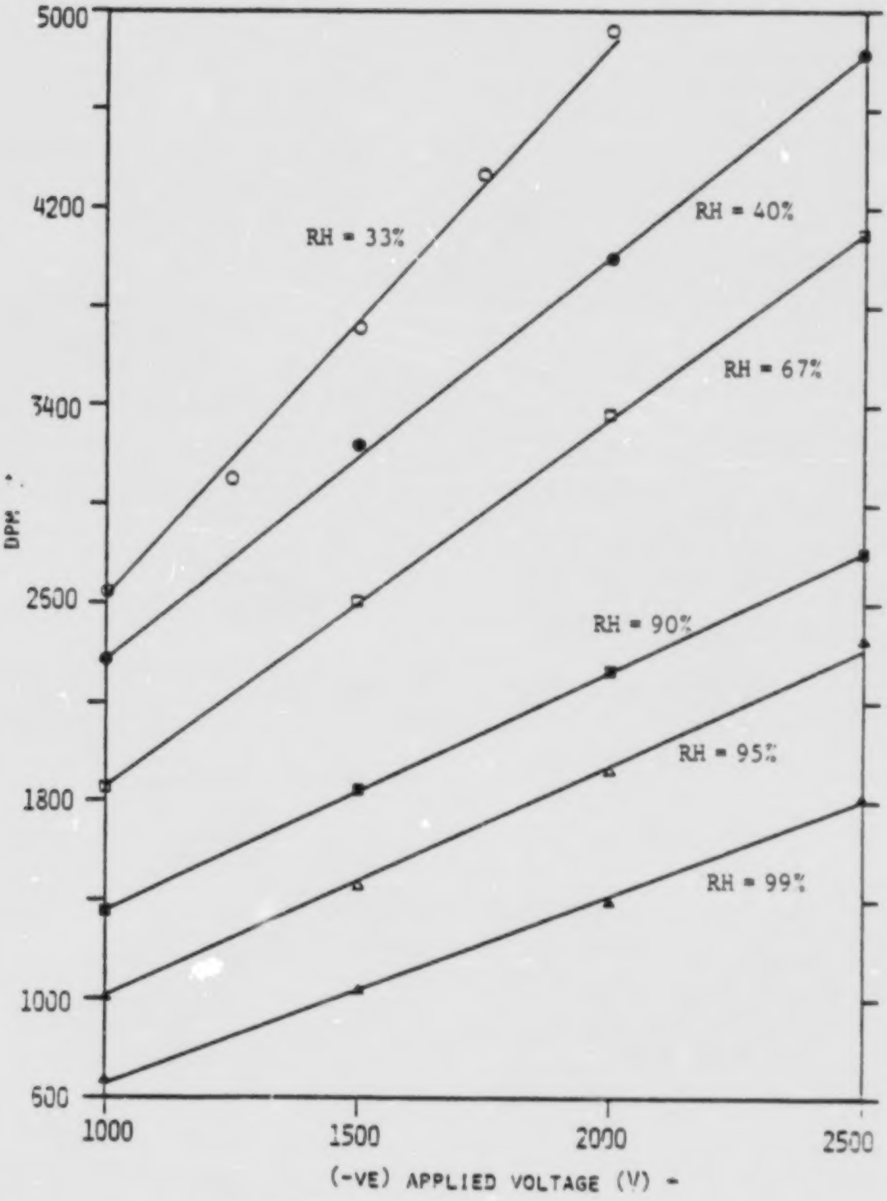

Fig. 7.2. Disintegrations per minute obtained from open face Al disc for different applied voltages (5 min exposure, 3 min waiting, 5 min counting).

applied voltage at voltages above 2000 V (Figs. 6.6 and 6.8). This observation has an important implication with respect to the mine environment. Since the humidity in underground mines is normally high (>70%) and electrets are formed generally with ±10% variations in surface potentials, the electrostatic deposition should, therefore, not be affected for electrets with surface potentials greater than 2000 V.

7.2 Effects of Other Parameters

In order to study the dependence of electrostatic deposition of aerosols on aerosol size and concentration, the unattached fraction of radon daughters, and the radon daughter concentration, the following experiments were conducted. Simultaneous measurements were made on an aluminum disc held at -1000 V applied and an open face filter in a filter holder driven by a pump at 3 L/min flow rate. Sampling was carried out for 5 minutes and discs and filters counted in two Trimet alpha counters in three counting intervals, each according to the optimized modified Tsivoglou method (Bu80) at 2-5, 7-15 and 25-30 minutes. The concentrations of RaA, RaB and RaC were determined from the set of equations given below:

$$C_2V = 0.1682\ I(2,5) - 0.11435\ I(7,15) + 0.09297\ I(25,30)$$

$$C_3V = -\ 0.0082\ I(2,5) - 0.02466\ I(7,15) + 0.07179\ I(25,30)$$

$$C_4V = -\ 0.02184\ I(2,5) + 0.04541\ I(7,15) - 0.04799\ I(25,30)$$

where C_2, C_3 and C_4 are the concentrations of RaA, RaB and RaC respectively in pCi/L, V is the sampling rate (L/min) and $I(t_1,t_2)$ is the number of alpha disintegrations obtained in the time interval t_1 to t_2 minutes after the end of sampling.

The concentrations of radon daughters were varied by varying the radon flow rate and the aerosol concentrations. The concentrations were measured in the chamber at least three times during each run and variations from the mean were always found to be within $\pm 10\%$. Also, at least two hours were allowed for the Working Level to become steady after turning the aerosol generator on. The aerosol concentrations were recorded by an Environment One condensation nuclei counter placed inside the radon chamber. Humidity and temperature were recorded during the course of sampling. The aerosol size distribution corresponding to each sampling was measured with diffusion batteries, using three rectangular channel-batteries located inside the radon chamber. Appendix A describes the experimental method and data. The count median diameter of the aerosols was calculated by using the method developed by Busigin (Bu78). The computer program is listed in Appendix C. The size and concentration of the aerosols for each measurement is required to determine the attachment rate of radon daughters to aerosols. The unattached fractions were then determined by the method outlined in Chapter 2. The results are listed in Table 7.1.

The electrostatic flow rate, Q_e, as defined in Chapter 6 was calculated by trial and error to give radon daughter concentrations close to the actual values. The computer program for these calculations is listed in Appendix C.

The relationship between the electrostatic flow rate of RaA and RaB and the attachment rate is represented in Fig. 7.3. The attachment rate was calculated from eqns. (2.4) and (2.14) using the mean thermal velocity of radon daughter atoms, $\bar{v} = 1.38 \times 10^{-4}$ cm/s and sticking probability, $S = 1$. The electrostatic flow rate of RaA is plotted against

TABLE 7.1

Experimental Data for Simultaneous Measurements on Radon Daughter Collection by -1000 V Aluminum Disc and Filter-Pump System

Expt. No.	Counting interval no.*	Al disc counts (-1000 V applied)	Filter counts (3 L/min flow rate)	Calculated Rn ds. data				Diseq. ratios $C_{RaA}:C_{RaB}:C_{RaC}$	Effective time (min)	WL	Aerosol concn. #/cm $(\times 10^{-3})$	Aerosol dia. (μm)	Attachment rate (#/S)	Relative humidity (%)	Temp. (°C)	Rn flow rate (Arbitrary units)
				Parameter	RaA	RaB	RaC									
1	1	993	12030	*C	433	236	152	100:54:35	40	2.2	80	0.08	0.05	98	21	32
	2	1243	22778	*q_E	0.5	0.21	-0.01									
	3	741	12095	*f	0.06	~8×10^{-4}	~10^{-6}									
2	1	1117	14778	C	536	311	166	100:58:31	40	2.7	75	0.09	0.05	97	21	32
	2	1474	28241	q_E	0.45	0.21	-0.02									
	3	915	15491	f	0.07	~9×10^{-4}	~10^{-6}									
3	1	1643	20137	C	696	365	251	100:52:36	40	3.5	135	0.05	0.03	97	22	28
	2	2885	37852	q_E	0.42	0.43	0.01									
	3	1953	19944	f	0.11	~0.002	~3×10^{-6}									
4	1	121	348	C	14	7	3	100:50:21	35	0.06	40	0.03	0.004	97	23	8
	2	198	621	q_E	1.8	1.5	-0.4									
	3	144	337	f	0.51	0.1	~3×10^{-5}									
5	1	235	1357	C	55	18	15	100:33:27	35	0.2	75	0.03	0.007	95	23	8
	2	354	2290	q_E	0.95	1.2	-0.2									
	3	254	1137	f	0.40	0.04	~6×10^{-5}									
6	1	1271	13571	C	478	228	170	100:48:36	40	2.3	100	0.03	0.01	94	21	10
	2	2055	24989	q_E	0.49	0.43	0.04									
	3	1311	12858	f	0.28	0.02	~2×10^{-5}									
7	1	2325	22514	C	767	408	285	100:53:37	40	3.9	165	0.03	0.02	96	24	10
	2	3663	42484	q_E	0.56	0.42	0.03									
	3	2317	22235	f	0.19	0.01	~10^{-5}									

cont'd.....

TABLE 7.1 (cont'd)

Expt. No.	Counting Interval No.	Al disc counts (-1000 V applied)	Filter counts (3 L/min flow rate)	Calculated Rn ds. data				Diseq. ratios $C_{RaA}:C_{RaB}:C_{RaC}$	Effective time (min)	WL	Aerosol concn. #/cm^3 (x10^{-3})	Aerosol dia (μm)	Attachment rate (#/S)	Relative humidity (%)	Temp. (°C)	Rn Flow rate (Arbitrary units)
				Parameter	RaA	RaB	RaC									
8	1	1757	19156	C	690	313	232	100:48:33	40	3.3	150	0.04	0.02	99	23	10
	2	2765	35262	q_E	0.49	0.41	0.01									
	3	1785	18360	f	0.15	0.005	~6x10^{-6}									
9	1	2210	21856	C	803	396	256	100:49:32	40	3.8	130	0.04	0.02	99	23	10
	2	3378	40310	q_E	0.51	0.40	0.02									
	3	2151	21264	f	0.17	0.006	~8x10^{-6}									
10	1	1247	11130	C	462	261	120	100:35:26	35	1.7	75	0.03	0.006	97	24	10
	2	1899	18903	q_E	0.55	0.61	-0.04									
	3	1269	9576	f	0.19	0.05	~7x10^{-5}									
11	1	1562	11591	C	485	172	123	100:35:25	35	1.8	150	0.02	0.01	100	21	10
	2	2167	19647	q_E	0.59	0.40	0.14									
	3	1180	10009	f	0.34	0.03	~5x10^{-5}									
12	1	1551	20212	C	733	364	241	100:50:33	40	3.5	170	0.06	0.06	100	23	12
	2	2280	37388	q_E	0.41	0.27	0.02									
	3	1396	19665	f	0.06	~7x10^{-4}	~10^{-6}									
13	1	1820	18983	C	782	271	208	100:35:26	35	3.0	140	0.05	0.03	97	22	10
	2	2649	32204	q_E	0.44	0.38	0.06									
	3	1557	16192	f	0.10	0.002	~3x10^{-6}									
14	1	223	6056	C	189	118	81	100:62:43	50	1.1	270	0.06	0.09	87	22	7
	2	305	11871	q_E	0.27	0.14	-0.3									
	3	210	6281	f	0.04	~3x10^{-4}	~3x10^{-7}									
15	1	277	6401	C	221	118	79	100:56:36	40	1.1	180	0.09	0.14	87	22	5
	2	413	12068	q_E	0.25	0.17	-0.0004									
	3	265	6357	f	0.02	~10^{-4}	~10^{-7}									
16	1	2064	14958	C	555	259	176	100:47:32	35	2.5	80	0.04	0.01	86	23	7
	2	3189	27264	q_E	0.8	0.27	0.03									
	3	1274	14222	f	0.20	0.01	4x10^{-}									

cont'd........

TABLE 7.1 (cont'd

Expt. No.	Counting Interval No.	Al disc counts (-1000 V applied)	Filter counts (3 L/min flow rate)	Calculated Rn ds. data				Diseq. ratios $C_{RaA}:C_{RaB}:C_{RaC}$	Effective time (min)	WL	Aerosol concn. #/cm³ ($\times 10^{-3}$)	Aerosol dia (µm)	Attachment rate (#/S)	Relative humidity (%)	Temp. (°C)	Rn Flow rate (Arbitrary units)
				Parameter	RaA	RaB	RaC									
17	1	2131	17180	C	590	297	219	100:50:37	40	2.9	150	0.04	0.02	84	24	7
	2	2973	32053	q_E	0.7	0.38	0.06									
	3	1730	16589	f	0.14	0.017	$\sim 2\times 10^{-5}$									
18	1	1397	14965	C	486	257	201	100:53:41	40	2.5	185	0.04	0.03	83	24	5
	2	1981	28328	q_E	0.57	0.33	0.02									
	3	1201	14562	f	0.10	0.01	$\sim 10^{-5}$									
19	1	2727	16869	C	637	298	193	100:47:30	35	2.9	180	0.01	0.02	86	22	6
	2	3424	30693	q_E	0.85	0.33	0.12									
	3	1795	16133	f	0.14	0.02	$\sim 3\times 10^{-5}$									

* Counting interval no. 1: 2-5 min, no. 2: 7-15 min, no. 3: 25-30 min; C = concentrations in pCi/L; q_E = electrostatic flow rate (L/min); f = unattached fraction.

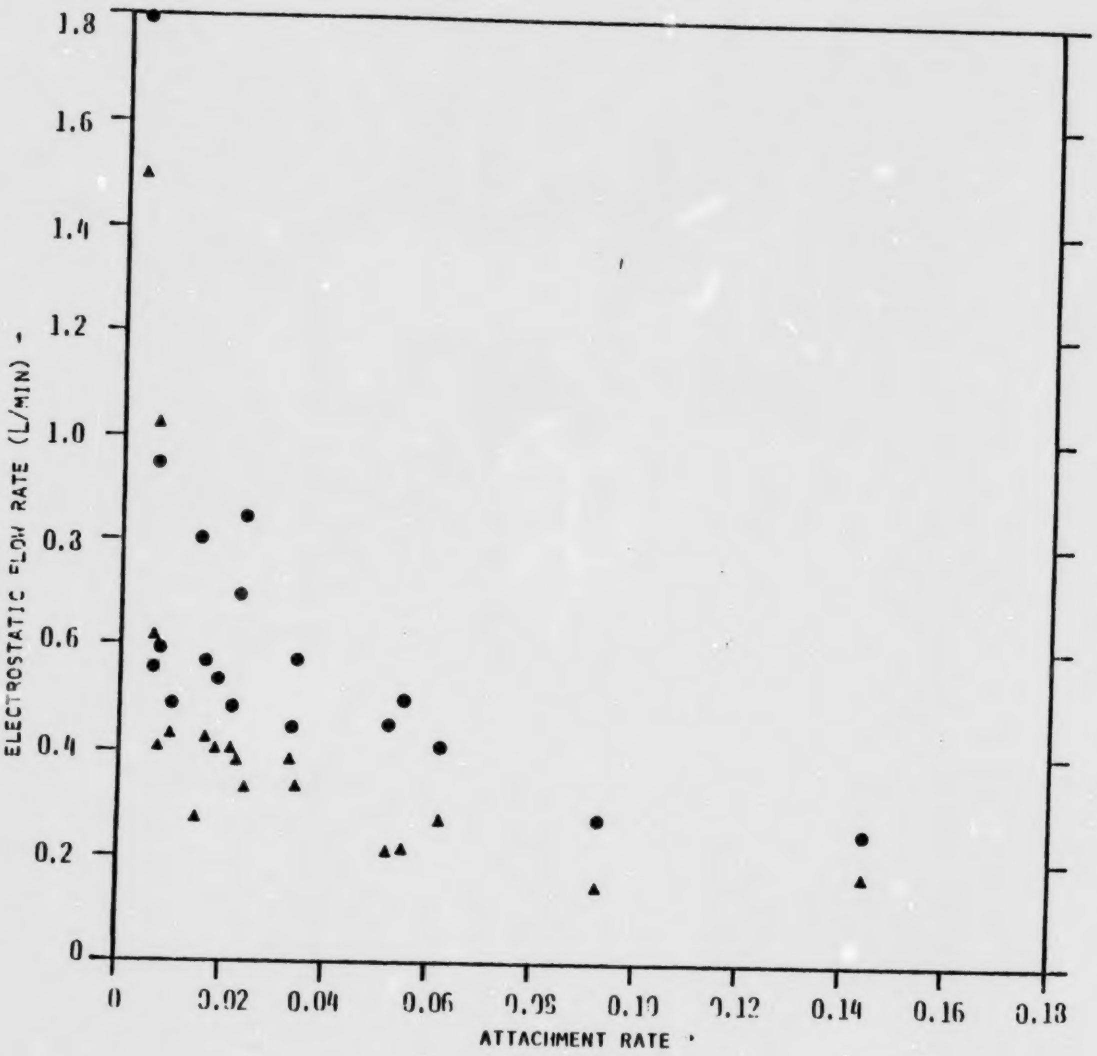

Fig. 7.3. Electrostatic flow rate of RaA (●) and RaB (▲) vs their attachment rate.

the unattached fraction of RaA in Fig. 7.4. The electrostatic flow rate is presented as a function of aerosol concentration in Fig. 7.5 and as a function of particle size in Fig. 7.6. The 2-5 minute counts vs. the RaA concentrations and 25-30 minute counts vs. RaC concentrations are presented in Fig. 7.7. The most important relationship from a dosimetry point of view is the one represented in Fig. 7.8. In this graph, the 25-30 minute counts, which are mainly due to RaC (and hence the RaC'), are plotted both for the filter and the disc against the Working Level. The filter counts are divided by a factor of 10 to scale them to the same order as the disc counts.

Error bars have not been shown for the experimental data points in any figure because of the poorly understood and complex interdependence of parameters such as unattached fraction of radon daughters, aerosol size, aerosol concentration and humidity. The errors involved cannot therefore be predicted with reasonable certainty. Errors due to the random nature of radioactive decay can be estimated as $\pm\sqrt{n}$ for n number of disintegrations.

The results presented in Fig. 7.3 - Fig. 7.8 are, however, to be interpreted with caution and are discussed in detail in Chapter 9.

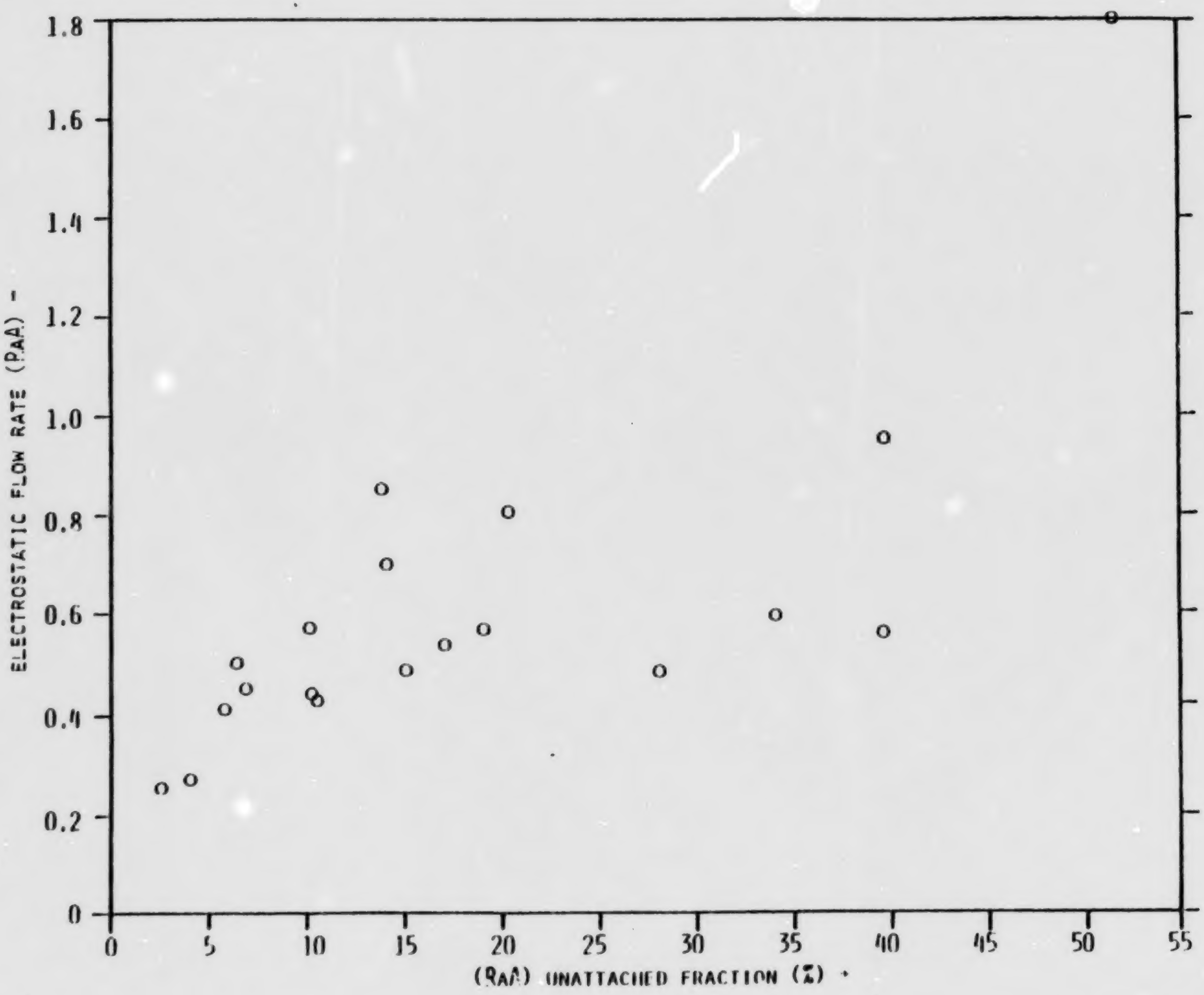

Fig. 7.4. Electrostatic flow rate of RaA versus the unattached fraction of RaA.

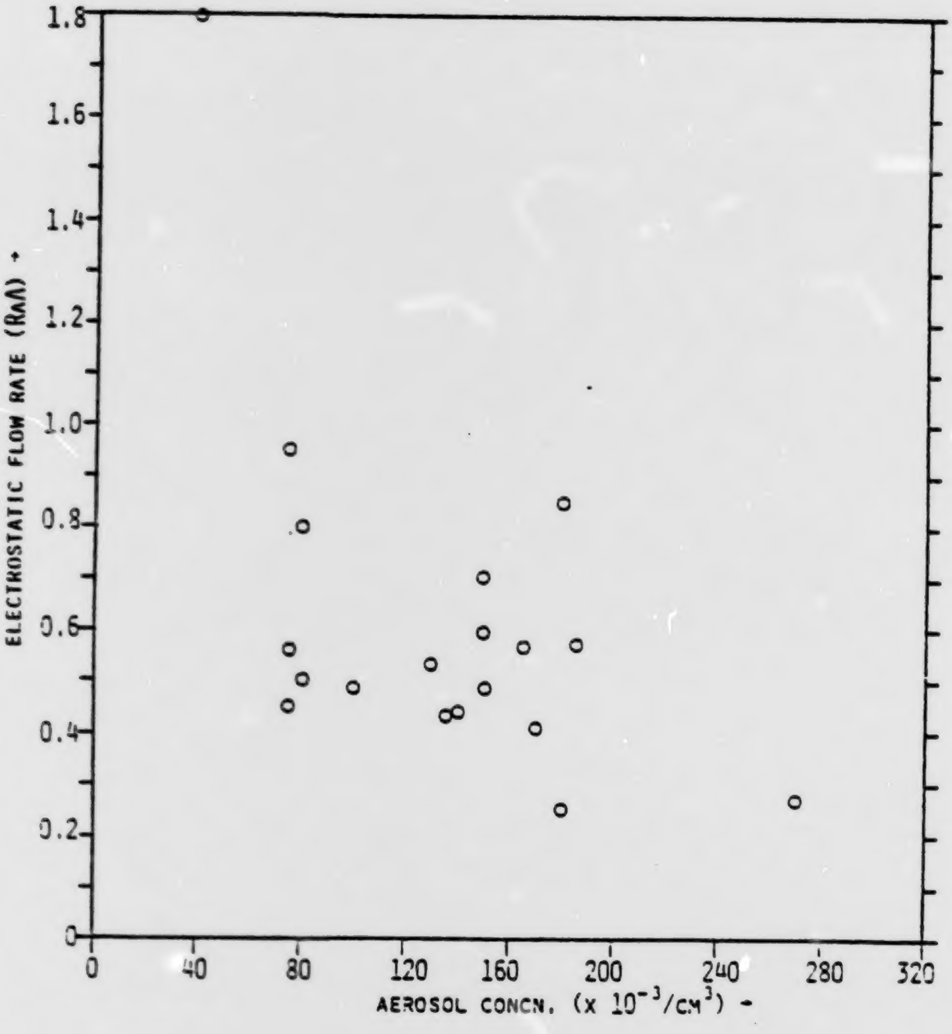

Fig. 7.5. Electrostatic flow rate of RaA vs the concentration of aerosols.

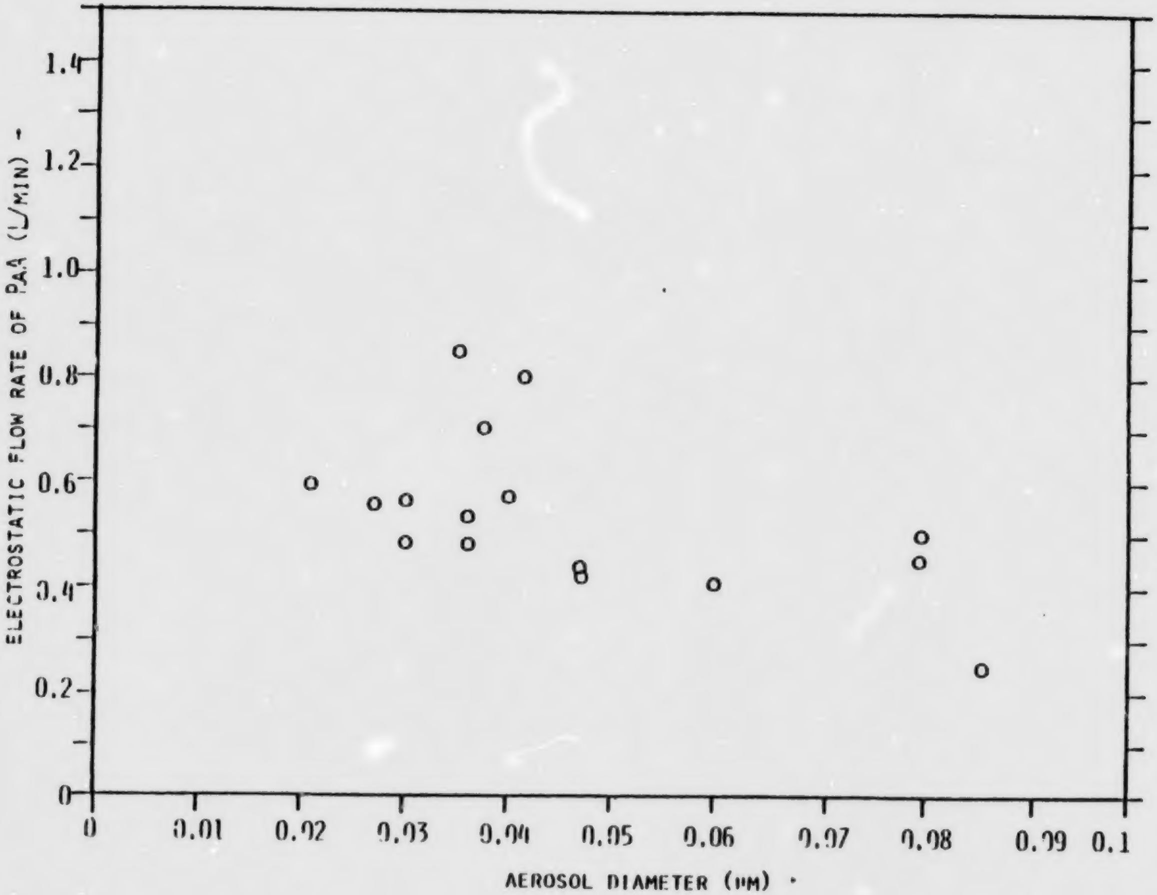

Fig. 7.6. Electrostatic flow rate of RaA plotted as a function of the aerosol diameter.

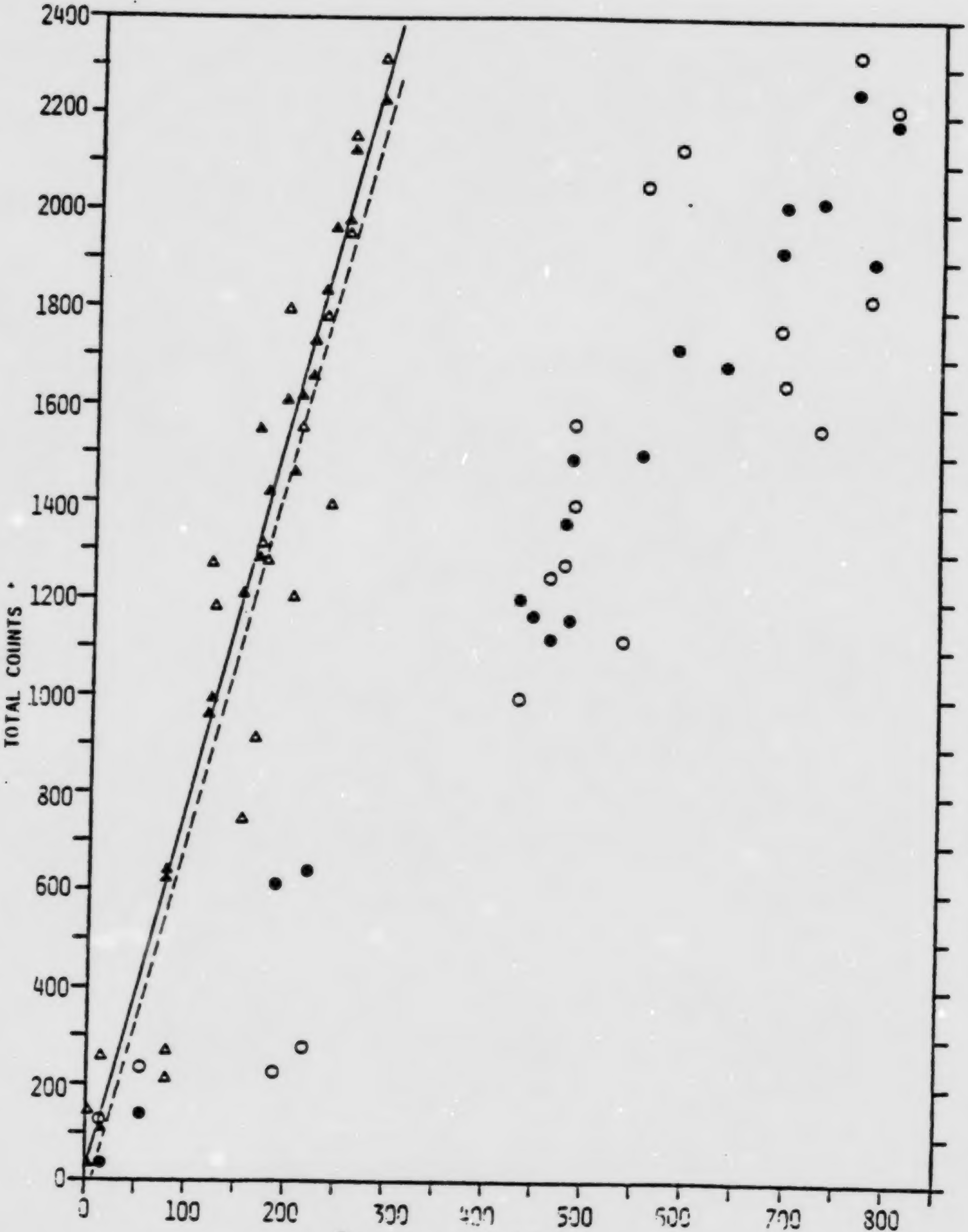

Fig. 7.7. 2-5 min counts obtained by using open face aluminum disc (-1000 V) vs RaA concentration O. 2-5 min counts obtained by using open face filter (3 L/min flow rate) RaA ●. 25-30 min counts obtained by using aluminum discs (-1000 V) vs RaC concentration △. 25-30 min counts obtained by using open face filter (3 L/min) vs RaC concentration.▲.

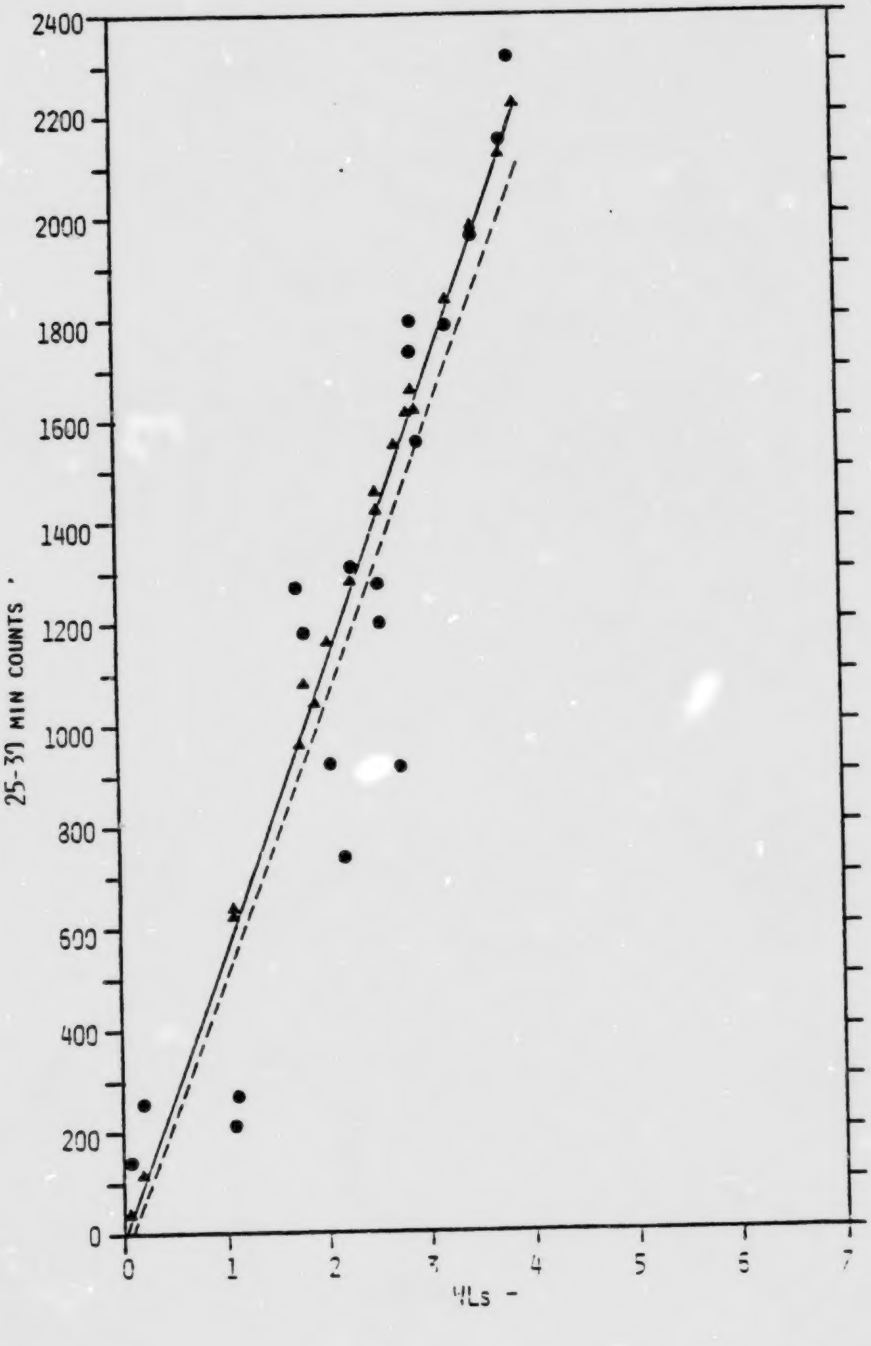

Fig. 7.8. Counts obtained at 25–30 min after 5 min sampling by
——— open face filter (3 L/min flow rate) ▲
----- aluminum disc (-1000 V) ●
vs Rn daughter Working Level.

8. PASSIVE ELECTRET DOSIMETER FOR RADON AND THORON DAUGHTERS: DESIGN AND PERFORMANCE

In the last chapter the similarity between electrostatic deposition on a charged surface and deposition on a pump-driven filter was established (Fig. 7.8). The next logical step in determining the feasibility of electrostatic deposition for passive radon daughter dosimetry is to design such a dosimeter and test it under laboratory and mine conditions.

8.1 Design of Dosimeter

A dosimeter for radon daughters consists of three parts: a dosimeter head containing the detector, a collection surface for aerosols, and an external housing to contain the detector and the collecting element (along with a pump, in active dosimeters). Since the main objective was to evaluate the performance of electrets as the aerosol collecting element, it was decided to use a replica of the CEA dosimeter head for the purpose of registering radon and thoron daughters, with an electret serving as the collecting element. The CEA dosimeter head is described in Appendix B.

The 6 mm gap between the collimators and the collecting surface in the CEA dosimeter was preserved by replacing the filter in the CEA dosimeter by the electret. However, the inlet for aerosols had to be made wider because of the short-range of the electrostatic forces. This modification was made by means of two spacers, each 6 mm long, with two long screws passing through the electret, to hold the aluminum base, the spacers, the dosimeter head and an aluminum cap on top of the detector (Fig. 8.1). A thin insulating ring of a non-static material was placed

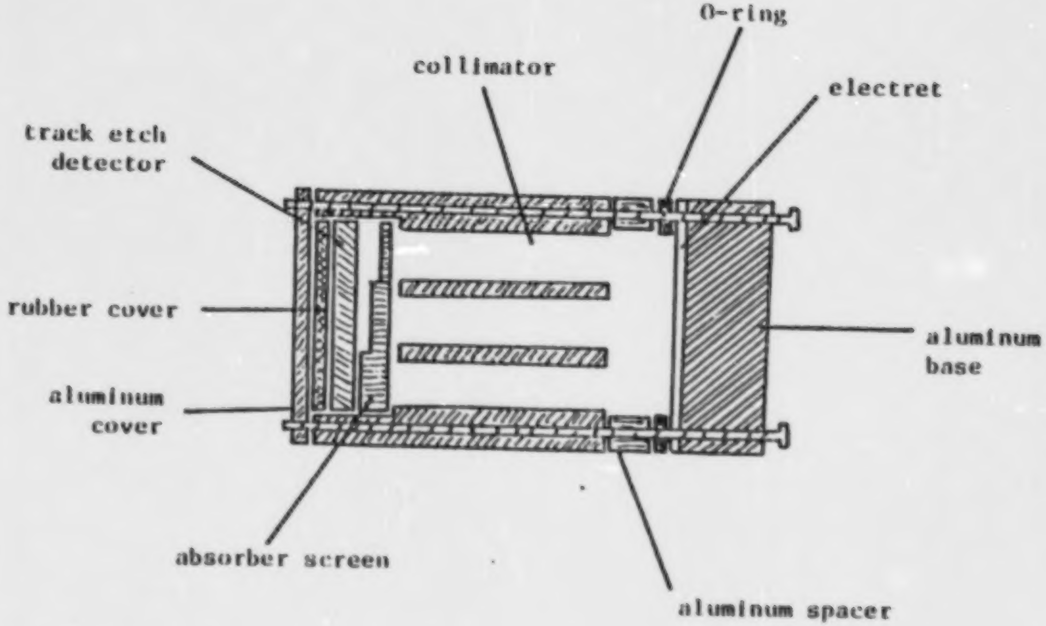
O-ring
collimator
electret
track etch detector
rubber cover
aluminum base
aluminum cover
absorber screen
aluminum spacer

Fig. 8.1. Schematic cross-section of the passive electret dosimeter.

on top of the electret, which was stretched across the surface of a 1 cm thick aluminum disc base. The diameter of the electret was approximately that of the base (2.9 cm), with allowance for the screws passing through the spacers. The insulating ring (of internal diameter 2.1 cm) placed on the electret covers any irregularities in the electret edges and exposes only a 2.1 cm diameter collecting surface. This arrangement also allows the electret to be handled by its edges (electrets lose charge on contact) and allows application of glue at the edges to hold the electret and the insulating ring in place.

As discussed in Chapter 6, a diffusion barrier is needed in order to isolate the system from external wind velocity effects. A cylindrical enclosure around the open area of the dosimeter was first tested. However, based on experiments carried out inside a small wind tunnel and on comparison with a CEA dosimeter exposed simultaneously with the electret dosimeter, cylindrical baffles were not found to be effective (Table 8.1).

The wind tunnel placed inside the radon chamber consisted of a galvanized steel tube, 18 cm diameter, 60 cm long, with a small axial fan located at one end. A support for the dosimeter was located at the centre of the tube and the position of the dosimeter could be adjusted radially by means of adhesive tape. The wind velocity at the centre of the tube was measured to be about 250 cm/s using a Florite air velocity meter.

As a result of large variations in registered activity with respect to the orientation of the dosimeter in the wind tunnel, the cylindrical barrier design was substantially modified. The modified housing consists of a complete enclosure for the dosimeter, with ten holes on the top and also on the bottom for entry and exit of air

TABLE 8.1

Results from Simultaneous Exposure of Electret Dosimeter (with Cylindrical Enclosures) and CEA Dosimeter in Wind Tunnel. R.H. 80-90%, Temp. 26-30°C

Expt. no.	Exposure time	Orientation	Diffusion Barrier dia (cm)	-2000 V Electret dosimeter No. of tracks counted		CEA dosimeter No. of tracks counted	
				RaA	RaC'	RaA	RaC'
1	1 h	Upright	3.8	104	37	108	23
2	1 h	Parallel to wind direction	3.8	160	69	68	29
3	45 min	Upright	3.3	26	16	56	20
4	75 min	Parallel to wind direction	3.6	144	60	110	22
5	75 min	Inclined at 45° angle	3.6	118	26	94	33

(Fig. 8.[illegible]. This diffusion barrier proved to be effective against external wind velocity effects. However the surface potential of the electret had to be increased to greater than 2500V as a result of the limited access of aerosols to the electret surface. Figures 8.3 and 8.4 show the number of tracks obtained by the electret dosimeter (-3000V electret), complete with external barrier, for different orientations of the dosimeter in the wind tunnel. The results are compared with a CEA dosimeter exposed simultaneously.

In order to confirm these track etch results, a silicon surface barrier detector in conjunction with an α-spectrometer was used in place of the dosimeter head. The results of five experiments, for 3000 sec exposures, are presented in Fig. 8.5. A typical α-spectrum obtained in such a run is shown in Fig. 8.6.

The dosimeter configuration as shown in Fig. 8.2 was adopted for two series of mine tests at Denison mines, Elliot Lake. The dosimeter weighs 120 g, compared to 320 g for the CEA dosimeter, and is about one third of the volume of the CEA dosimeter. The mine tests are described in the next section.

8.2 Mine Tests of Passive Electret Dosimeter

8.2.1 Initial Test

In the first series of tests, electrets were prepared from 25 μm thick foil electret material (supplied by the Sheldahl Company, Minnesota). Although in previous laboratory tests it had been found that this material could not hold surface potentials of -3000 V, and could only hold -2500V for more than a week, it was nevertheless decided to use the

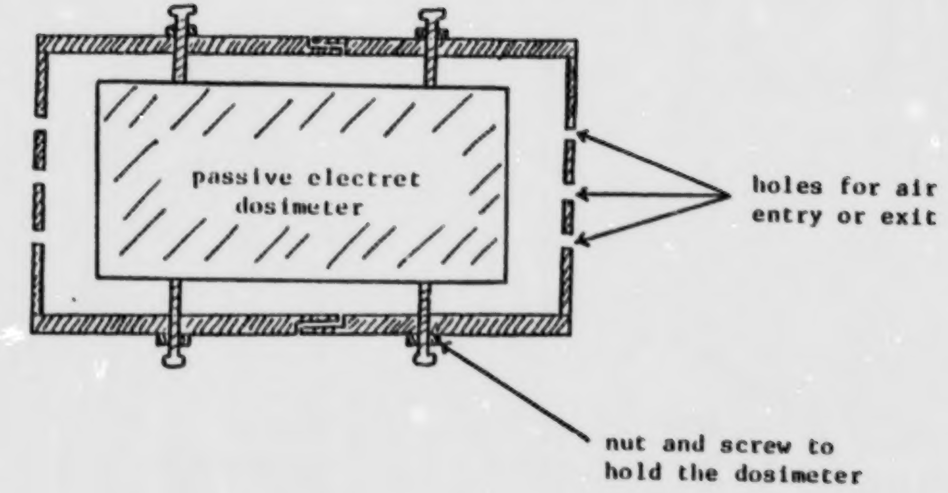
passive electret dosimeter
holes for air entry or exit
nut and screw to hold the dosimeter

Fig. 8.2. Diffusion barrier with the passive electret dosimeter in place.

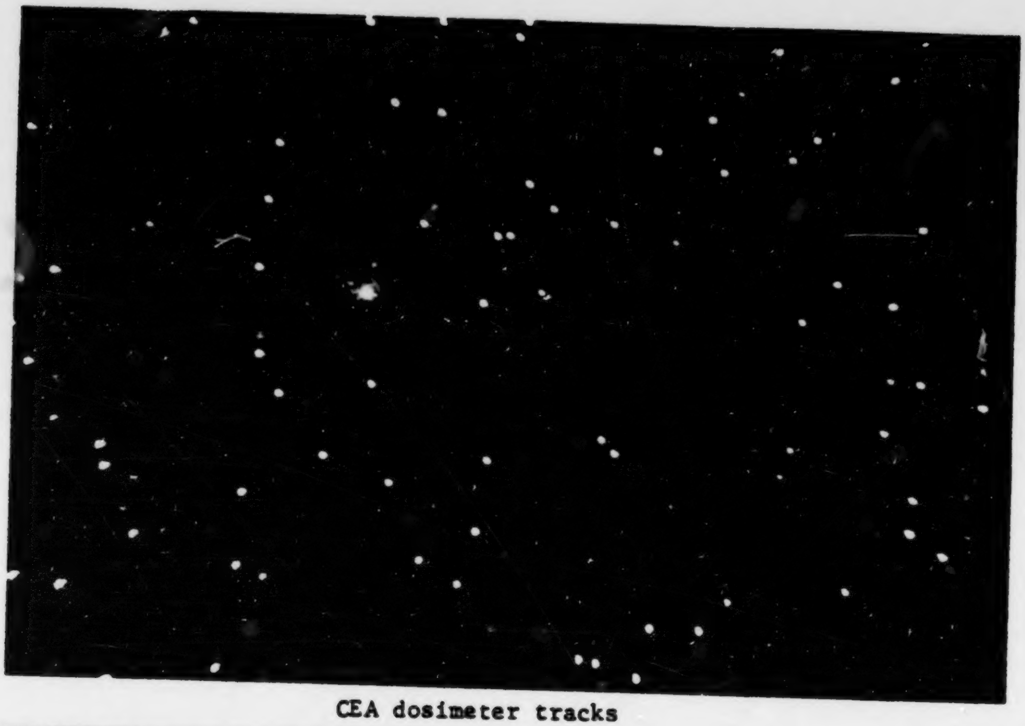

CEA dosimeter tracks

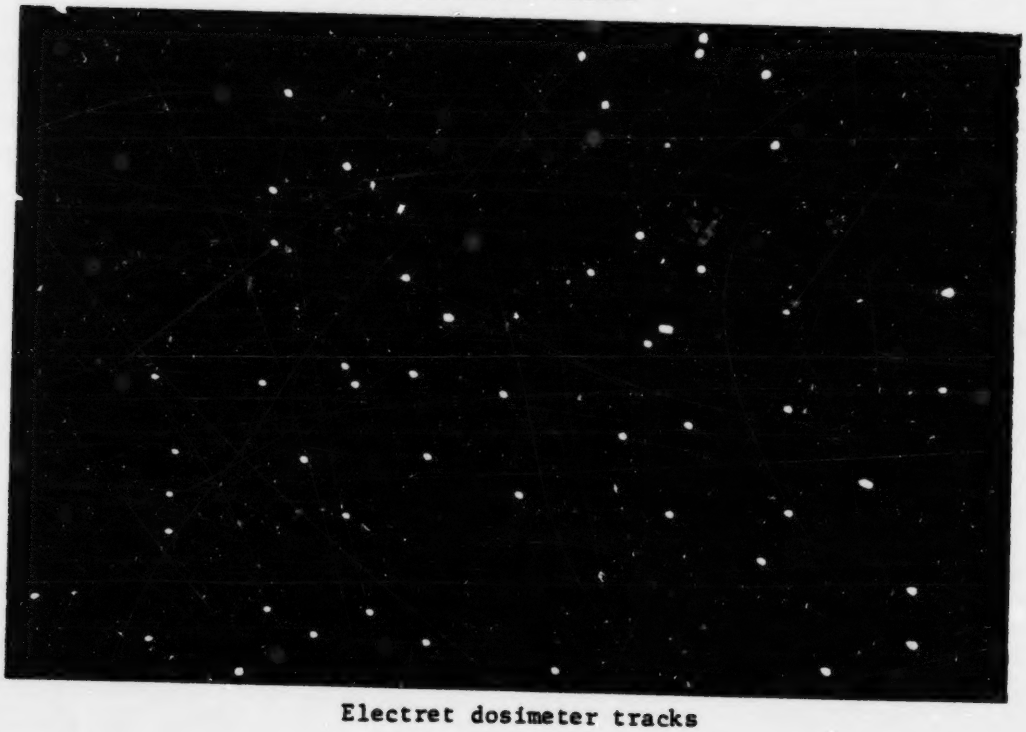

Electret dosimeter tracks

Fig. 8.3. Comparison of electret dosimeter in wind tunnel with simultaneously exposed CEA dosimeter held parallel to wind direction (100% R.H. at 22°C; 4 WL; exposure time = 2 hr).

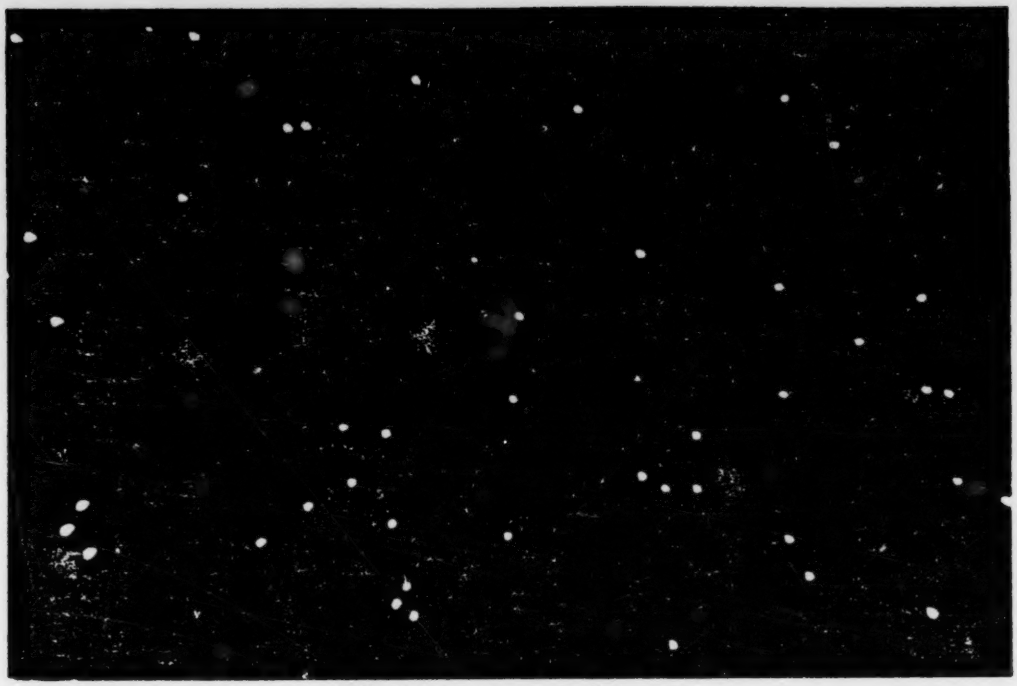

CEA dosimeter tracks

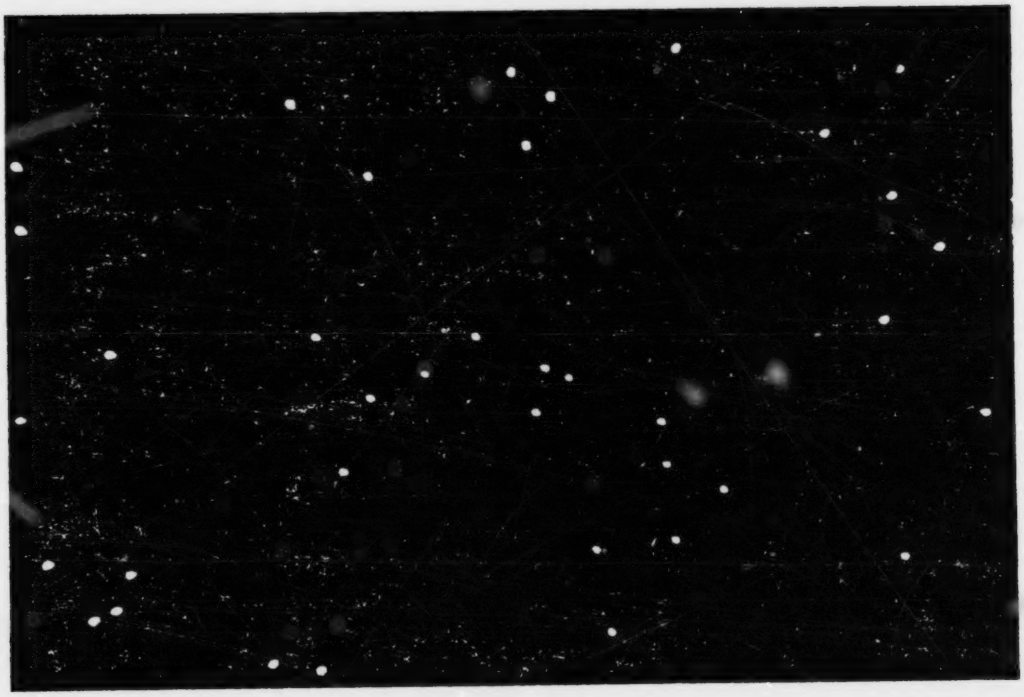

Electret dosimeter tracks

Fig. 8.4. Comparison of electret dosimeter in wind tunnel with simultaneously exposed CEA dosimeter held perpendicular to wind direction (100% R.H. at 21°C; 3.2 WL; exposure time = 2 hr).

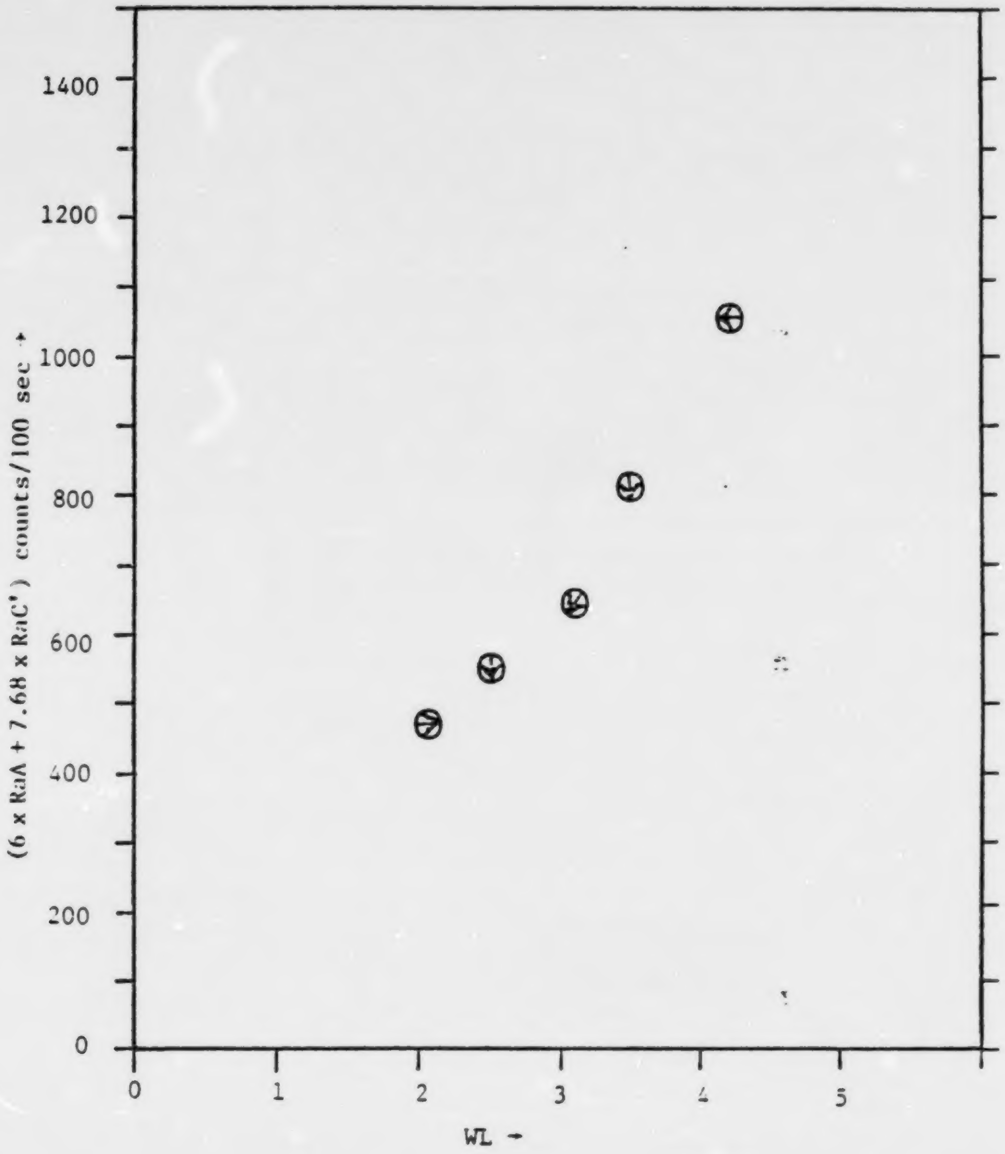

Fig. 8.5. Integrated alpha counts obtained from the α-spectrometer for the electret dosimeter at different orientations in the wind tunnel. The arrows indicate position of the dosimeter with respect to wind direction (→).

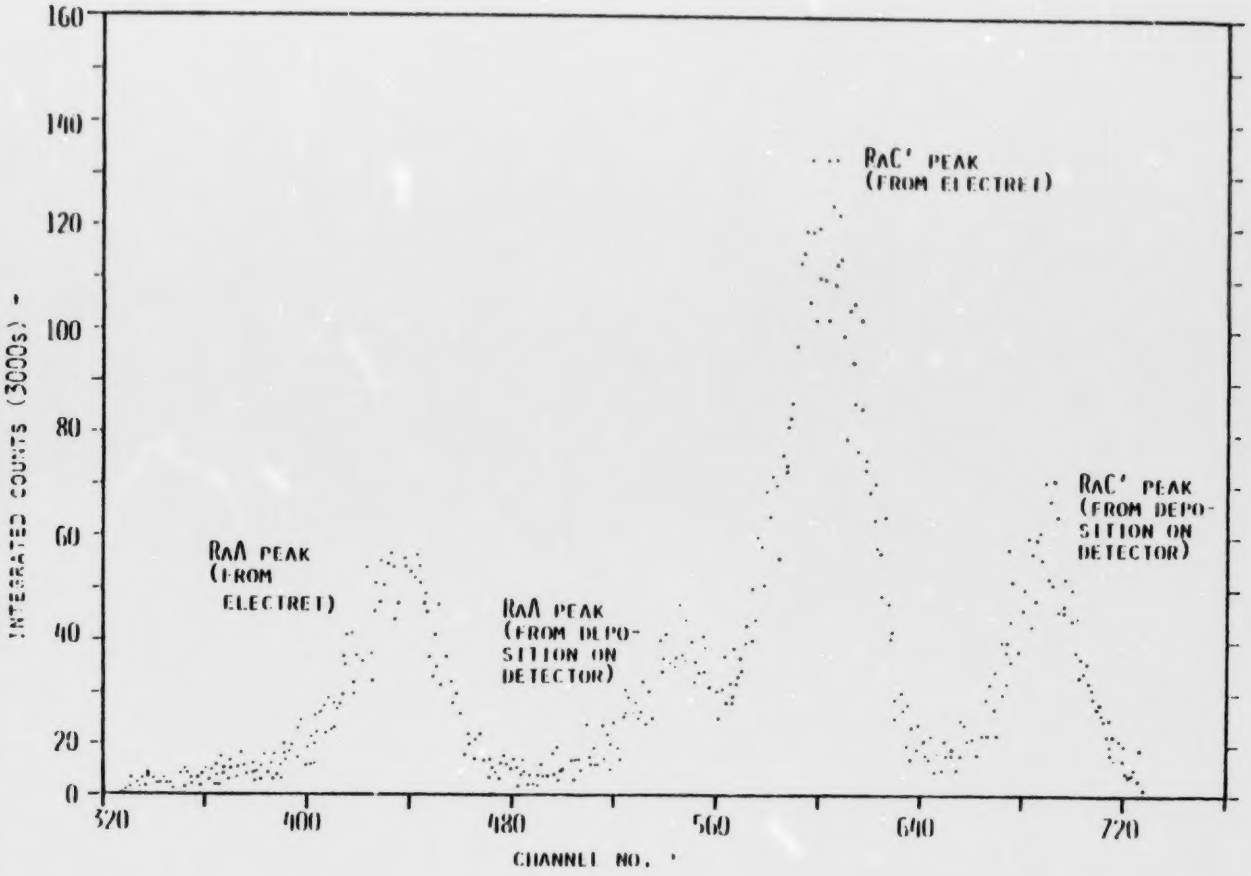

Fig. 8.6. A typical α-spectrum from activity collected in an electret dosimeter.

material at its highest surface potential because of its commercial availability. Ten electrets were formed at 10 KV applied for 1 minute. The electrets were then stored in a drawer to allow the charge to stabilize. Based on measurements of charge decay over three days, six electrets were chosen for incorporation into the dosimeters. Each electret was carefully stretched across the surface of the aluminum base after trimming its edges to make provision for the screws passing through the two spacers. A protective Teflon FEP film (non-aluminized) of 25 um thickness was placed on top of the electret to protect it against dirt and moisture. The protective cover was found to display a similar surface potential to that of the electret underneath as a result of induced polarization.

A small amount of glue was carefully applied to the electret edges and a thin insulating ring placed over it to secure the ring, the electret and the Teflon cover to the aluminum base. The assembly had to hold the electret firmly in place under the anticipated harsh mine conditions. Small pieces of adhesive tape were used to further secure the assembly to the dosimeter base. Cellulose nitrate (LR-115, type II) track etch detector films were placed on top of the aluminum strip with the appropriate energy absorbers in the dosimeter head. The dosimeter lid was then put together with two long screws passing through two thin spacers, acting as pillars to hold the dosimeter head (Fig. 8.1). A small rubber strip was inserted between the dosimeter lid and an aluminum cover for the detector to allow the lid to be tightened properly. Finally, the assembled dosimeter was placed inside the external housing (diffusion barrier) and held in place with the help of three nuts and screws each at two positions equally spaced from the ends. A vinyl belt was secured between two parallel screws in order to enable the dosimeter to be worn on a miner's belt. Identification numbers were marked on the dosimeter. Each miner was assigned a reference CEA dosimeter to be worn along with the passive dosimeter.

For the first test electret potentials could only be measured a few days after the test (when the dosimeters were to arrive by mail). Under these circumstances, there would have been no way of knowing, in the event of charge loss, when an electret showed the first signs of charge decay. The dosimeters were therefore exposed for 1, 2, 3, 4 or 5 days. The sixth dosimeter was exposed for one day. The surface potentials of the electrets were checked on January 11 and the dosimeters were assembled and mailed to Elliot Lake the same day. The tests were conducted January 17-21 and the dosimeters were returned by February 4. The exposed track etch dosimeters were etched but large clusters of tracks around the collimator edges region made it impossible to count the actual tracks. The surface potential decay pattern was, however, obtained (Fig. 8.7). The decrease in surface potential seems to increase with the exposure period. Greatest deterioration in surface potential occurred for dosimeter no. 5, exposed by mistake for six days (with a 2-day gap before the last day of the exposure) instead of for five days as had been originally planned. However, since the potentials were read 12-15 days after exposure, the exact pattern of decay could not be established. The probable patterns of decay are shown in Fig. 8.7.

The following conclusions may be drawn from this initial mine test:

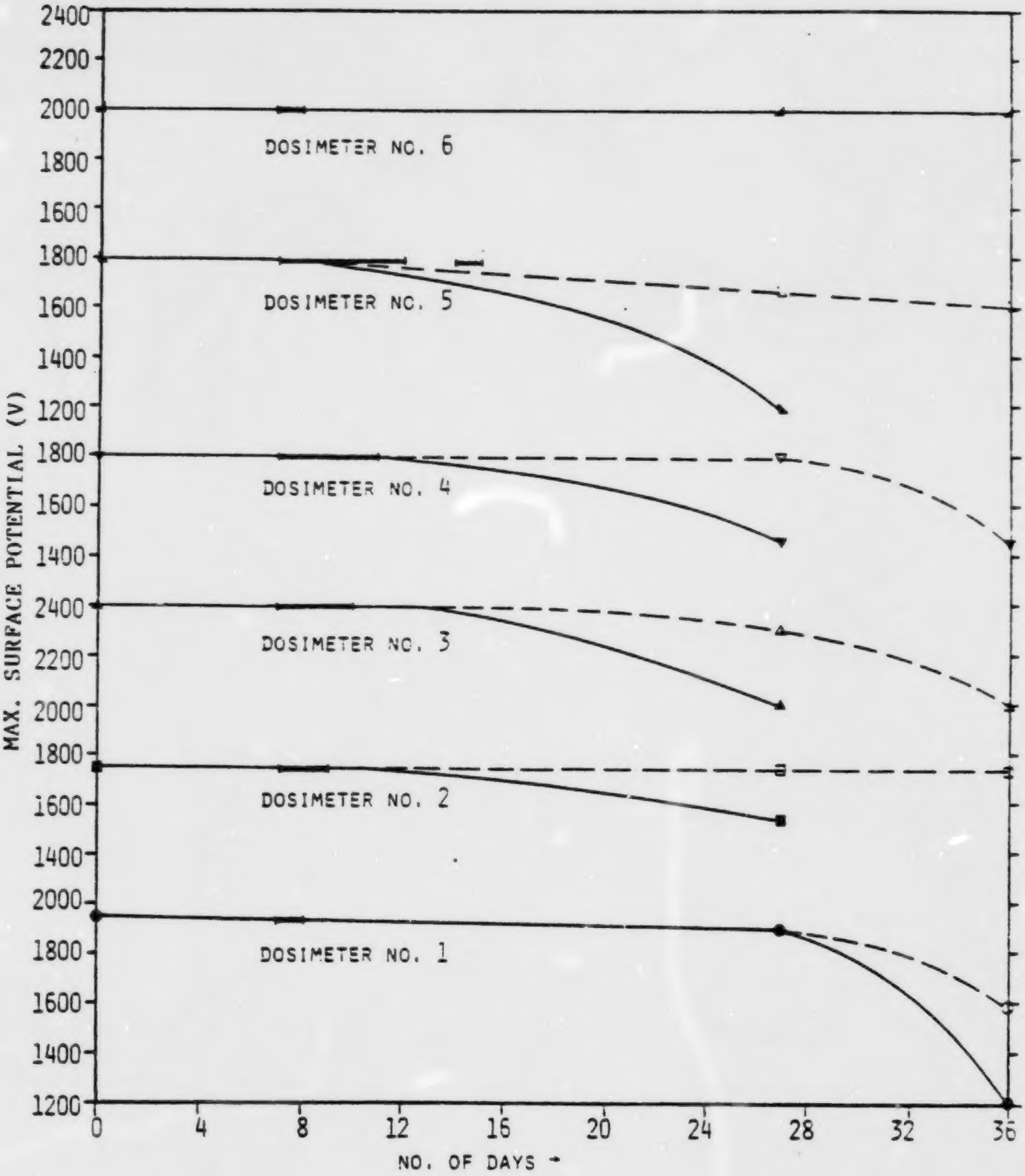

Fig. 8.7. The pattern of electret charge decay with cover (———) and without cover (-----) in mine test no. 1. Exposure period is indicated by thick horizontal bars.

i) In order to obtain useful track etch data, precautions should be taken to eliminate any possibility of contamination of detector films which causes track clusters to form due to the deposited dust.

ii) In order to measure the charge decay characteristics of an electret after exposure under mine conditions, the electret potential should be measured at the end of each day.

iii) The electrets should also be checked at the end of each day for any visible contamination that might affect their potential.

iv) If the surface potential is degraded only on the cover of the electret and if the electret itself is intact (as in dosimeter no. 2 and no. 4 in Fig. 8.7), the protective cover should be replaced.

v) An attempt should be made to form electrets with higher surface potentials and better stability.

vi) The dosimeters proved rugged enough to be used in a mine environment.

8.2.2 Second Mine Test

Drawing upon the conclusions of the initial mine test, another test was planned. Further experiments on electret formation were carried out in an attempt to obtain more stable electrets with higher surface potentials. Doubly aluminized Teflon FEP, which was earlier rejected in favour of the commercial electret-foil, was found to be capable of holding high surface potentials ($\geq$3000 V) for a minimum of one week when formed at 10 KV applied for 1 minute. Electrets for the second test were therefore prepared with this material.

Equipment for making electrets and measuring surface potentials was transported to Elliot Lake and arrangements were made to check the dosimeters at the end of each day. The tests were conducted for five days (April 4-8) and all six dosimeters were exposed for the same period of five days. A CEA dosimeter for reference was worn by each miner along with the passive dosimeter. The track etch detector side of each dosimeter was securely sealed with black adhesive tape so that dust could not reach the detector surface or the collimator edges on the absorbers. Table 8.2 summarizes daily measurements on the electret dosimeters. Table 8.3 compares the electret dosimeters with the reference CEA dosimeter. (Detailed grab sampling data are shown in Table 8.3a.) These results are shown in the next chapter.

TABLE 8.2

Summary of the Electret Behaviour During the Second Mine Test

Dosimeter No.	April 4	April 5	April 6	April 7	April 8
1	Initial voltage on April 3 = -1800 V After exposure, max. potential = -1300 V Clean surface	Max. pot. = -2800 V Clean surface	Max. pot. = -2500 V Clean surface	Max. pot. = -2500 V Clean surface	Max. pot. = -2300 V Clean surface
2	Initial voltage on April 3 = -3600 V After exposure, max. potential = -3500 V	Max. pot. = -3200 V	Max. pot. = -2700 V	Max. pot. = -2700 V VISIBLE CONTAMINATION	Max. pot. = -2300 V
3	Initial voltage on April 3 = -3400 V After exposure, max. pot. = -3000 V Clean surface	Max. pot. = -1500 V Under the cover, max. pot. = -3600 V Cover replaced New pot. = -3600 V	Max. pot. = -2800 V	Max. pot. = -1500 V Under the cover max. pot. = -2400 V VISIBLE CONTAMINATION Cover replaced New pot. = -2400 V	Max. pot. = -2000 V

cont'd......

TABLE 8.2 (cont'd)

Dosimeter No.	April 4	April 5	April 6	April 7	April 8
4	Initial voltage on April 3 = -3600 V After exposure, Max. pot. = -1200 V Clean surface	Max. pot. = -2800 V Clean surface	Max. pot. = -2600 V Clean surface	Max. pot. = -1600 V Under cover, max. pot. = -2500 V VISIBLE CONTAMINATION Cover replaced New pot. = -2500 V	Max. pot. = -1200 V
5	Initial voltage on April 3 = -3000 V After exposure, max. pot. = -2800 V Slightly contaminated	Max. pot. = -2000 V Visible contamination Electret replaced New pot. = -3600 V	Max. pot. = -1800 V Smear from glue noticed Electret replaced New pot. = -3800 V	Max. pot. ∿-3500 V in one half and -1500 in other half	Max. pot. -2500 V in one half and -1500 V in other half
6	Initial pot. = -3000 V After exposure = -3000 V on 3/4 of surface 1/4 of surface contaminated, with +500 V on a contaminated spot.	Max. pot. = -2300 V Electret replaced New pot. = -3800 V	Max. pot. = -1000 V Under cover, max. pot. = -2800 V Cover replaced New pot. = -2800 V	Max. pot. = -1800 V Under cover, max. pot. = -2400 V Water drops in the dosimeter Cover replaced	Max. pot. = -1400 V

TABLE 8.3

Summary of the Electret Dosimeter Results Obtained from the Second Mine Test

Miner No.	Occupation	Passive dosimeter data				CEA dosimeter data							
		Dos. no.	E.S. flow rate (ℓ/hr)	RnWL (R_1)	TnWL (T_1)	Dos. no.	Flow rate (L/hr)	RnWL (R_2)	TnWL (T_2)	ΔRnWL $(\frac{R_1 - R_2}{R_2})$	ΔTnWL $(\frac{T_1 - T_2}{T_2})$	Grab sample average (RnWL)	Comments
1	Electrical foreman	1	1	0.13	0.13	D-86	3.72	0.08	0.13	0.625	0	0.09	
2	Electrician	2	1	0.20	0.15	D-89	4.06	0.21	0.12	0.05	0.25	0.08	4 days exposure. Did not report for work on Apr. 7
3	Jumbo drill	3	1	*0.45	*0.25	D-88	3.72	0.49	0.24	0.08	0.04	0.92	*Calculated for 3 day exposure. Voltage dropped below 2000 V on 2 days
4	Shift supervisor	4	1	*0.36	*0.13	D-50	3.04	0.36	0.24	0	0.46	0.15	*Calculated for 3 days. Voltage dropped below 2000 V on 2 days
5	Underground mechanic	5	-	-	-	D-60	3.89	0.08	0.076	-	-		Too many inconsistencies. Electret data rejected.
6	Underground mechanic	6	-	-	-	D-87	3.72	0.20	0.15	-	-	0.15	Same as above.

*Average over the test period. Data given in Table 8.1a.

TABLE 8.3a

Grab Sampling Data for the Second Mine Test

Miner No.	Day No.	Hours spent at one location	Location sample WL	Daily average WL	Average WL (over the test period)
1	1	3	0.03	0.064	0.087
		2	0.01, 0.07		
		2	0.2, 0.13		
		1	0.01		
	2	4	0.01, 0.07	0.062	
		2	0.15		
		1	0.03		
		1	0.01		
	3	2	0.01, 0.07	0.10	
		5	0.15		
		1	0.01		
	4	2	0.06	0.92	
		4	0.15		
		2	0.01		
	5	2	0.03	0.11	
		3	0.15		
		2	0.01, 0.07		
		1	0.01		
2	1	1	0.01, 0.07	0.12	0.082
		7	0.10, 0.14, 0.15		
	2	1	0.01, 0.07	0.08	
		7	0.14, 0.04		
	3	1	0.01, 0.07	0.06	
		7	0.06		
	4	Did not report for work			
	5	1	0.01, 0.07	0.07	
		7	0.12, 0.03		

cont'd....

TABLE 8.3a (cont'd)

Miner No.	Day No.	Hours spent at one location	Location sample WL	Daily average WL	Average WL (over the test period
3	1	5	1.01	1.01	0.92
		3	1.01		
	2	2	1.01	1.01	
		3	no sample taken		
		3	1.01		
	3	4	1.01	0.75	
		4	0.35, 0.65		
	4	3	0.35, 0.65	0.82	
		3	1.01		
		2	1.01		
	5	4	1.01	1.01	
		1	1.01		
		1	1.01		
		2	1.01		
4	1	8	0.15	0.15	0.15
	2	8	0.15	0.15	
	3	8	0.15	0.15	
	4	8	0.15	0.15	
	5	8	0.15	0.15	
5	1	4	0.12	0.075	0.08
		4	0.03		
	2	0.5	0.15	0.073	
		2	0.06		
		1.5	0.18		
		4	0.03		
	3	8	0.03	0.03	
	4	4	0.57, 0.4	0.135	
		1	0.15		
		3	0.13		
	5	4	no sample taken	0.105	
		3	0.13		
		1	0.03		

cont'd...

TABLE 8.3a (cont'd)

Miner No.	Day No.	Hours spent at one location	Location sample WL	Daily average WL	Average WL (over the test period)
6	1	5	0.28	0.29	0.15
		1	0.15		
		2	0.38		
	2	6	0.12	0.12	
		2	0.13		
	3	3	0.13	0.12	
		3	0.12		
		1	0.15		
		1	0.03		
	4	4	0.15	0.14	
		2.5	0.12		
		1	0.13		
	5	3	0.12	0.10	
		3	0.13		
		2	0.03		

9.0 DISCUSSION OF RESULTS

Experiments described in the last two chapters need to be discussed in detail because of the inter-relationships of various parameters. This chapter discusses the results obtained both by using aluminum discs in the laboratory and by exposing passive electret dosimeters in the mine.

9.1 Results from Aluminum Disc Experiments

Before interpreting the results, it should be noted that, under the experimental conditions, only limited control over the unattached fraction, aerosol size and concentration and the radon daughter concentrations was possible. Therefore each experiment corresponds to a random combination of these parameters, and data points do not represent identical conditions. For example in Fig. 7.1 each data point was obtained on a different day because after changing humidity in the radon chamber, at least 24 hours were allowed for the conditions in the chamber to become stable. The Working Level and the aerosol parameters could not be reproduced exactly in each experiment. The results in Figs. 7.1 and 7.2 should therefore be interpreted only with respect to trends.

Figures 7.3 and 7.4 show the variation of electrostatic flow rate with the attachment rate and the unattached fraction of radon daughters, respectively. A conclusion common to the two graphs is that the electrostatic flow rate increases with increasing unattached activity, particularly for unattached fractions greater than 40%. It would have been useful if charged fraction measurements were available for comparison. However, charged fraction measurements were not attempted in the radon chamber for the following reasons: (a) The existing methods for charged fraction measurements are not sufficiently reliable because they do not take into account neutral aerosols collected due to induced polarization; (b) The radon chamber has a limited space for equipment. The condensation nuclei counter, the diffusion batteries, the water reservoirs, the wind tunnel and the assembly for aluminum disc measurements occupied a major fraction of the available space. It was not practical to operate additional equipment, such as Zeleny tubes for charged fraction measurements, via the glove ports.

Theoretical estimates were therefore made of the unattached fractions corresponding to the aerosol size and concentration in each experiment. The relationship between the unattached fraction and the electrostatic flow rate (Fig. 7.4) suggests the presence of high charged fractions of radon daughters at low attachment rates. The points at 51% and 40% unattached fraction correspond to electrostatic flow rates as high as 1.8 and 0.95 L/min respectively. Since these points indicate situations unlikely to occur in a mine atmosphere they were excluded from the statistical analysis presented later. The general trends of electrostatic deposition for a variety of combinations of related parameters, with respect to the parameter indicated on the x-axis, are shown in Figs. 7.3-7.6 and can be summarized as follows:

The electrostatic flow rate does not vary appreciably at attachment rates greater than 0.07/S, unattached fractions less than 40%, aerosol sizes greater than 0.04 μm and aerosol concentrations less than 270,000/cm^3. Since the constancy of the electrostatic flow rate is extremely important for a passive dosimeter based on electrostatic diffusion, a statistical analysis was performed. The electrostatic flow rate data were found to be normally distributed with 70% of the data well within ±σ and 94% of the data well within ±2σ of mean (Fig. 9.1). The experimental conditions were typical of a mine, namely random combinations of aerosol concentration (75,000-270,000/cm^3), aerosol size (0.02-0.08 μm), unattached fractions (<40%) and Working Levels (<4) at high humidity (R.H. 83-100%, temperature 21-24°C).

At aerosol concentrations in the higher range (≥200,000/cm^3) the electrostatic flow rate appears to decrease by about 50%. However, the data points in the range of >200,000/cm^3 and <75,000/cm^3 aerosol concentration were comparatively few and definite conclusions cannot be drawn.

Good correlation is observed between the RaC concentrations and the electrostatically collected activity (in a 25-30 minute interval after sampling) (Fig. 7.7). Figure 7.8 shows that the activity collected by the -1000 V open face disc (1.8 cm dia) is comparable to that of a 0.3 L/min pump (the pump flow rate was 3 L/min and the filter counts, after division by 10, are plotted in Fig. 7.8). An interesting comparison can be made with the earlier experiments reported in Chapter 6 where Fig. 6.3 shows that the performance of a similar -1000 V disc is comparable to that of a 0.3 L/min pump operated for 5 minute sampling, 3 minute waiting and 5 minute counting time.

The negative values for the electrostatic flow rate of RaC in Table 7.1 could be related to the negligibly small unattached fraction of RaC, which might indicate the absence of a charged fraction of RaC. Strong coulombic forces would therefore be absent and the electrostatic flow rate would therefore decrease. Unknown factors may also be responsible.

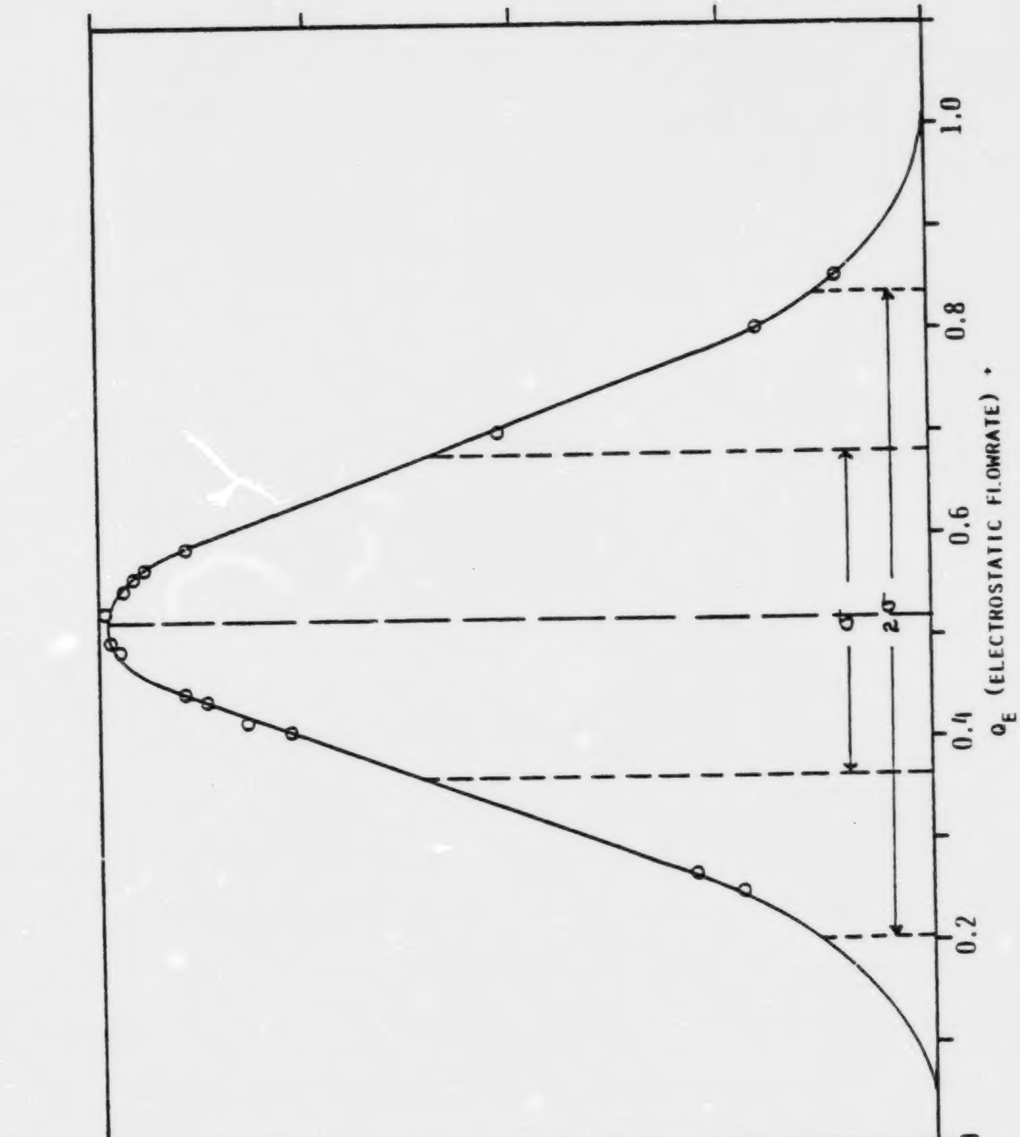

Fig. 9.1. Normal distribution of electrostatic flow rate of RaA.

The effective time in Table 7.1 is the parameter 't' used for calculating the unattached fractions of radon daughters as described in Chapter 2. The effective time (as termed by Evans) is the approximate time required to attain the prevailing disequilibrium conditions in accordance with Evans' estimations (Ev69).

Since radon concentrations were not required for evaluation of results the radon flow rates in Table 7.1 indicate the flowrate meter readings. Calibration was not carried out as only relative flow rates were needed.

9.2 Results from Electret Dosimeter Tests

From the charge stability data of electrets reported in Chapter 4 it was evident that foil electrets could hold surface potentials up to -2000 V for a minimum of one week. Foil electret material was used for making electrets in the first series of mine tests. Degradation of surface potential, however, called for improvements in the electrets used for the second mine tests. Electrets with much higher surface potentials ($\sim$-3800 V) were prepared, and these retained a maximum of -2300 V after five days exposure in the mines. Electret covers were changed when the surface potential was found to be less than 2000 V on the cover but greater than 2000 V on the electret underneath. However, each changing appeared to lower the electret charge. Electrets were changed during the second test in dosimeters no. 5 and 6 which behaved unpredictably. Sealing the dosimeter heads helped in eliminating contamination of the detector films and subsequent track cluster formation due to dust deposition. Contamination has also been observed in the CEA head (Ca82).

Two of the six dosimeters (dosimeters nos. 1 and 2) did not require a cover or electret change during the test period. Covers had to be replaced twice in dosimeter no. 3 and once in dosimeter no. 4. Dosimeters no. 5 and 6, which suffered maximum deterioration in electret potential, were both worn by underground mechanics. Dosimeter no. 5 suffered a setback when smear from glue was noticed under the electret surface (changed one day earlier) at the end of the third day of tests, while no. 6 had water drops inside on at least one occasion. Dosimeters nos. 5 and 6 were also found to be the dirtiest of the six dosimeters each day after mine exposure. Exposure readings from these latter dosimeters were rejected due to inconsistencies in their electret behaviour (Table 8.2). Relative to the reference CEA dosimeter exposure data, the three remaining passive dosimeters gave radon daughter Working Levels within $\leq$8% of the reference and thoron daughter Working Levels within $\leq$25% of the reference.

The electrostatic flow rate for the passive dosimeter was found to be about 1/4 - 1/3 of that of the CEA dosimeter, possibly as a result of a lower unattached fraction at the high aerosol concentrations in the diesel-operated mines wherein the test was carried out (Appendix A). As seen in Fig. 7.5, the electrostatic flow rate for a -100 V open face disc is 0.27 L/min at 270,000 aerosols/cm^3 in comparison with a mean electrostatic flow rate of 0.52 L/min (Fig. 9.1). In a dosimeter configuration the efficiency of collection would suffer a similar decrease in the electrostatic flow rate.

The presence of a smaller fraction of unattached radon daughters could result in a decrease in the collected activity due to a lower electrostatic aerosol migration velocity, as can be seen from the following explanation. If the attached fraction is large, the average size of the radon daughter-carrying particles will be large, and these large particles will experience large drag forces. Further, fewer coulombic forces would exist since the carrier aerosol would neutralize many radon daughter ions during the process of attachment. The presence of fewer coulombic forces would again reduce the electrostatic flow rate. Unfortunately, the behaviour of the electrostatic flowrate outside of the range of aerosol concentration of 70 000-180 000 particles/cm^3 cannot be determined from the data, which are too few in number outside the specified range. In high aerosol concentrations the unattached fraction of radon daughters would be negligible, thereby limiting the number of radon daughters existing as free ions. Polarization of aerosols alone would become the dominant mechanism responsible for electrostatic collection. The absence of coulombic forces could therefore cause a decrease in the electrostatic flow rate. In mine operations, this effect should not be significant because of the consistency of the aerosol concentration therein (see Appendix A). However, the relationship of electrostatic flow rate to aerosol concentration needs to be investigated more thoroughly in the high and low ranges of aerosol concentration.

There is no apparent reason why the voltage stayed above 2300 V for two dosimeters (no. 1 and no. 2), particularly given that the surface of the electret in dosimeter no. 2 looked dirty (with a splash-like mark on it) at the end of the very first day of tests. In three of the remaining four dosimeters, the surface potential started to decay after two of three days of exposure.

In general, the electret dosimeter proved to be rugged enough for use in the mine atmosphere and no part of the dosimeters suffered any physical damage in the mine tests.

10. SUMMARY, CONCLUSIONS AND RECOMMENDATIONS

10.1 Summary and Conclusions

The open face disc measurements established trends of radon daughter deposition in an electrostatic field with varying humidity, aerosol size and concentration, unattached fraction of radon daughters and radon daughter concentrations. The results allowed an electrostatic flow rate, similar to a pump flow rate, to be defined. The electrostatic flow rate was found to be reasonably constant for unattached fractions of less than 40%, particle sizes greater than 0.04 μm and aerosol concentrations between 70,000/cm^3 and 180,000/cm^3. Although earlier experiments had indicated that the effect of humidity was noticeable in the higher humidity range (Fig. 7.1), this effect was not found to be cause for concern in later experiments (Table 7.1). The electrostatic flow rate was found to change only at very high (>180,000/cm^3) or very low (<70,000/cm^3) aerosol concentrations, possibly corresponding to lower and higher unattached fractions, respectively.

Electrets were formed with two different materials, a commercial 'electret-foil' and a locally aluminized Teflon FEP film, both 25 μm thick. The former material could retain surface potentials only up to ∿2000 V. The latter material could, however, retain potentials up to or greater than 3000 V for at least a week and was therefore selected for use in the final dosimeter tests.

Two dosimeter tests were carried out in Denison mines, Elliot Lake, for a period of up to five days in each case. In the first test, although the data were marred by contamination of the track etch detectors, valuable information was obtained to allow improvements to be made in the electret surface potentials and protection of the detectors from dust. Improved dosimeters with up to -3800 V electrets were tested in Denison Mines for a five-day period. Four of the six dosimeters were compared with reference CEA dosimeters exposed simultaneously. The efficiency of the electret dosimeter was found to be about 1/3 that of the CEA dosimeter. Three of the four dosimeters agreed to within 8% of the radon daughter Working Level recorded by the CEA dosimeter and within 25% of the thoron daughter Working Level.

The major conclusions with respect to electret dosimeters can be summarized as follows:

i) Electrostatic deposition of aerosols on charged surfaces can be achieved in a manner similar to that on filters driven by pumps.

ii) Depending upon the area of the charged disc, an electrostatic flow rate for radioactive aerosols can be defined and correlated with the flow rate of a pump drawing similar aerosols through a filter. Unlike the pump flow rate, however, the electrostatic flow rate is not identical for RaA, RaB and RaC in the air. Over the 5 minute sampling time, the electrostatic flow rate of RaC was found to be negligibly small whereas for RaB it was equal to or less than that for RaA. This result could have been due to differences in the charge state of the radon daughter.

iii) The charged fraction and the unattached fraction may not be the same species but the experiments consistently indicated relatively greater electrostatically deposited activity in the presence of higher unattached fractions.

iv) An electret surface potential greater than (-)2500 V was found to be suitable for the passive dosimeter developed in this work.

v) The success of the electret formation technique depends upon the correct combination of formation voltage and time, cleanliness of surfaces and good contact between surfaces.

vi) The electret retains its surface potential better in a covered than in an uncovered state. The proposed dosimeter configuration provides a reasonable cover for the electret in order that it may stay charged for longer periods.

vii) Electrets with surface potentials less than 1000 V have been known to be stable over long periods (∿years). However, higher surface potentials (greater than (-)2500 V) can be retained for no more than ∿15 days under ambient room conditions and for up to a week if exposed to a mine environment.

viii) A Teflon FEP (non-aluminized) cover provides adequate protection of the electret surface, and the electret charge (of the same sign) appears on the cover as a result of induced polarization. Changing the cover results in some loss of charge from the electret surface.

ix) Contamination from dirt or moisture settling on the electret cover does not necessarily destroy its charge.

x) A diffusion barrier must be provided in order to make a passive dosimeter reliable. However this requirement considerably decreases the efficiency of the dosimeter.

xi) The electrostatic flow rate was found to be constant for 0.03 μm < particle diameter < 0.09 μm, 70,000/cm^3 < aerosol concentration < 180,000/cm^3 and unattached fraction < 0.40. The data do not allow conclusions to be drawn about the electrostatic flow rate outside of these particle diameters, aerosol concentrations and unattached fraction ranges.

xii) The dosimeter design can be used for one week in its present state. However improvements in design and in electret performance are desirable.

10.2 Recommendations

The following recommendations are made for future work:

i) The nature of unattached fractions of radon daughters is not yet fully understood. The present work suggests that higher charged fractions are associated with higher unattached fractions. It is recommended that further study be made of the nature of unattached radon daughters and the relationship of the unattached fraction to the charged fraction.

ii) The existing charged fraction measurement methods should be modified to correct for the neutral particles collected due to induced polarization. Since induced polarization is independent of the sign of the electric field, required corrections can be made by reversing the sign of the field after appropriate calibration.

iii) It is a well-known fact that mine aerosols are of diverse chemical nature. However, some information on their collective electrical behaviour is required to understand the electrostatic diffusion mechanism in a mine atmosphere. It is therefore recommended that the electrical properties of mine aerosols be studied. In particular, the dielectric constant of mine aerosols should be determined.

iv) In view of the difference in aerosol concentrations in diesel and non-diesel mines and the different nature of aerosols in the two types of mines, a comparative large scale evaluation of passive dosimeter performance should be carried out in such mines. The relationship between the electrostatic collection efficiency and the aerosol concentration needs more study.

v) Electret formation techniques and materials have been studied in the past mainly for obtaining surface potentials of less than (-)1000 V. It is recommended that the existing techniques be improved and new avenues explored to obtain electrets with better stability and surface potentials greater than (-)2500 V.

vi) The present work was primarily directed towards passive collection of radon daughter aerosols and attention was not paid to the detector system. However, in view of the tediousness of the readout procedure with the track etch detectors, it is recommended that alternative energy discriminatory detectors be used.

vii) The design of the passive dosimeter developed in this work needs to be optimized with respect to the geometry of the system to attain the maximum possible efficiency. The diffusion barrier design also needs to be improved. A small mesh-size-screen in place of the holes in the diffusion barrier may allow better control of accumulation of dust inside the dosimeter. Also, a larger external housing may improve the efficiency of the electret dosimeter.

REFERENCES

An73 Anderson, E.W., Blyler, L.L., Johnson, G.E., Link, G.L., in Proc. Electrochemical Society, Princeton 1973, pp. 424-435.

Ba66 Baust, E., 1966, "The Attachment of Radioactive Atoms and Ions to Spherical Aerosol Particles", Zeit. für Physik, 199, 187.

Ba78 Bauser, H. and Ronge, W., 1978, "The Electret Ionization Chamber: A Dosimeter for Long Term Personnel Monitoring", Health. Phys., 34, 97-102.

Bh74 Bhatnagar, C.S., 1964, Ind. J. Pure Appl. Phys., 2, 331.

Bi71 Billard, F., Madelain, G., Chapuis, A., Fontan, J. and Lopez, A., "Contribution to the Study of Air Pollution in Uranium Mines", Radioprotection, 6(1), 45.

Bi83 Bigu, J., 1983, Personal communication.

Br53 Brazier, L.G., 1953, Engineer, 196, 637.

Br66 Bricard, J. and Pradel, J., 1966, "Electric Charge and Radioactivity of Naturally Occurring Aerosols:, in 'Aerosol Science', (C.N. Davies, ed.), Academic Press, New York, pp. 87-108.

Br67 Brock, J.R., 1967, "The Thermal Force in the Transition Region", J. Colloid Sci., 23, 448-452.

Br71 Broome, D. and Khan, I., 1971, "The Mechanism of Soot Release from Combustion of Hydrocarbon Fuels", in 'Air Pollution Control in Transport Engines', p. 185, Institution of Mech. Engrs. London.

Br81 Brown, R.C., 1981, "Capture of Dust Particles in Filters by Line-Dipole Charged Fibres", J. Aerosol Sci., 12(4), 349-356.

Bu78a Busigin, A., 1978, "Measurement of the Total and Radioactive Aerosol Size Distribution in a Uranium Mine", M.A.Sc. thesis, University of Toronto.

Bu78b Busigin, A., van der Vooren, A.W. and PXillips, C.R., 1978, "Attached and Unattached Radon Daughters: Measurements and Measurement Techniques in Uranium Mines and in the Laboratory", AECB-1169 (Dec. 1978).

Bu80 Busigin, A., van der Vooren, A.W. and Phillips, C.R., 1980, "A Technique for Calculation of Aerosol Particle Size Distributions from Indirect Measurements", Aerosol Sci., 11, 359-366.

Bu81 Busigin, A., van der Vooren, A.W., Babcock, J. and Phillips, C.R., 1981, "The Nature of Unattached RaA (^{218}Po) Particles", Health Phys., 40, 333.

Bu83 Busigin, C.J., Busigin, A. and Phillips, C.R., 1983, "Measurement of Charged and Unattached Fractions of Radon and Thoron Daughters in Two Canadian Uranium Mines", Health Phys., 44(2), 165-167.

Ca80 Cameron, J. and Mascarenhas, S., 1980, "A Cylindrical Electret Ionization Chamber", Nuc. Inst. Meth., 175, 117-118.

Ca82 Carson, D.W., Townsend, M.G. and Tremblay, R.J., "Mixtures of Radon ant Thoron Daughters in Underground Atmospheres: Measurement Procedures, a Portable α-Spectrophotometer, a Semi-Automatic Spark Counter for Reading Track Etch Films from Personnel Dosimeters", Proc. Conf. on 'Radiation Hazards in Mining', Golden, CO. 845.

Ch56 Chamberlain, A.C. and Dyson, E.D., 1956, "The Dose to the Trachea and Bronchi from the Decay Products of Radon and Thoron", Brit. J. Radiology, 29(342),

Ch 70 Chapuis, A., Lopez, A., Fontan, J., Billard, F. and Madelaine, G.J., 1970, "Spectre Granulometrique des Aerosols Radioactifs dans une Mine d'Uranium", Aerosol Sci., 1, 243.

Ch72 Chudleigh, P.W., 1972, "Charging of Polymer Foils Using Liquid Contacts", App. Phys. Lett., 21(11).

Ch76 Chudleigh, P.W., 1976, J. App. Phys., 47, 4475.

Ch78 Chapuis, A.M., Duport, P. and Zettwoog, P., 1978, "Individual Dosimeter for Radon and Thoron Daughters", Proc. Specialist Meeting of NEA on Radon Monitoring, Paris, OECD.

Ch81 Chittaporn, P., Eisenbud, M. and Harley, N.H., 1981, "A Continuous Monitor for the Measurement of Environmental Radon", Health Phys., 41, 405-410.

Co53 Cohn, S.H., Skow, R.K. and Gong, J.K., 1953, A.M.A. Arch. Ind. Hyg., 7, 500.

Co77 Coover, S.R., Rosenboro, J.H. and Watson, J.E.Jr., 1977, "Electret Charger for Pocket Ion Chamber Dosimeters", Health Phys., 33, 474-477.

Cr66 Craft, B.F., Oser, J.L. and Norris, F.W., 1966, "A Method of Determining Relative Amounts of Combined and Uncombined Radon Daughter Activity in Underground Uranium Mines", Amer. Ind. Hyg. Assoc. J., 27, 154.

Cr67 Cross, J.D., 1967, "Thermoelectrets", 'Static Electrification', Inst. of Physics, London, pp. 22-28.

Da74 Davis, C.N., 1974, "Size Distribution of Atmospheric Particles", J. Aerosol Sci., 5, 293.

Eg19 Eguchi, M., 1919, "On Dielectric Polarization", Proc. Physico-Mathematical Soc. Japan, Series III, 1, 326.

Ep24 Epstein, P.S., 1924, Phys. Rev., 23, 710.

Ev69 Evans, R.D., 1969, "Engineers Guide to the Elementary Behaviour of Radon Daughters", Health Phys., 17, 229-252.

Fa39 Faraday, M., 1839, "Experimental Researches in Electricity", Richard and John Edward Taylor, London.

Fa71 Fabel, G.W. and Henisch, H.K., 1971, "Polymer Thermoelectret Dosimetry", Phys. Stat. Solidi (a) 6, 535.

Fe53 Feaster, G., 1953, "Electrets", Ph.D. Thesis, University of Kansas.

Fo69 Fontan, J., Blanc, D., Huertas, M.L. and Marty, A.M., 1969, "Mesure de la Mobilite et du Co-efficient de Diffusion des Particles Radioactives", in 'Planetary Electrodynamics', (S.C. Coroniti and J. Hughes, editors), Vol. 1, Gordon and Breach, New York.

Fr61 Fridkin, V.M. and Zheludev, I.S., 1961, "Photoelectrets and the Electrophotographic Process", Consultants Bureau, New York.

Fr77 Friedlander, S.K., 1977, "Smoke, Dust and Haze: Fundamentals of Aerosol Behaviour", John Wiley and Sons, Toronto.

Fu67 Fusamura, N., Kurosawa, R. and Maruyama, M., 1967, "Determination of f-value in Uranium Mine Air", in 'Assessment of Airborne Radioactivity in Nuclear Operations', IAEA, Vienna, p. 213.

Fu64 Fuchs, N.A., 1964, "The Mechanics of Aerosols", McMillan, Co. New York.

Fu82 Fu, M.A., 1982, "Radioactive Aerosol Plate-out in Alpha Dosimeter Heads", M.A.Sc. thesis, University of Toronto.

Ge35 Gemant, A., 1935, Phil. Mag., 20, 929.

Ge53 Gemant, A., 1953, "Electrets, Their Mechanism and Potentialities", Direct Current, Sept. 1953, pp. 145-147.

Ge69 George, A.C. and Breslin, A.J., 1969, "Deposition of Rn Daughters in Humans Exposed to Uranium Mine Atmospheres", Health Phys., 17, 115.

Ge72 George, A.C. and Hinchliffe, L., 1972, "Measurement of Uncombined Radon Daughters in Uranium Mines", H. Phys., 23, 791-803.

Ge77 George, A.C. and Breslin, A.J., 1977, "Measurements of Environmental Radon with Integrating Instruments", presented at Atomic Industrial Forum, Uranium Mill Monitoring Workshop, Albuquerque, N.M.

Gr32 Gray, S., 1732, Phil. Trans. Roy. Soc. London, Ser. A: 37, 285.

Gr44 Gross, B., 1944, "Experiments on Electrets", Phys. Rev., 66, 26-28.

Gr49 Gross, B., 1949, J. Chem. Phys., 17, 866.

Gr58 Gross, B., 1958, J. Polymer Sci., 27, 135.

Gr59 Gross, B., 1959, Z. Phys., 155, 479.

Gr63 Gross, B. and Murphy, P.V., 1963, J. Chem. Phys., 38(10), 2400.

Gr71 Gross, B., 1971, "The Electret", Endeavour, 30, 111, 115-119.

Gu48 Gutmann, F., "The Electret", Revs. Mod. Phys., 20(3), 457-472.

He92 Heaviside, O., 1892, "Electrical Papers", Chelsea, New York, pp. 488-493.

ICRP59 Publication 2, Report of Committee II on Permissible Dose for Internal Radiation, Pergamon Press, Oxford.

Ja61 Jacobi, W.V., 1961, "The Attachment to Natural Aerosols of Naturally Occurring Radioactive Aerosols", Geofisica Pura e Applicata, 50, 260.

Ja82 Jackson, P.O., Cooper, J.A., Langford, J.C. and Petersen, M.R., 1982, "Characteristics of Attached Radon-222 Daughters under both Laboratory and Underground Uranium Mine Environment", Proc. Conf. on 'Radiation Hazards in Mining', Golden, CO, 1031-1042.

Je70 Jefimenko, O. and Walker, D.K., 1970, Conf. on Dielectric Materials Measurements and Applications, IEEE, London, 146-149.

Jo68 Johnson, V.A., 1968, "Electrets - Applications Unlimited?", in 'Electrets and Related Electrostatic Charge Storage Phenomena', Electrochem. Soc., New York, pp. 100-103.

Ka69 Kawano, M., Ikebi, Y. and Shimo, M., 1969, "Measurement of the Attachment Coefficient of Small Ions and Radioactive Ions to Condensation Nuclei", in 'Planetary Electrodynamics' (S.C. Coroniti and J. Hughes, editors), Vol. 1, Gordon and Breach New York.

Ke62 Keefe, D. and Nolan, P.J., 1962, Proc. Royal Irish Academy, 62, 43.

Ko75 Kotrappa, P., Bhanti, D.P. and Dhandayutham, R., 1975, "Diffusion Sampler Useful for Measuring Diffusion Coefficients and Unattached Fraction of Radon and Thoron Decay Products", Health Phys., 29, 155-162.

Ko76 Kotrappa, P. Bhanti, D.P. and Raghunath, B., 1976, Diffusion Coefficients for Unattached Decay Products of Thoron - Dependence on Ventilation and Relative Humidity, 31, 378-380.

Ko78 Konikoff, J.J. and West, J.E., 1978, Ann. Rep. Conf. Elect. Insul. Diel. Phenom. (NAS, Washington), 304-310.

Ko80 Kotrappa, P., Gupta, P.C. and Dua, S.K., 1980, "Design and Performance of a Teflon Electret Dosimeter Charger", Health Phys., 39, 566-568.

Ko81 Kotrappa, P., Dua, S.K., Gupta, P.C. and Kayya, Y.S., 1981, "Electret - A New Tool for Measuring Concentrations of Radon and Thoron in Air", Health Phys., 41, 35-46.

Ko82 Kotrappa, P., Dua, S.K., Pimpale, N.S., Gupta, P.C., Nambi, S.V., Bhagwat, A.M. and Soman, S.D., 1982, "Passive Measurement of Radon and Thoron using TLD or SSNTD on Electrets", Health Phys., 43, 399-404.

Kr55 Kraemer, H.F., Johnstone, H.F., 1955, "Collection of Aerosol Particles in Presence of Electrostatic Fields", Ind. & Eng. Chem., 47(12), 2426-2434.

Kr76 Kruger, J. and Andrews, M., 1976, "Measurement of the Attachment Coefficients of Rn-220 Decay Products to Monodisperse Polystyrene Aerosols", J. Aerosol Sci., 7, 21-36.

Kr79 Kruger, J. and Nöthling, J.F., 1979, "A Comparison of the Attachment of the Decay Products of Radon-220 and Radon-222 to Monodisperse Aerosols", J. Aerosol Sci., 10, 571-579.

La60 Lassen, L. and Rau, G., 1960, "The Attachment of Radioactive Atoms to Aerosols", Zeitschrift für Physik, 160, 504.

La70 Lapple, C.E., 1970, "Electrostatic Phenomena with Particulates", in 'Advances in Chemical Engineering', Vol. 8.

Li56 Linden, E.G., 1956, "Electrets", IRE Convention Record, New York, Vol. 4, Pt. 3.

Lu73 Luus, R. and Jaakola, T.H.I., 1973, "Optimziation by Direct Search and Systematic Reduction of the Size of Search Region", A.I.Ch.E. Journal, 19(4), 760.

Ma66 Madelaine, G., 1966, "Behaviour of Radon and Thoron Daughters in Aerosol-free Air", Tellus, 18(2), 593.

Ma73 Mascarenhas, S., 1973 in "Electrets, Charge, Storage and Transport in Dielectretics", Electrochem. Soc. Princeton, N.J., pp. 650-656/657-660.

Mc72 McLaughlin, J.P., 1972, "The Attachment of Radon Daughter Products to Condensation Nuclei", Proc. R.I.A., Vol. 72, Sect. A, 51.

Me73 Mercer, T.T., 1973, "Aerosol Technology in Hazard Evaluation", p. 164, Academic Press, New York and London.

Me80 Menon, V.B., Kotrappa, P. and Bhanti, D.P., 1980, "A Study of the Attachment of Thoron Decay Products to Aerosols Using an Aerosol Centrifuge", J. Aerosol Sci., 11, 87-93.

Mu73 Murphy, P.V. and Merchants, S., 1973, in 'Electrets, Charge Storage and Transport in Dielectrics', Electrochem. Soc. Princeton, N.J., pp. 627-649.

Na37 Nadjakoff, G., 1937, C.R. Acad. Sci., 204, 1865.

Ne78 Nelson, G.O., Bergman, W., H.H. Miller, Taylor, R.D., Richards, C.P. and Biermann, A.H., 1978, "Enhancement of Air Filtration Using Electric Fields", Amer. Ind. Hyg. Assoc. J., 39, 472-479.

Ni50 Nielsen, 1950, "What about Electrets? How Soon Will They be Workable Design Tools?", Elec. Manufact. Dec. 1950.

Pa64 Palmer, H.E., Perkins, R.W. and Stuart, B.O., 1964, "The Distribution and Deposition of Radon Daughters Attached to Dust Particles in the Respiratory Systems of Humans Exposed to Uranium Mine Atmospheres", Health Phys., 10, 1129.

Pe68 Parlman, M.M., 1968, "Review of Phenomenological Theories of Electrets", in 'Electrets and Related Electrostatic Charge Storage Phenomena', edited by M.M. Perlman, Electrochem. Soc., New York.

Pe72 Perlman, M.M. and Reedyk, C.W., 19 72, "Polycarbonate Electrets" 'Electret devices for air pollution control' (Thomas Kallard, editor), pp. 79-83, Optosonic Press, 1972.

Pe79 Perlman, M.M., Kao, K.J. and Bamji, S.S., 1979, "Silicone Resin Electrets", J. App. Phys., 50(5), 3622-2627.

Pi72 Pillai P.K.C., Jain, K. and Jain, V.K., 1972, "Thermoelectrets and Their Applications", Phys. Stat. Sol. (a) 13, 341.

Po68 Porstendörfer, J., 1968, "The Diffusion Coefficients and Mean Free Paths of the Neutral and Charged Radon Decay Products in Air", Zeitschrift für Physik, 213, 384.

Po73 Pohl, H.A., 1973, "Non-uniform Field Effects: Dielectrophoresis" in 'Electrostatics and Its Applications', ed. by A.D. Moore, Wiley, New York.

Po78 Porstendörfer, J. and Mercer, T.T., "Diffusion Coefficients of Radon Decay Products and Their Attachment Rate to the Atmospheric Aerosols", Proc. Symp. 'Natural Radiation Environment III', Houston, Texas, April 23-28.

Po78a Porstendörfer, J. and Mercer, T.T., 1978, "Adsorption Probability of Atoms and Ions on Particle Surfaces in Submicrometer Size Range", J. Aerosol Sci., 9, 469-474.

Po79 Porstendörfer, J. and Mercer, T.T., 1979, "Influence of Electric Charge and Humidity upon the Diffusion Coefficient of Radon Decay Products", Health Phys., 37, 191-199.

Po79a Porstendörfer, J., Röbig, G. and Ahmed, A., 1978, "Experimental Determination of the Attachment Coefficients of Atoms and Ions on Monodisperse Aerosols", J. Aerosol Sci., 10, 21-28.

Pr79 Prodi, F., Santachiara, G. and Prodi, V., 1979, "Measurements of Thermophoretic Velocities of Aerosol Particles in the Transition Region", J. Aerosol Sci., 10, 421-425.

Ra68 Raabe, O.G., 1968, "Measurement of the Diffusion Coefficient of RaA", Nature, 217, 1143.

Ra68a Raabe, O.G., 1968, "The Adsorption of Radon Daughters to Some Polydisperse Submicron Polystyrene Aerosols", Health Phys., 14, 397.

Ra69 Raabe, O.G., 1969, "Concerning the Interactions that Occur Between Radon Decay Products and Aerosols", Health Phys., 17, 177-185.

Ra71 Raabe, O.G., 1971, "Particle Size Analysis Utilizing Grouped Data and the Log-normal Distribution", J. Aerosol Sci., 2, 289-303.

Ra79 Raghunath, B. and Kotrappa, P., 1979, "Diffusion Coefficients of Decay Products of Radon and Thoron", J. Aerosol Sci., 10, 133-138.

Ri62 Rivers, R.D., 1962, "Non-ionizing Electrostatic Air Filters", ASHRAE Journal, Feb., 37-40.

Ro82 Rose, V.E. and Perkins, J.L., 1982, "Passive Dosimetry - State of the Art Review", Am. Ind. Hyg. Ass. J., 43(8), 605-621.

Sc62 Schaeffer, R.M. and Oughton, C.D., 1962, J. Opt. Soc. Am., 34, 1787.

Se38 Selenyi, P., 1938, J. App. Phys., 9, 637.

Se62 Sessler, G.M. and West, J.E., 1962, J. Acous. Soc. Am., 34, 1787.

Se70 Sessler, G.M. and West, J.E., 1970, App. Phys. Lett., 17, 507.

Se72 Sessler, G.M. and West, J.E., 1972, "Production of High Quasi-permanent Charge Densities on Polymer Foils by Application of Breakdown Fields", J. App. Phys., 3, 43.

Se73 Sessler, G.M., and West, J.E., 1973, "Electret Transducers: A Review", J. Acous. Soc. Am., 53(6), 1589-1600.

Se75 Sessler, G.M. and West, J.E., 1975, "Electrets Formed by Low Energy Electron Injection", J. Electrostat., 1, 111-123.

Se80 Sessler, G.M. and West, J.E., 1980, in "Electrets", Topics in Applied Physics, 33, Springer Verlag, New York.

Si56 Silverman, L., Connors, E.W.Jr., and Anderson, D.M., 1956, "Electrostatic Mechanisms in Aerosol Filtration by Mechanically Charged Fibre Media and Related Studies", USAEC Report NYO 4610, Harvard Univ., Sept. 4, 1956.

St82 Stranden, E and Berteig, L., 1982, "Radon Daughter Equilibrium and Unattached Fraction in Mine Atmospheres", Health Phys., 42(4), 479-487.

Th59 Thomas, J.W. and Woodfin, E.J., 1959, "Electrified Fibrous Air Filters", AIEE Trans. Pt. II (Applications and Industry), 78, 276-278, Nov. 1959.

Th70 Thomas, J.W., 1970, "A Study of the Two-Filter Method for Rn-222", Health Phys., 18, 113.

Tu71 Turnhout, J. Van., 1971, Polymer Journal, 2(2), 173-191.

Tu75 Turnhout, J. Van., 1975, "The Use of Polymers for Electrets", J. Electrostat., 1, 147.

Tu75a Turnhout, J. Van., 1975, "Thermally Stimulated Discharge of Electrets", Elsevier, Amsterdam.

Tu79 Turnhout, J. Van., Albers, J.H.M., Hoenveld, W.J., Adamse, J.W.C., and Rossen, L.M. Van., "Non-woven Electret Fibre: A New Filtering Medium of High Efficiency", in 'Static Electrification', Int. Phys. Conf. Ser. No. 48, 337-349.

Tu80 Turnhout, J. Van., Adamse, J.W.C., and Hoeneveld, W.J., 1980, "Electret Filters for High Efficiency Air Cleaning", J. Electrostat., 8, 369-379.

Ty55 Tyler, R.W., Weble, J.H. and York, W.C., 1955, J. App. Phys., 26, 61.

Va71 VanPelt, W.R., 1971, "Attachment of Rn-222 Decay Products to a Natural Aerosol as a Function of Particle Size", Ph.D. Thesis, New York University.

Va82 van der Vooren, A., Busigin, A. and Phillips, C.R., 1982, "An Evaluation of Unattached Radon Daughter Measurement Techniques", Health Phys., 42, 801.

Vu76 Vuk, C.T., Jones, M.A. and Johnson, J.H., 1976, "The Measurement and Analysis of the Physical Character of Diesel Particulate Emissions", SAE paper No. 760131, Feb. 1976.

Wa66 Waldmann, L. and Schmitt, K.H., 1966, "Thermophoresis and Diffusiophoresis of Aerosols", Chap. VI in Davies, C.N. (Ed.), 'Aerosol Science', Academic Press, New York.

We14 Wellisch, E.M., 1914, "Experiments on the Active Deposits of Radium", Phil. Mag., 28(166), 417.

Wi53 Wiseman, G.G. and Linden, E.G., 1953, "Electrets", Elec. Eng., 869-872.

Wi53a Wieder, H.H. and Kaufman, S., 1953, "Plastic Electrets", J. App. Phys., 24(2), 156-161.

Wi66 Wilkening, M.H., Kawano, M. and Lane, C., 1966, "Radon Daughter Ions and Their Relation to some Electrical Properties of the Atmosphere", Tellus, 18, 2.

Wi78 Wilkening, M.H., 1978, "Radon Daughter Ions in the Atmosphere", Symp. on Natural Radiation Environ., Houston, Texas.

NOMENCLATURE

a	$12 \pi\mu Q$ or radius of the collecting disc
B	Attachment coefficient (cm^3/s)
C	Coulombs (Chaps. 1-4, 6-10)
	Number of alpha particles recorded by the detector per unit time (Chap. 5)
C(d)	Aerosol size distribution function
C_{RaA}	Concentration of RaA (pCi/L)
C_{RaB}	Concentration of RaB (pCi/L)
C_{RaC}	Concentration of RaC (pCi/L)
C_p	Slip correction factor
C_t	Thermophoretic velocity
d	Aerosol diameter (μm)
$\bar{d}$	Count median diameter (μm)
d_p	Particle size (Chap 5)
D	Counts recorded in the counting interval (α,β) (Chap. 5)
	Diffusion coefficient (cm^2/s) (Chapts. 1-4,6-10)
D_i	Diffusion coefficient of the radioactive aerosols (Chap. 5)
e	Electronic charge ($= 1.6 \times 10^{-19}$ coulombs)
E	Electric field strength (V/cm)
E_i	Internal field of an electret (V/cm)
f	Friction coefficient
f_1	Charged fraction of aerosols
f_A	Unattached fraction of RaA
f_B	Unattached fraction of RaB
f_C	Unattached fraction of RaC

F	thermophoretic force
F_C	Coulombic force (dynes)
F_e	Total electrostatic force (dynes)
F_p	force due to induced polarization in dielectric particles (dynes)
F_p'	Force due to induced polarization in conducting particles (dynes)
H	Distance between hot and cold plates
J_i	Flux of radioactive aerosols towards the detector plate
k	Thermal conductivity of the gas
k_p	Thermal conductivity of the particle (W/mK, watts/metre, °K)
K	Mobility of an ion (cm^2/v-s)
K_1	Relative dielectric constant of the medium
K_2	Relative dielectric constant of the particle
l	Mean free path of the gas, about 0.065 μm in air at N.T.P (Chap. 5).
ℓ	Thickness of the electret film (Chap. 4)
M_i	Number of atoms of radioactive aerosols transferred to the disc per unit time
n	Number of elementary charges per particle
n_i	Concentration of radioactive aerosols
$n_{i\infty}$	Atmospheric concentration of radioactive aerosols
$n_i{}^*$	$n_i/n_{i\infty}$
N_i	Number of atoms of radioactive aerosols on the disc surface (Chap. 5) Number of atoms of radon or its daughters (Chaps. 1-4, 6-10)
N_{if}	Number of atoms of unattached radon daughters
$\bar{N}_i$	Number of atoms of radionuclide at the end of sampling
P	Pressure

P_e	Dimensionless parameter $\frac{a^2 c_t}{D_i H}$
P	Dipole vector
Q	Thermal creep first code coefficient, $\frac{3}{4}\left(\frac{d_p}{\pi T}\right)^{1/2}$
Q_e	Electrostatic flow rate (cm^3/s)
Q_E	Electrostatic flow rate (L/min)
R	Particle radius
R_1	$\frac{\lambda_1 \lambda_2 \lambda_3}{(\lambda_1 - \lambda_2)(\lambda_3 - \lambda_2)}$
R_2	$\frac{\lambda_1 \lambda_2 \lambda_3}{(\lambda_1 - \lambda_2)(\lambda_1 - \lambda_3)}$
R_3	$\frac{\lambda_2 \lambda_3}{\lambda_3 - \lambda_2}$
r	radial coordinate
r*	$\frac{r}{a}$
S	Area of the collecting disc (Chap. 5)
S_m	Constant related to the reflection coefficient of molecules striking the particle surface
S_t	Constant related to the thermal accommodation coefficient
T	Temperature or sampling time
T_0	Cold temperature of the bottom plate
T_1	Hot temperature of the top plate
t	Collection time
v	Migration (or drift) velocity of particles in an external force field (cm/s)
$\bar{v}$	Mean thermal velocity of radon daughter atoms or ions (cm/s)
v_e	Electrostatic drift velocity (cm/s)
V	Volts
V_m	Maximum surface potential that can be retained by an electret
x_1	Dielectric support thickness (cm)

x_2	Thickness of air gap between electret surface and electrode (cm)
x_3	Thickness of electret film (μm)
z	Axial coordinate
z^*	z/H
Z	Aerosol concentration ($\#/cm^3$)

Greek Symbols

ν	Kinematic viscosity of the gas
α	Accommodation coefficient (~ 0.9) or beginning of a counting interval (Chap. 5)
	Recoil fraction of RaA which becomes unattached RaB upon decay (Chap. 1-4, 6-10)
α_p	Polarizability of a dielectric particle
β	End of counting interval (Chap. 5)
θ	Time after collection
μ	Coefficient of viscosity of the gas
λ	Radioactive decay constant of the aerosol (Chap. 5)
λ_i	Radioactive decay constant of radon daughters (Chaps. 1-4, 6-10)
λ_s	Attachment rate of radon daughter atoms to aerosols (#/s)
σ	Dimensionless coefficient defined in the relationship between the slip velocity at the particle surface and the temperature gradient in the gas, ∇T (Chap. 5)
	Surface charge density (C/cm^2) (Chaps. 1-4, 6-10)
σ_g	Geometric standard deviation of aerosol size distribution
η	Counting coefficiency
π	Dimensionless parameter $\frac{C_t}{\lambda_i H}$

ϵ_0	Permittivity of free space ($=8.854 \times 10^{-12} \frac{C}{V-m}$)
ϵ	Dielectric constant

Subscripts: i = 1 for RaA, i = 2 for RaB, i = 3 for RaC (Chap. 5)

i = 1 for Rn, i = 2 for RaA, i = 3 for RaB, i = 4 for RaC (Chaps. 1-4, 6-10)

APPENDIX A: AEROSOL AND ACTIVITY SIZE DISTRIBUTION MEASUREMENTS

A.1 Theoretical Aspects

A lognormal size distribution can be represented by a count median diameter, $\bar{d}$, and a geometric standard deviation σ_g. Busigin (Bu78) developed a technique to calculate the parameters $\bar{d}$ and σ_g from diffusion battery data. A diffusion battery is an assembly of a number of cylindrical or rectangular channels. The comparative penetration of aerosols through different sizes of diffusion batteries at similar flow rates can yield an estimate of the aerosol size distribution. The calculation technique used is based upon in iterative, direct search optimization technique utilizing random numbers and reduction of the size of the search region developed by Luus and Jaakola (Lu73). An optimal fit is obtained of the kth approximation of the size distribution $n^{(k)}(d)$ to the actual distribution n(d) using the experimental diffusion battery data.

The probability of a particle passing through a diffusion battery is

$$P = \sum_{i=1}^{\infty} a_i e^{-b_i \mu} \qquad (A.1.1)$$

where $\mu = 2\,WLD/FH$ for a diffusion battery composed of rectangular plates.

W = width of each rectangular plate (cm)

L = length of each rectangular plate (cm)

D = diffusion coefficient of the particle (cm^2/s)

F = volume flow rate through a single channel in the diffusion battery (cm^3/s)

2H = height of a plate in the diffusion battery (cm) ($2H \ll W$).

The penetration constants a_i and b_i for parallel plate diffusion batteries are:

$a_1 = 0.91035$, $a_2 = 0.5314$, $a_3 = 0.01529$, $a_4 = 0.0068$,
$b_1 = 1.88517$, $b_2 = 21.4317$, $b_3 = 62.3166$, $b_4 = 124.5$

The experimentally measured penetration, g, of aerosols through a diffusion battery is related to the theoretically calculable penetration probability, $P_j\cdot(d)$ by

$$g_j = \int_0^\infty P_j\cdot(d)\; n(d)\; d(d) \qquad \text{(A.1.2)}$$

where n(d) is the required aerosol size distribution.
The aim of the optimization calculation therefore is to minimize the difference between g_j as given by eqn. (A.1.2) and the approximation $g_j^{(k)}$ where $g_j^{(k)} = \int_0^\infty P_j(d)\; n^{(k)}(d)\; d(d)$.

Some constraints on the values of d and σ_g are required to ensure a reasonable solution. The computer program based on this technique is given in Section A.2. The diffusion batteries with appropriate couplings for filter holders and sampling pumps used for measurements in the present work are shown in Fig. A.1.1. The dimensions of diffusion batteries are given in Table A.1.1.

At a sampling rate of 3 L/min, diffusion battery (D.B.) no. 3 would remove 50% of the 0.02 μm particles, D.B. no. 4 would remove 50% of the 0.08 μm particles and D.B. no. 5 would remove 24% of 0.2 μm particles. The experimental method for estimating size distribution of aerosols and of RaA, RaB and RaC is described in Section A.3.

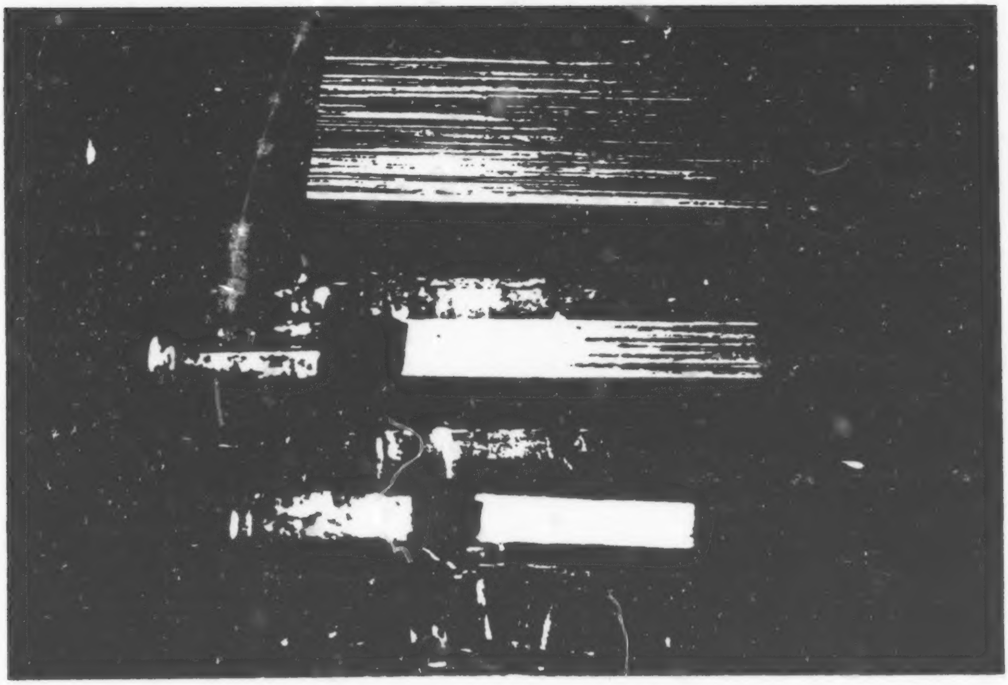

Fig. A.1.1. Diffusion batteries for aerosol and activity size distribution measurements. Air is drawn through a filter placed at the outlet (the left end of each battery in the photograph). Each diffusion battery is a stack of rectangular plates. Each rectangular plate is of length L and width W. H is the spacing between two neighbouring plates.

TABLE A.1.1.

Dimensions of Diffusion Batteries

D.B. no.	No. of channels	Width (cm)	Length (cm)	Spacing between plates (cm)
3	25	10	19	0.08
4	50	10	30	0.04
5	140	10	43	0.04

A.2 Experimental Data

The aerosol size distribution was determined by drawing air through each diffusion battery separately. The pump operated through a condensation nuclei counter in order to provide an indication of the number of aerosol particles penetrating the battery. The number of aerosols registered in the absence of the diffusion battery was then used for calculating the penetration g_3, g_4 and g_5 through diffusion batteries nos. 3, 4 and 5. Input of these values into the computer program (Section C.1) allows estimation of the count median diameter $\bar{d}$ and the geometric standard deviation σ_g.

For the activity size distribution determination glass fibre filters of 0.45 μm pore size and 47 mm diameter were placed in the magnetic filter holders at the air exit ends of the diffusion batteries. Each diffusion battery was preceded by a pump. Sampling was carried out for 10 minutes followed by counting at 2-5, 6-12, 25-35 minutes from the end of sampling. The overall sampling and counting schedule was as follows:

Time (min)	Action to be taken
0	Start sampling through first diffusion battery using filter no. 1
10	Stop sampling with filter no. 1
11	Start sampling through next diffusion battery with filter no. 2
12	Start counting filter no. 1
15	Stop counting filter no. 1, record total counts and reset counter.

16 Restart counting filter no. 1

21 Stop sampling with filter no. 2

22 Stop counting filter no. 1, record total counts and reset counter.

23 Start counting filter no. 2

26 Stop counting filter no. 2, record total counts and reset counter

27 Restart counting filter no. 2

33 Stop counting filter no. 2, record total counts and reset counter

35 Restart counting filter no. 1

45 Stop counting filter no. 1, record total counts and reset counter.

46 Restart counting filter no. 2

56 Stop counting filter no. 2, record total counts and reset scaler.

The concentrations were calculated from the following equations:

$$\eta C(2)V = 0.370265\ I(1) - 0.27601\ I(2) + 0.064683\ I(3)$$

$$\eta C(3)V = -0.011373\ I(1) - 0.02496\ I(2) + 0.03988\ I(3)$$

$$\eta C(4)V = -0.043756\ I(1) + 0.080482 I(2) - 0.029094\ I(3)\ ,$$

where the symbols have their usual meaning.

Portable condensation nuclei counters and pumps were used for measurements inside mines. The results for the aerosol and activity size distributions are listed in Table A.2.1 for both diesel and non-diesel mines.

With respect to Table A.2.1, some data were rejected owing to large concentration fluctuations during sampling, in some cases caused by blasting during the measurement procedure. Under mine conditions, such errors could arise from the instability of the radon daughters and aerosols concentrations over the sampling period. Variations in pump flow rate and the inherent inaccuracy of the portable condensation nuclei counter could have also introduced some errors into the measurements.

In the radon chamber the activity size distribution had earlier been observed to be very similar to the aerosol size distribution by a co-worker (Fu82). Therefore, only the size distribution of aerosols was measured in the laboratory experiments. The data corresponding to the experiments reported in Table 8.1 are reported in Table A.2.2.

TABLE A.2.1

(i) Rio Algom Mines Data:

July 14, 1982 (a) Counts recorded:

Set no.	Counting Interval (min)	Open face	D.B. 3	D.B. 4	D.B. 5
I	2-5	4323	3899	2440	915
	6-12	7017	6497	4315	1586
	25-35	9420	8585	5720	2043
II	2-5	4263	4033	2611	849
	6-12	7138	6738	4374	1411
	25-35	9727	8870	5870	1988
III	2-5	4307	4079	2615	885
	6-12	7210	6987	4365	1517
	25-35	9538	9096	5991	1940
V	2-5	4326	4170	2783	940
	6-12	7145	7270	4819	1624
	25-35	9764	9615	6211	2098
Pump flow rate (V) L/min		2.63	2.7	2.75	2.59
counting efficiency (η)		0.423	0.435	0.437	0.4415

(b) Concentrations (pCi/L)

I	RaA	97.5	69.5	27.2	11.5
	RaB	54	45.9	30.6	10.9
	RaC	36.2	34.6	24.4	9.8
II	RaA	84.7	70.0	45.9	18.6
	RaB	57.5	47.2	31.4	11.9
	RaC	37.4	36.4	22.1	6.45

TABLE A.2.1 (cont'd)

Set no.	Counting Interval (min)	Open face	D.B. 3	D.B. 4	D.B. 5
III	RaA	79.1	57.5	49.9	11.9
	RaB	54.0	48.0	31.4	10.2
	RaC	40.8	40.3	22.1	9.3
V	RaA	93.2	53.8	33.7	12.33
	RaB	57.7	52.2	31.6	11.26
	RaC	36.3	36.0	28.2	9.9

(c) Calculated size distribution data

Set no.	Aerosol concn. (/cm^3)	Count median diameter (μm); σ_g in brackets			
		RaA	RaB	RaC	Aerosol
I	63,000	0.03 (2.29)	0.07 (1.85)	0.09 (1.66)	0.06 (2.58)
II	63,000	0.06 (2.28)	0.06 (2.29)	0.07 (1.52)	0.06 (2.58)
III	41,000	0.06 (2.35)	0.07 (1.55)	0.07 (1.89)	0.04 (2.51)
V	30,000	0.03 (2.43)	0.07 (1.67)	0.10 (1.62)	0.03 (2.49)

cont'd

TABLE A.2.1 (cont'd)

(ii) Denison Mines Data:

July 17, 1982 (a) Counts recorded:

Set no.	Counting Interval (min)	Open face	D.B. 3	D.B. 4	D.B. 5
I	2-5	3348	2522	2379	1048
	6-12	5562	4229	3816	1678
	25-35	7520	5744	5266	2285
III	2-5	3569	2606	2450	1226
	6-12	5467	4281	4047	1826
	25-35	7649	5800	5371	2620
V	2-5	3537	2804	2684	1228
	6-12	5870	4580	4282	2037
	25-35	7863	6193	5831	2683
Pump flow rate (V) L/min)		2.59	2.7	2.75	2.63
Counting efficiency (η)		0.437	0.423	0.435	0.441

(b) Concentrations (pCi/L)

I	RaA	67.0	48.0	47.6	24.8
	RaB	43.1	32.9	29.1	12.76
	RaC	28.9	21.9	16.5	7.76
III	RaA	100.8	55.1	45.6	40.8
	RaB	44.9	32.9	28.3	15.4
	RaC	21.5	21.5	20.6	5.8
V	RaA	69.5	60.7	62.7	22.6
	RaB	44.5	35.0	31.6	14.4
	RaC	31.2	22.8	19.1	11.0

con'd.....

TABLE A.2.1 (cont'd)

(c) Size Distribution Data

Set no.	Aerosol concn. (/cm^3)	count median diameter (μm); σ_g in brackets			
		RaA	RaB	RaC	Aerosol
I	238,000	0.07 (2.65)	0.08 (2.49)	0.06 (2.56)	0.04 (2.39)
III	300,000	0.04 (2.69)	0.07 (2.81)	0.12 (1.49)	0.04 (2.50)
V	270,000	0.12 (1.54)	0.09 (2.44)	0.07 (2.42)	0.04 (2.69)

TABLE A.2.2

Expt. no.	Open face Aerosol concn. (/cm^3)	Aerosol concn. after passing through			count med. dia. (μm)	σ_g
		D.B. 3	D.B. 4	D.B. 5		
1 & 2	70,000	60,000	42,000	24,000	0.08	2.21
3	125,000	80,000	60,000	25,000	0.04	2.37
4 & 5	44,000	24,000	17,000	2,000	0.03	2.39
6	70,000	40,000	22,000	4,000	0.03	2.21
7	225,000	120,000	80,000	25,000	0.03	2.4
8 & 9	150,000	90,000	60,000	25,000	0.04	2.48
10	170,000	90,000	45,000	20,000	0.03	2.36
11	150,000	70,000	30,000	10,000	0.02	2.43
12	80,000	62,000	40,000	20,000	0.06	2.13
13	120,000	90,000	50,000	20,000	0.05	2.2
14&15	215,000	160,000	110,000	50,000	0.06	2.48
16	150,000	85,000	65,000	45,000	0.04	2.65
17	190,000	115,000	75,000	40,000	0.04	2.58
18	200,000	130,000	85,000	40,000	0.04	2.51
19	180,000	110,000	60,000	30,000	0.03	2.45

APPENDIX B

B.1 Importance of Energy Discrimination for Radon Daughter Dosimetry

Energy discrimination in radon and thoron daughter dosimetry implies a capability to register RaA, RaC' and ThC' separately in separate energy channels. An integrated alpha count does not indicate the disequilibrium ratios of radon and thoron daughters. Knowledge of this ratio is important for exact exposure estimation. An energy discrimination option in a dosimeter provides a better estimate of Working Level through separate registration of RaA, RaC' and ThC'. Especially in the case of atmospheres containing thoron, as in certain Canadian uranium mines, measurement of integrated alphas alone can yield an overestimation of the radon daughter Working Levels due to the presence of thoron daughters.

B.2. The CEA Dosimeter

The CEA dosimeter consists of a cylindrical body and a detection head. The body contains a turbine, motor and rechargeable batteries. The motor is capable of driving the centrifugal turbine at 18000 rpm for 18 hours after one time charging.

The detection head consists of three collimating channels, a screen with appropriate energy absorbers for RaA, RaC' and ThC', the detector film with a cover and a Millipore filter with a support screen (Fig. B.2.1).

Detection Principle: The CEA dosimeter uses a cellulose nitrate (LR-115, type II) film manufactured by Kodak-Pathé Ltd. for detection of alpha particles. The film consists of a 13 μm thick sensitive layer,

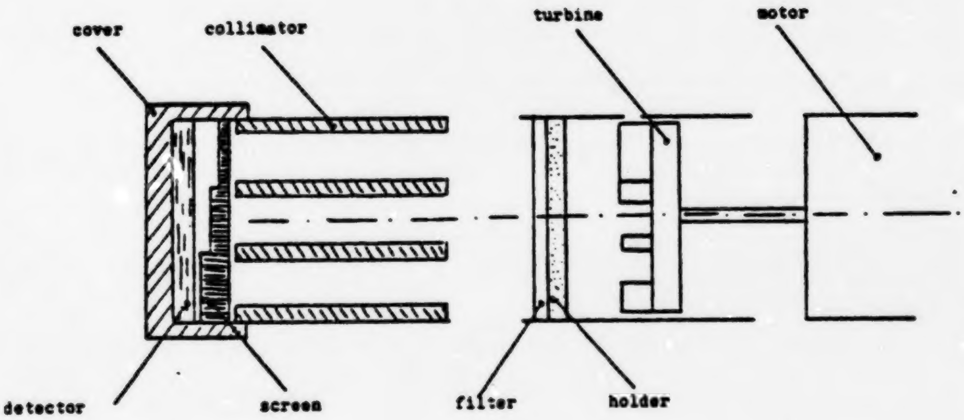
cover
collimator
turbine
motor
detector
screen
filter
holder

Fig. B.2.1. The CEA dosimeter head.

red in colour, deposited on a transparent mylar film. When an alpha particle of energy in the approximate range 3 ± 0.5 MeV makes an impact on this type of film, the alpha track can be enlarged under appropriate etching conditions (2.5 N NaOH, 60°C for 90 minutes) to appear as a 5-7 μm diameter hole. Such holes can be counted against the red background, under a microscope.

The alpha energy from radon and thoron daughters is degraded to the ∿3 ± 0.5 MeV range by means of appropriate absorbers placed below the detector film. The aerosols are driven towards and retained on a 0.8 μm pore size Millipore filter. The alphas emitted from the aerosols on the filter traverse the length of a cylinder containing three collimators and associated absorbers. The thickness of each absorber is designed to allow detection of only one of the three alpha energies of interest. After etching the three regions on the detector film contain tracks registered by the appropriate energy alpha particle.

APPENDIX C: COMPUTER PROGRAMS

C.1 Aerosol Size Distribution Calculation

```
1 REM AEROSOL SIZE DISTRIBUTION
16 FOR I=1 TO 30:PRINT:NEXT I
17 P0=-66620:P1=2.401E-11:P2=2.5066283
18 P3=1.6273E-5:P4=5.485E-6
20 PRINT: INPUT"NO.OF STEPS IN INTEGRATION";M
30 PRINT:INPUT"HOW MANY MEASUREMENTS";N
40 DA=5E-7:DB=1E-4
50 A(1)=.91035:A(2)=.05314
55 A(3)=.01529:A(4)=6.8E-3
60 B(1)=1.88517:B(2)=21.4317:B(3)=62.3166:B(4)=124.5
70 PL(1)=1:PL(2)=1:PL(3)=25:PL(4)=50:PL(5)=140
80 W(1)=10 :W(2)=15.7:W(3)=10:W(4)=10:W(5)=10
90 HT(1)=.2:HT(2)=.1:HT(3)=.08:HT(4)=.04:HT(5)=.04
100 LG(1)=6.25:LG(2)=12.7:LG(3)=19:LG(4)=30:LG(5)=43
110 FOR I=1 TO N
118 PRINT:PRINT:PRINT
120 PRINT"INPUT DATA FOR MEASUREMENT";I
121 PRINT"**************************"
130 PRINT:INPUT"DIFFUSION BATTERY NUMBER";C(I)
140 PRINT:INPUT"PENETERATION";F(I)
150 PRINT:INPUT"FLOWRATE IN ML/S";Q(I)
155 PRINT:PRINT:PRINT
160 NEXT I
170 H=LOG(DB/DA)/M
180 REM
190 REM INITIAL PARAMETER GUESSES
200 DH=1E-5
210 SH=2
215 DP=DH:SP=SH
220 PI=1000000
240 RX=0.2*H*M
250 RS=0.5
260 PRINT:INPUT"HOW MANY ITERATIONS";NI
270 PRINT:INPUT"GUESSES PER ITERATION";NG
275 PRINT
276 PRINT "*********************"
277 PRINT:PRINT:PRINT:PRINT
280 FOR J=1 TO NI
285 PRINT "PROGRAM ON ITERATION";J;"OF";NI
286 PRINT
290 RX=0.8*RX:RS=0.8*RS
300 FOR L=1 TO NG
305 PRINT "PROGRAM ON GUESS";L;"OF";NG:PRINT:PRINT
307 PRINT:PRINT"THEORETICAL CALCULATIONS"
308 PRINT
310 S=ABS(SH+RS*(RND(S)-0.5))
315 LS=LOG(S)
330 XX=ABS(LOG(DH/DA)+RX*(RND(S)-0.5))
340 DM=DA*EXP(XX)
```

```
345 LD=LOG(DM)
350 D1=EXP(LD-4*LS)
360 D2=EXP(LD+4*LS)
370 H=LOG(D2/D1)/M
380 REM
390 REM PI IS A FUNCTION OF N MEASUREMENTS
400 REM
405 Z=0
410 FOR K=1 TO N
420 FT=0
430 REM
440 REM INTEGRATION ROUTINE
450 REM
460 FOR U=1 TO M
470 DI=D1*EXP(H*U)
480 XY=P0*DI
490 IF XY<-80 THEN XY=-80
500 D=(P1/DI)*(1+P3/DI+(P4/DI)*EXP(XY))
510 CC=C(K)
520 MU=2*PL(CC)*W(CC)*LG(CC)*D/HT(CC)
525 MU=MU/Q(K)
530 P=0
540 FOR V=1 TO 4
545 XY=-B(V)*MU
546 IF XY<-80 THEN XY=-80
550 P=P+A(V)*EXP(XY)
560 NEXT V
570 X=1/(DI*P2*LS)
580 XY=LOG(DI/DM)/LS
590 X=X*EXP(-XY*XY/2)
600 IF U=M THEN GOTO 620
610 FT=FT+P*X*(EXP((U+1)*H)-EXP((U-1)*H))
620 NEXT U
625 XY=-66620*D1
630 D0=(P1/D1)*(1+P3/D1+(P4/D1)*EXP(XY))
640 XY=LOG(D1/DM)/LS
650 X0=1/(D1*P2*LS)
660 X0=X0*EXP(-XY*XY/2)
670 MU=2*PL(CC)*W(CC)*LG(CC)*D0/(HT(CC)*Q(K))
680 PP=0
690 FOR V=1 TO 4
695 XY=B(V)*MU
696 IF XY<-80 THEN XY=-80
700 PP=PP+A(V)*EXP(-XY)
710 NEXT V
720 FT=FT+PP*X0*(EXP(H)-1)+P*X*(EXP(M*H)-EXP((M-1)*H))
730 FT=FT*D1/2
740 XY=FT-F(K)
745 Z=Z+XY*XY*XY*XY
```

```
 750 PRINT 'PENETERATION OF D.B.';C(K);'=';FT
 755 FP(K)=FT
 760 NEXT K
 765 Z=SQR(Z):Z=SQR(Z)
 770 IF Z>PI THEN GOTO 790
 780 SP=S:DP=DM:PI=Z
 785 FOR K=1 TO N:FH(K)=FP(K):NEXT K
 790 PRINT 'PI=';PI
 795 PRINT:PRINT
 810 LH=DP:SH=SP
 820 NEXT J
 830 FOR I=1 TO 20:PRINT:NEXT I
 840 PRINT 'FINAL RESULTS'
 850 PRINT '---------------'
 860 PRINT:PRINT:PRINT
 870 PRINT 'MEAS';TAB(6);'D.B.';
 880 PRINT TAB(12);'FEXP';TAB(20);'FTHEOR'
 885 PRINT'----';TAB(6);'----';TAB(12);'----';TAB(20);
 886 PRINT'------'
 888 PRINT
 890 FOR K=1 TO N
 900 PRINT K;TAB(6);C(K);TAB(11);F(K);TAB(19);FH(K)
 910 NEXT K
 930 PRINT'PERFORMANCE INDEX=';PI
 940 PRINT 'CNT MEDIAN DIAOETER=';DP
 950 PRINT 'GEOMETRIC S.D.=';SP
 965 PRINT
 970 PRINT:INPUT'HOW MANY MORE ITERATIONS';NI
 980 IF NI>0 THEN GOTO 275
 990 END
OK
```

C.2 Electrostatic Flow Rate Calculations

```
10 REM OPTIMISED MODIFIED TSIVOGLOU'S METHOD
24 C(1)=100:C(2)=60:C(3)=40
26 PRINT:INPUT"FLOWRATE 1";V(1)
28 PRINT:INPUT"FLOWRATE 2";V(2)
30 PRINT:INPUT"FLOWRATE 3";V(3)
32 ST=5
45 T(1)=2:T(2)=5:T(3)=7:T(4)=15:T(5)=25:T(6)=30
48 PRINT:INPUT"I(1)=";I(1)
50 PRINT:INPUT"I(2)=";I(2)
54 PRINT:INPUT"I(3)=";I(3)
60 EFF=.433
70 L(1)=.22726:L(2)=.025864:L(3)=.035185
80 FOR J=1 TO 3:C(J)=2.22*C(J)/L(J):CC(J)=C(J):NEXT J
120 A(1,1)=(1-EXP(-L(1)*ST))/L(1)
130 A(2,1)=(1-EXP(-L(2)*ST))/L(2)
140 A(2,1)=A(2,1)+(EXP(-L(2)*ST)-EXP(-L(1)*ST))/(L(2)-L(1))
150 A(2,2)=(1-EXP(-L(2)*ST))/L(2)
160 A(3,1)=(1-EXP(-L(3)*ST))/L(3)
170 A(3,1)=A(3,1)+(EXP(-L(3)*ST)-EXP(-L(2)*ST))/(L(3)-L(2))
180 W=L(2)*(EXP(-L(2)*ST)-EXP(-L(3)*ST))
185 W=W/((L(3)-L(2))*(L(2)-L(1)))
190 A(3,1)=A(3,1)+W
200 W=L(2)*(EXP(-L(3)*ST)-EXP(-L(1)*ST))
210 A(3,1)=A(3,1)+W/((L(3)-L(1))*(L(2)-L(1)))
220 A(3,2)=(1-EXP(-L(3)*ST))/L(3)
230 A(3,2)=A(3,2)+(EXP(-L(3)*ST)-EXP(-L(2)*ST))/(L(3)-L(2))
240 A(3,3)=(1-EXP(-L(3)*ST))/L(3)
250 FOR J=1 TO 3
260 N(J)=0
270 FOR M=1 TO 3
280 N(J)=N(J)+A(J,M)*V(M)*C(M)
290 NEXT M
300 NEXT J
410 FOR Q=1 TO 3
420 W=1+L(2)*L(3)/((L(3)-L(1))*(L(2)-L(1)))
425 W=W*(EXP(-L(1)*T(2*Q-1))-EXP(-L(1)*T(2*Q)))
430 AL(Q,1)=W
440 W=L(1)*L(3)/((L(1)-L(2))*(L(3)-L(2)))
445 W=W*(EXP(-L(2)*T(2*Q-1))-EXP(-L(2)*T(2*Q)))
450 AL(Q,1)=AL(Q,1)+W
460 W=L(1)*L(2)/((L(1)-L(3))*(L(2)-L(3)))
470 W=W*(EXP(-L(3)*T(2*Q-1))-EXP(-L(3)*T(2*Q)))
480 AL(Q,1)=AL(Q,1)+W
490 W=L(3)/(L(3)-L(2))
500 W=W*(EXP(-L(2)*T(2*Q-1))-EXR(-L(2)*T(2*Q)))
510 AL(Q,2)=W
520 W=L(2)*(EXP(-L(3)*T(2*Q-1))-EXP(-L(3)*T(2*Q)))/(L(2)-L(3))
530 AL(Q,2)=AL(Q,2)+W
540 AL(Q,3)=EXP(-L(3)*T(2*Q-1))-EXP(-L(3)*T(2*Q))
542 NEXT Q
```

```
 653 FOR M=2 TO 3
 654 FOR J=2 TO 3
 655 X(M,J)=AL(M,1)*AL(1,J)-AL(1,1)*AL(M,J)
 656 NEXT J
 657 NEXT M
 658 Y(3,3)=X(3,2)*X(2,3)-X(2,2)*X(3,3)
 659 H(1,1)=1
 660 H(2,1)=AL(2,1)
 670 H(2,2)=-AL(1,1)
 680 H(3,1)=AL(2,1)*X(3,2)-AL(3,1)*X(2,2)
 685 H(3,2)=-AL(1,1)*X(3,2)
 688 H(3,3)=AL(1,1)*X(2,2)
 690 FOR M=1 TO 2
 700 FOR J=(M+1) TO 3
 710 H(M,J)=0
 720 NEXT J
 730 NEXT M
 740 FOR J=1 TO 3
 750 E(3,J)=H(3,J)/Y(3,3)
 760 E(2,J)=(H(2,J)-(X(2,3)*E(3,J)))/X(2,2)
 770 E(1,J)=(H(1,J)-(AL(1,2)*E(2,J))-(AL(1,3)*E(3,J)))/AL(1,1)
 780 NEXT J
 790 FOR M=1 TO 3
 800 D(1,M)=E(1,M)/A(1,1)
 810 D(2,M)=(E(2,M)-(A(2,1)*D(1,M)))/A(2,2)
 820 D(3,M)=E(3,M)/A(3,3)-A(3,2)*D(2,M)/A(3,3)
 824 D(3,M)=D(3,M)-A(3,1)*D(1,M)/A(3,3)
 830 NEXT M
 840 FOR J=1 TO 3
 850 C(J)=C(J)*L(J)/2.22
 860 NEXT J
 880 FOR M=1 TO 3
 890 FOR J=1 TO 3
 900 D(J,M)=D(J,M)*L(J)/2.22
 910 NEXT J
 915 NEXT M
 920 FOR J=1 TO 3
 930 C(J)=0
 940 FOR M=1 TO 3
 941 C(J)=C(J)+((D(J,M)*I(M))/(V(J)*EFF))
 942 NEXT M
 943 NEXT J
 944 RWL=(1.03*C(1)+5.07*C(2)+3.73*C(3))/1000
 945 PRINT"C(1)=";C(1)
 946 PRINT"C(2)=";C(2)
 947 PRINT"C(3)=";C(3)
 950 PRINT"RWL=";RWL
 994 END
OK
```